Dissertation

博士論文

Study on Spatial and Temporal Variations in Single Cell Rheology Measured by Atomic Force Microscopy

原子間力顕微鏡による単一細胞レオロジーの時空間変化に関する研究

Graduate School of Information Science and Technology
Hokkaido University

北海道大学大学院情報科学研究科

PingGen Cai

蔡萍根

Content

Chapter 1: General Introduction

1.1 Cell Mechanics and Structure

The cell is the basic unit of life: every living organism is made up of cells. Each individual cell has an internal polymer network for maintaining its shape and internal organization, called cytoskeleton (CSK). CSK enables cells to adapt mechanically to their dynamic functions including crawling, contraction, intracellular trafficking and division in response to the external environment and stimuli. Thus, cells can transit their mechanical states from fluid-like to solid-like, exhibiting viscoelastic property. The viscoelastic property or the so-called rheological property of cells could be investigated by studying the relationship between forces and deformations when the forces are applied to cells.

The CSK that is composed of three main types of protein fibers including actin filaments, intermediate filaments, and microtubules exhibits a high heterogeneous structure. These kinds of filaments are distributed throughout the cell in an organized manner. A schematic of the typical distribution of CSK is shown in Fig. 1.1. Actin filaments are long and flexible helical polymer fibers formed by polymerization of the monomeric globular form of the protein (G-actin). The actin filaments are distributed within cell to form a network. It can also come into being dense, rigid bundles cross-linked through association with motor myosin II. The bundles called stress fibers can develop forces and lead to cellular contraction or cytoskeletal reorganization [1-4]. One of the remarkable properties of actin filaments is that they can undergo rapid reorganizations depending on physical or chemical conditions. For example, the stiffness of cells can be changed owning to pharmacological or mechanical stimulus [3-9]. The disruption of actin filaments by drugs such as latrunculin A or cytochalasin D leads to a significant decrease in cellular stiffness and also weakens the ability of cells

to move and contract [3-9]. In contrast, the enhancements of the actin polymerization and the actin-myosin formation induce an increment in cellular stiffness for some cell types [3-11].

The structure of microtubules is a hollow cylindrical geometry formed by polymerization of tubulin α, β dimmers. In interphase, the microtubules radiate out from the microtubule-organizing center (called centrosome) located close to the cell center. Compared to actin filaments, the microtubules exist in smaller numbers. The role of microtubules in cell mechanical properties has not been fully elucidated. Some results reported that the disruption of microtubules has induced a slight drop in cell stiffness by using drugs, such as nocodazole or colchicines. In contrast, the polymerization of microtubules caused an increase in cell stiffness by using drugs, such as paclitaxel [1,12-14].

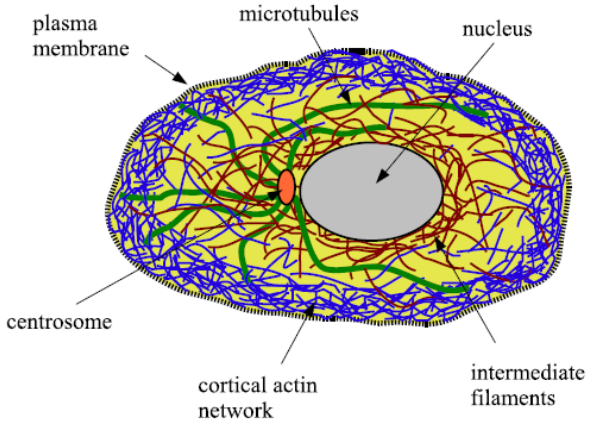

Figure 1.1 Schematic of the typical organization of the cytoskeletal filaments inside a cell. Figure adapted from [4].

The intermediate filaments are a variety of filaments with common sequences and structures and usually bonded to other parts of the cytoskeleton via linking proteins. It is considered that the intermediate filaments do not have highly dynamical behavior compared with the other two components of cytoskeleton. Thus, to date, the role of

intermediate filaments in cell mechanical property has not yet been interested rather than the other two filament types [4].

1.2 Experimental Techniques for Probing Cell Mechanics

Following the development of modern rheological techniques, it became possible to quantitatively measure the mechanical properties of single living cells with nanometer resolution with the forces in the piconewton (pN) to nanonewton (nN) range carrying out measurements under liquid environment. These techniques are atomic force microscope, magnetic twisting cytometry, optical cell stretcher, laser tweezers, microplates and particle tracking microrheology (Fig. 1.2) [15,16], which are classified into active technique involving the application of forces and passive technique examining the motion of the particles or micro-beads due to thermal fluctuations. Each technique has its particular characteristics, advantages, and limitations.

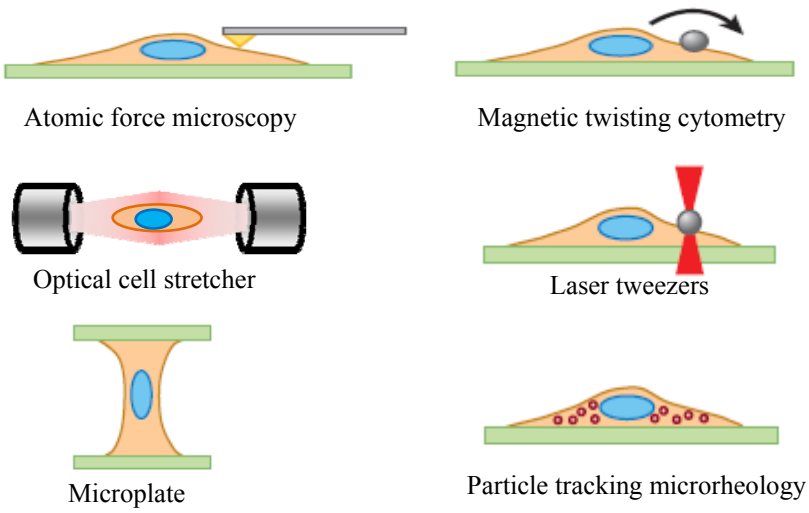

Figure 1.2 Schematic of different microrheology techniques for measuring the rheological properties of living cells. Figure adapted from [15,16].

1.2.1 Atomic force microscopy

Atomic force microscopy (AFM) was invented by Binning *et al*. in 1986 [17]. It only took five years from the application in basic physics to in biology [18,19]. Firstly, AFM was applied to image the cell by Radmacher *et al*. [18] and Henderson *et al*. [19]. Then, Tao *et al*. [20] used it to probe the microelasticity of soft biological samples. Hoh *et al*. were the first time to use AFM to measure the mechanical properties of living cells [21]. AFM can probe the cell mechanical properties in a submicrometer resolution with the forces in the range of 0.1-1 nN and the frequency in the range of 0.1-300 Hz by adding a force via a flexible force-calibrated cantilever [22]. In order to obtain the accurate measurement of cellular properties, the recent AFM studies on cellular mechanics have utilized the polystyrene bead to modify the tip of the cantilever [23-26]. As AFM has the advantages of a high resolution, easy sample preparation and precise controlment of probe position, and has the benefit to get the images and probe the mechanics of biological samples under the real physiological condition, AFM has now become a valuable tool in probing the viscoelastic properties of cells [7-8,22-25].

1.2.2 Magnetic twisting cytometry

Magnetic twisting cytometry (MTC) is also an active method to measure cell rheology. This technique measures the mechanical response of cells by generating well defined forces on magnetic beads with an electromagnet in which the magnetic beads are attached to the cytoskeleton structure of cell through specific receptors. The displacement of the bead in response to an applied force is monitored [5,6]. The applied force can be adjusted from pN to nN by adjusting the current in the coil. MTC has an advantage to measure a large number of cells in a short time period, whereas the limitations are that the binding site that the bead adheres to the cell surface cannot be controlled and the focal adhesion complexes will be formed at the binding sites by

bounding the beads to the cell surface [5,6]. Furthermore, it is difficult to determine the degree of the microbead embedding inside the cell.

1.2.3 Optical cell stretcher

Optical cell stretcher developed by Käs *et al*. is a novel laser tool to measure cell rheology [27]. Combined with microfluidic delivery, it can deform individual suspended cells by optically inducing surface forces at rates [27], capture cells from a flow in a microfluidic system and center them automatically, thus allowing the measurements of flow-cytometric single cell with high throughput without making mechanical contact. The drawback of this technique is less effect of the spatial resolution and the relative stiff cells.

1.2.4 Laser tweezers

Laser tweezers focus laser beams to exert forces onto small dielectric particles [28]. They have an effect in biology for measuring pN forces generated by motor proteins or measuring mechanical properties of cell organelles. Laser tweezers have also been used extensively for cell microrheological measurement [28]. Additionally, an alternative approach to optical tweezers is to use two opposing beams to capture and deform non-adhering cells. However, the limitation is that the applied force is much smaller to drive cell deformation because living cell samples would be damaged under higher laser power.

1.2.5 Microplate

The microplate method can be used to measure the mechanical properties of surface-adherent cells. In this technique, a cell is held between two glass microplates [29], in which one plate is a rigid microplate coated with fibronectin, and the other is a flexible microplate acted as a force transducer. The deflection in the flexible microplate is measured by using an optic fiber technique which allows for the accurate

measurement of the stress imposed on the cell. Applying forces to induce deformations of the cells, this technique can be used to study the non-linear behavior and the creep responses of living cells over a long time [29].

1.2.6 Particle tracking microrheology

Particle tracking microrheology is a passive technique for measuring cell rheology by tracking the random Brownian dynamics of organelles or microinjected particles [30]. The technique provides sub-nanometer and near-microsecond resolutions by the laser optoelectronic detection. According to the motion of the particle, the rheological properties of the interior of the cell can be obtained. Later, two particles method was utilized in the passive microrheology experiment by calculating the cross-correlation between the individual movements of two particles [31]. Recently, a new fluorescence laser-tracking microrheometer was developed to measure cell rheology by using fluorescent microspheres at tracer particles [32]. The advantage of this technique is non-invasive because no mechanical perturbation is applied.

1.3 Current Results of Cell Mechanics

1.3.1 Elastic clues in disease detection

The mechanical measurement has been used to distinguish the different cancerous states at the population level [33-35]. Cross *et al*. have measured the mechanical properties of benign and cancer cells taken from patients by AFM [35]. They reported that the stiffness of cancer cells was 70% less than that of benign cells as shown in Fig. 1.3. Moreover, the distribution of the Young's modulus of cancer cells was narrower than that of benign cells.

The mechanical identification of different cancerous states has been attempted at the tissue level where the stiffness of ex vivo human breast tissues was investigated by

indentation-type atomic force microscopy (IT-AFM) [36]. The authors reported that the stiffness distributions were largely different among different cancerous states such as normal, benign and invasive cancer tissues (Fig. 1.4). The benign lesion showed a large stiffness and a broad distribution compared with normal tissues [Fig. 1.4 (a) and (b)]. Furthermore, the invasive cancer tissue exhibited a complex stiffness distribution in which a soft peak appeared for malignant tumor [Fig. 1.4 (c)]. Those findings clearly demonstrate that the measurement of cell mechanical properties is potentially useful for detecting the cancerous states of living cells not only at the cell population level [35] but also at the tissue level [36] where both the mean value and the standard deviation of the mechanical distribution are key indicators for diagnosing cancerous states.

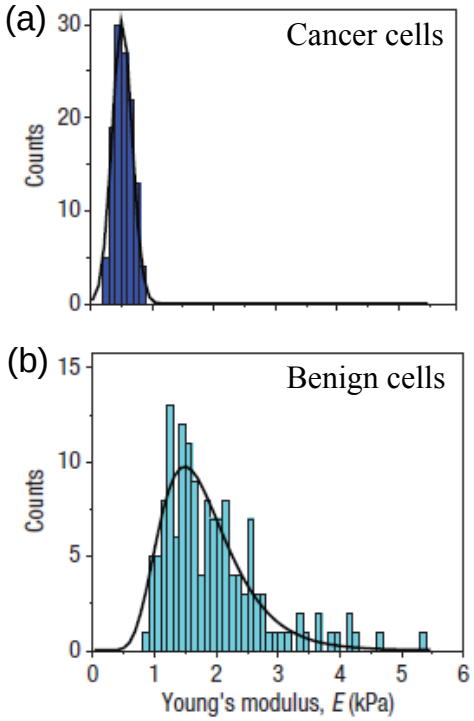

Figure 1.3 Histograms of the Young's modulus *E* for cancer (a) and benign (b) cells. The solid lines represent the Gaussian fit for cancer cells in (a) and the log-normal fit for benign cells in (b), respectively. Figure adapted from [35].

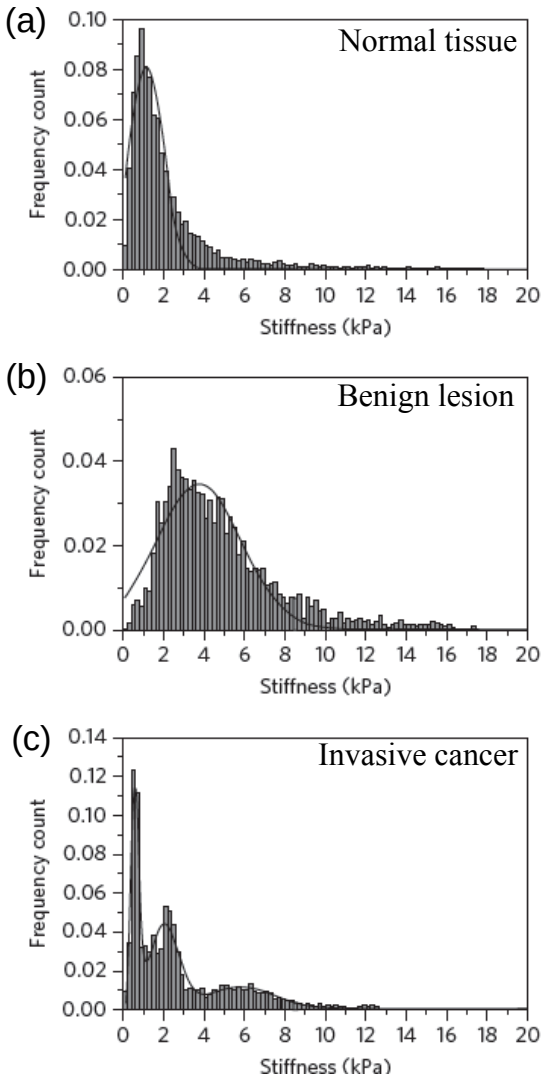

Figure 1.4 Stiffness distributions for normal tissue (a), benign lesion (b) and invasive cancer (c). Figure adapted from [36].

1.3.2 Frequency-dependent ensemble averaged cell rheology

The cells behave not only elastic properties but also viscous properties. In contrast to the static elastic properties, it is important to investigate the rheological properties of cells as a function of frequency or time. As described above, a variety of the experimental methods and approaches have been developed to measure cell rheology [4-6,8,11,12,15,16,22-25,37-56]. The studies on different cell types showed the data in

different forms, such as creep response $J(t)$, stress relaxation response $F(t)$, and complex shear modulus $G^*(f)$ [4-6,8,11,12,15,16,22-24,37-56]. The results revealed that the magnitude of the stiffness of living cells varied more than four orders from tens of Pa to hundreds of kPa, depending on cell types, the heterogeneous structures of cells and the probing instrumentation as shown in Fig. 1.5 [4-6,8,11,12,15,16,22-25,37-56]. However, the stiffness measured by the different methods follows single or multiple power-law behaviors over an exceeding large range of timescales or frequencies.

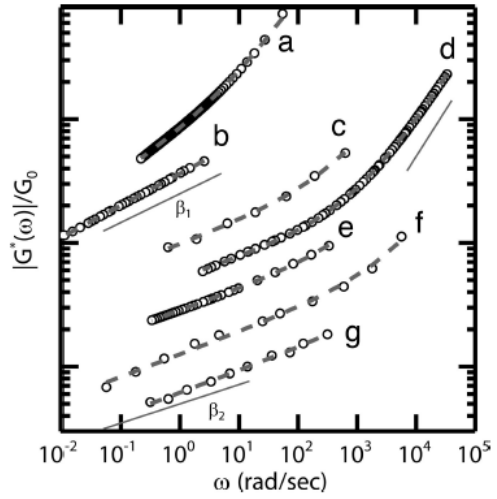

Figure 1.5 Frequency-dependent complex shear modulus. From top to bottom: mechanical measurements from cell creep (magnetic pulling) (a), uniaxial rheometry (b), atomic force microscopy (c), particle tracking microrheology in the lamellae (d), cell creep (magnetic bead twisting) (e), MTC (f), and optical tweezers (g). Figure adapted from [48].

For single power-law behavior of G^*, a more detailed information of cell rheological properties was obtained by performing the measurement under the CSK modifications with different drugs [5-6,8,11-12,46]. Fabry *et al*. measured the frequency dependence of complex shear modulus G^* composed of storage G' and loss G'' moduli of Human Airway Smooth Muscle (HASM) cells under the effects of different drugs using MTC technique [5,6]. They reported that the ensemble averaged storage modulus G' increased

with increasing frequency f as single power-law in a large frequency range of 10^{-2} to 10^{3} Hz as shown in Fig. 1.6 (a). Furthermore, G' increased with a decrease in power-law slope after the activation by contractile agonist histamine and G' decreased with an increase in power-law slope after the relaxation with DBcAMP or the disruption of actin filaments by cytochalasin D. The ensemble averaged loss modulus G'' also exhibited power-law behavior and varied with the CSK modifications [Fig. 1.6 (b)]. The results showed a strong relation between the ensemble averaged G' and G'' and the CSK structure organization. Interestingly, the common intersection was found in G' when the power-law curves of G' under different conditions were extrapolated to higher frequencies [Fig. 1.6 (c)]. The same results were reported by Smith *et al*. [8].

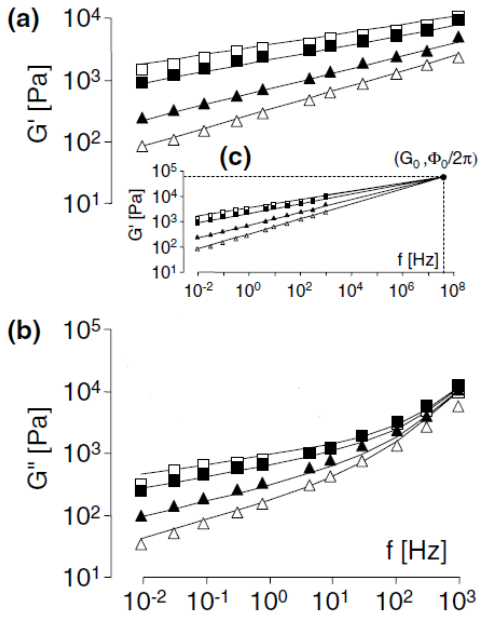

Figure 1.6 G' (a) and G'' (b) of HASM cells vs. frequency under different conditions: control conditions (■), and after 10 min treatment with histamine (□), DBcAMP (▲) and cytochalasin D (△). The solid lines are the fitting of power-law as $\sim f^{\alpha}$. (c) Extrapolation of curves for G' in (a) to higher frequencies yields crossover at coordinate. Figure adapted from [5].

Single power-law behavior has been observed in various cultured cell types with

different techniques over the limited timescales range of 10^{-2}-10^{2} s using creep [40] and frequency range of 10^{-2}-10^{3} Hz using oscillatory measurement [5,6,8]. However, in some studies, the multiple power-law behavior was also found in the rheological properties of cells [44,48,55,56]. For example, Stamenovic *et al*. measured the rheological properties of HASM cells by twisting magnetometry technique in the frequency range of 10^{-3}-10^{0} Hz and 10^{-1}-10^{3} Hz [55]. They found two distinct power-law rheological properties of the frequency-dependent $|G^*|$ in those two different frequency regimes at 10^{-3}-10^{-1} Hz and 10^{0}-10^{3} Hz (Fig. 1.7). The power-law slope in the frequency regime at 10^{-3}-10^{-1} Hz was much larger than that in the frequency regime at 10^{0}-10^{3} Hz. These two power-law behaviors were considered to result from noncovalent protein-protein bond rupture during the near-equilibrium loading [56]. In another example, Hoffman *et al*. measured the rheological properties corresponding to the cortical and intracellular networks of cells by four measurement techniques [48]. The results clearly revealed that both regions displayed weak power-law rheology at low frequencies, crossing over to a steeper dependence at high frequencies with slope 0.75 as shown in Fig. 1.8. The large slope in the higher frequency was considered to probably arise from entropic fluctuations of a semiflexible-filament regime, and a soft-glass-like dynamics [44]. The result for two different multiple power-law cases in the frequency regime at 10^{0}-10^{2} Hz was consistent with the result of single power-law rheology as described above [5,6].

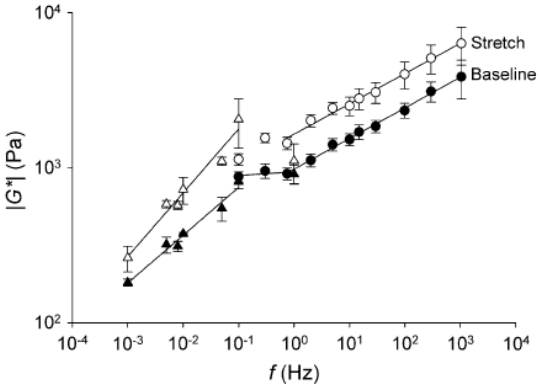

Figure 1.7 Magnitude of the dynamic modulus $|G^*|$ versus frequency f relationship measured in HASM cells at the baseline (solid symbols) and after cell stretching by an ~12% uniform substrate strain (open symbols) using oscillatory magnetic cytometry. Figure adapted from [55].

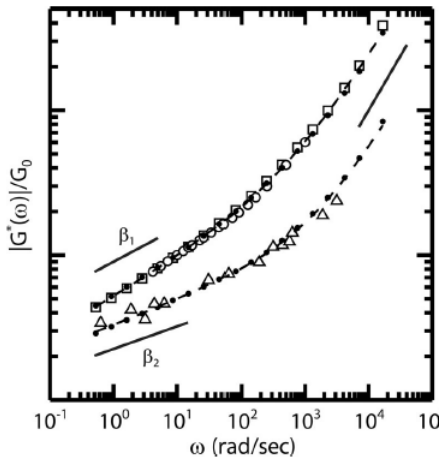

Figure 1.8 Normalized shear modulus for cells collapse onto two master curves. The squares are cell-averaged internal laser tracking microrheology data, triangles are a typical single-cell magnetic twisting cytometry response, and open circles are cell-averaged two point microrheology. The small black points are from single tracer external bead laser tracking microrheology trajectories, which can correspond to either curve. Figure adapted from [48].

1.3.3 Variations in cell elasticity and rheology

Cells exhibit an individual difference even if they are cultured in the same condition as introduced in Section 1.3.1. This manifests the importance of understanding the cell-to-cell variation of cell mechanics. Balland *et al*. investigated the number distribution of G^* of epithelial alveolar cells A549 by optical tweezers [45]. The results

revealed that the number (ensemble) distribution of G_0 where G_0 is the storage modulus factor at $f = 1$, exhibited a log-normal distribution whereas the power-law slope for cells exhibited a normal distribution as shown in Fig. 1.9. The frequency-dependent cell-to-cell variation in cell rheology was, for the first time, investigated by Hiratsuka *et al*. [24]. The complex shear modulus of NIH3T3 cells was measured at different frequencies by AFM combined microarray technique in which cells were cultured in the wells of microarray where the shapes and sizes of cells were strictly restricted. The number distributions of G' and G'' of NIH3T3 cells at different frequencies are shown in Fig. 1.10. The ensemble averaged G' and G'' increased with increasing frequency. Moreover, the distributions of G' and G'' became narrower with increasing frequency.

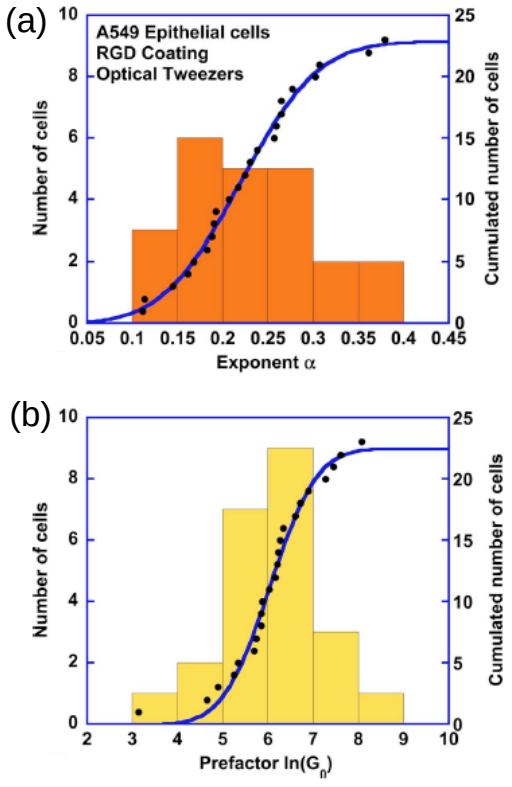

Figure 1.9 Histograms of the distributions of the power-law slope α (a) and of the logarithms of the prefactors $\ln(G_0)$ (b), measured with the optical tweezers on a set of 23 epithelial alveolar cells A549. The distributions of α and G_0 are normal and log-normal, respectively. Figure adapted from [45].

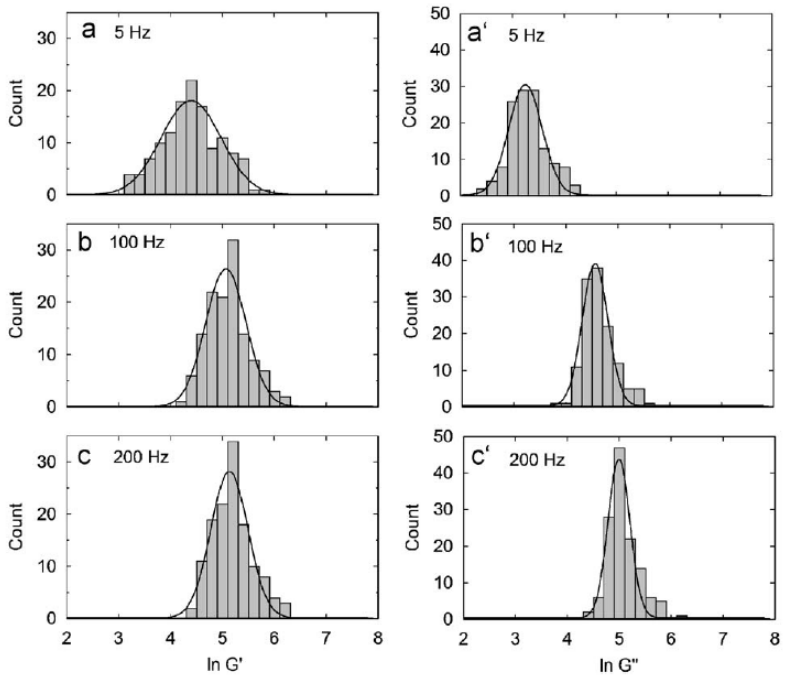

Figure 1.10 Number distribution of storage G' (left) and loss G'' (right) moduli of NIH3T3 cells in the wells of the microarray at different frequencies of (a) 5, (b) 100 and (c) 200 Hz. Solid lines represent the fits to a log-normal distribution function. Figure adapted from [23].

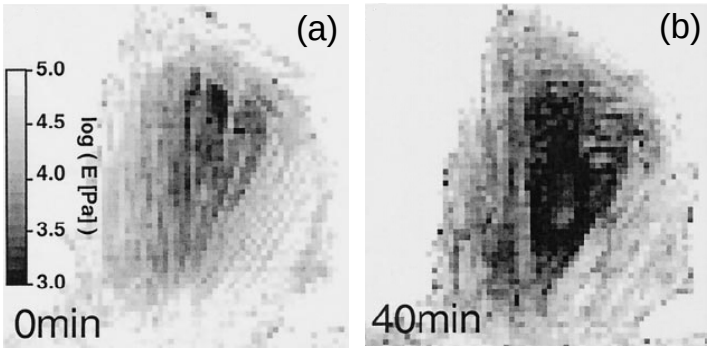

Figure 1.11 Elasticity map of single cell under control (a) and cytochalasin D-treated conditions (b). Figure adapted from [7].

The elastic and rheological properties of cells exhibit spatial distributions due to inherent heterogeneous structures of CSK [7,52]. The elasticity map of the fibroblast cells was probed by AFM under the various drugs affecting the integrity of CSK [7]. As

shown in Fig. 1.11, the elasticity exhibits a spatial distribution in which the elasticity on the nucleus is smaller than that of the periphery of nucleus under control condition [Fig. 1.11 (a)]. After the actin filaments structure was disrupted by drug cytochalasin D, the stiffness of cells significantly decreased [Fig. 1.11 (b)]. In addition to elasticity of single cell, Park *et al*. investigated the local heterogeneity of the ensemble-averaged shear modulus by measuring a large number of single cells that were cultured on micropatterned substrates [52]. They reported that the stiffness depended on the measurement position (Fig. 1.12). Moreover, the stiffness decreased gradually from the corners toward the center which was consistent with the result of elasticity in Fig. 1.11. Combination of the distributions of Figs. 1.11 and 1.12, we can know that the spatial distribution depends on the configuration of cells.

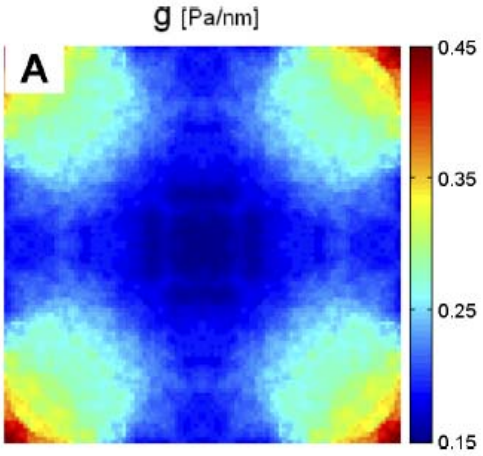

Figure 1.12 Distribution of local stiffness *g* measured by optical magnetic twisting cytometry. Figure adapted from [52].

Besides spatial heterogeneities of cell rheology, it also largely fluctuates with time owning to the dynamically self-remodeling and highly adaption of CSK in response to the surrounding environments and external stresses [47,53,54]. Such a temporal

variation of rheological properties of adherent singe cells cultured on a flat substrate was simultaneously measured at two frequencies by monitoring the motion of micro-beads attached to the actin filaments in the cells under external forces [47]. The experiments showed that the amplitudes of bead largely fluctuated with time under two frequencies in which the variations in rocking amplitude at both frequencies were found to be highly correlated and directly proportional (Fig. 1.13). Moreover, the temporal distributions of cell mechanical parameters are consistent with those observed in the ensemble (number) distributions [23,45], that is, the frequency-dependent shear modulus exhibits a log-normal distribution.

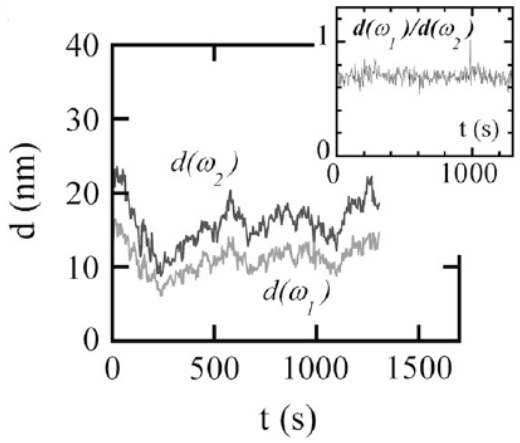

Figure 1.13 Time-dependent variations of the rocking amplitude $d(\omega_1)$ and $d(\omega_2)$ measured simultaneously at two different frequencies in response to a double sinusoidal driving torque: $\omega_1 = 1.3$ Hz, $\omega_2 = 63$ Hz. Figure adapted from [47].

1.3.4 Role of prestress in cell rheology

The relation between the cell stiffness and the internal prestress has been investigated in a variety of cell types under different modifications of the internal prestress by biochemical or mechanical stimuli [57-62]. Wang *et al*. estimated the averaged prestress within individual cultured cells by the traction force microscopy technique and measured the shear modulus by MTC under the treatment with different concentrations

of histamine [58,59]. The result revealed that both the prestress and the shear modulus increased with the concentration of histamine. Furthermore, a linear relationship was found between the prestress and the shear modulus. They explained that CSK structure of cell regulated its shape stability through the prestress and concluded that the tensile might play an important role in cell mechanical stability and stiffness [58,59].

1.4 Theoretical Modeling

Along with the experimental measurements, a number of models have been developed to understand the characteristic features of the mechanical properties of living cells as well as the relationships between complex shear modulus, power-law exponent, and prestress. The commonly applied models include spring-dashpots models, tensegrity model, power-law structure damping model, and soft grassy rheology. They are phenomenological models resting on generic principles that are valid independently of the details of the microscopic structure. Certainly, no single model captures the full phenomenology of cell mechanical behavior. In this section, I review those classical models of cell rheology.

1.4.1 Spring-dashpots models

Cells have viscoelastic behavior [4-6,8,11,12,15,16,22-25,37-56]. In the region of engineering, viscoelastic materials are usually described by mechanical equivalent circuits using the connection of Hookean elastic springs and Newtonian viscous dashpots [15]. As shown in Fig. 1.14, three well known classical models include the Maxwell model, formed by a spring and a dashpot in series; the Voigt model, made of a spring and a dashpot in parallel; and the Kelvin model, a Maxwell body in parallel with an additional spring. The linear viscoelastic behavior of living cells is modeled by these three models as the networks of springs and dashpots arranged in series or in parallel

(Fig. 1.14). The different structural elements of cell are reflected by the different elastic and viscous elements. However, spring-dashpots models explain the simple result with one parameter of time constant [29,63-65]. Following the development of more sophisticated experimental techniques, the more complex models of cell mechanics are extremely needed for the increasing accessible ranges of time and frequency, and resolution of the obtained data.

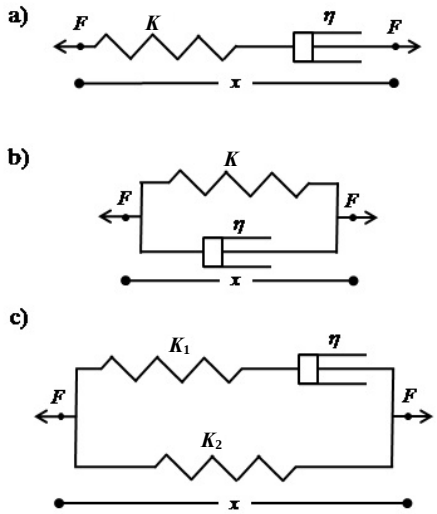

Figure 1.14 Schematic of spring-dashpots models: a) Maxwell, b) Voigt, c) Kelvin. F= force, K = spring constant, η = damping coefficient, x = distance.

1.4.2 Tensegrity model

Tensegrity model that takes the name from architecture principles is a more complex theoretical model based on the structural organization and composition of cells. It states that cells are structures under prestress in which the tensions can be generated by the actin-myosin network, by cellular force generation through focal adhesions, by cell-cell adhesions and polymerization of cytoskeletal elements as shown in Fig. 1.15 [66,67]. The quantitative prediction of a linear relationship between cellular prestress and cell stiffness by the tensegrity model has been demonstrated by experiment [58,59].

However, tensegrity does not provide a complete model of cell mechanics, such as the strong nonthermal or thermal fluctuations and frequency dependence [30,37,48,68].

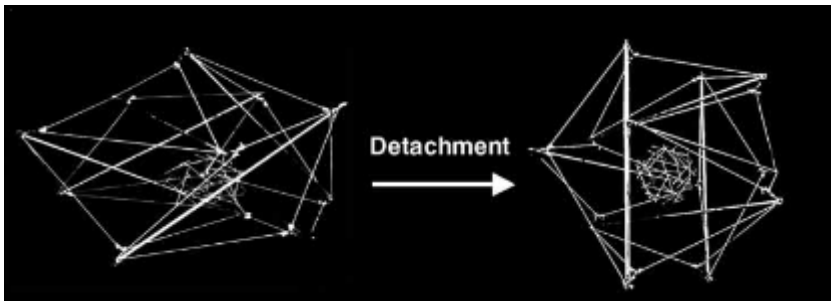

Figure 1.15 Tensegrity cell models of a nucleated cell when adherent and spread on a rigid substrate (left) or detached and round (right). The cell model is composed of large struts and elastic cord; the nucleus contains sticks and elastic strings. The large struts conceptually represent microtubules; the elastic cords correspond to microfilaments and intermediate filaments that carry tensional forces in the cytoskeleton. Figure adapted from [66].

1.4.3 Power-law structural damping model

Using an oscillatory measurement with a wide range of frequencies on cell, the results were founded that complex shear modulus G^* increased with frequency following a weak power-law [4-6,8,11,12,15,16,22-25,37-56]. Then, the power-law structural damping model was introduced to explain the power-law behavior of G^* on frequency as [5,6,69]

$$G^* = G_0 g(\alpha)[1 + i\eta(\alpha)]\left(\frac{f}{f_0}\right)^{\alpha} + i\mu f , \qquad (1.1)$$

where α is the power-law exponent of the model and $g(\alpha)$ is $\Gamma(1-\alpha)\cdot\cos(\pi\alpha/2)$ in which Γ denotes the gamma function. G_0 is a scale factor of the modulus at a scale factor of frequency, f_0, which is defined to be 1 Hz. $\eta(\alpha)$ is the hysteresivity, which is expressed by $\tan(\pi\alpha/2)$ and μ is the Newtonian viscous damping coefficient. The state of the cells is described by power-law exponent α. Furthermore, Eq. 1.1 describes the relation

between the transition of cell from solid-like ($\alpha = 0$) to liquid-like ($\alpha = 1$) and the change of α. The transition can be regulated by the activity or intracellular agitation of the cytoskeletal structure [5,6].

1.4.4 Soft glassy rheology

The timescale-invariance and glass transition features of power-law moduli of cells has noticed that cells have the features as soft glassy matter, such as foams, slurries or colloids. The disordered and metastable properties are the common features of those materials. Soft glass rheology (SGR) is extended and used to explain the power-law behavior of cell rheology by Fabry *et al*. [5,6]. In this theory, soft glassy elements are trapped in energy wells with a landscape formed by their neighboring elements, in which thermal activation is very small compared with the typical trap depths E (Fig. 1.16) [70-72]. Thus, the trapped elements are unable to escape from the wells. If the enough active energy is applied to the system, the elements can escape from their traps and hop from one energy well to another well. The parameter ($\alpha + 1$) is interpreted as an effective temperature. It is related to the rate at which elements can hop out of a trap assuming as the form $\exp[-E/(\alpha+1)]$. In the case of cells, α will reflect the ability of the cytoskeleton to resist force (small α) or to deform and flow (large α). When $\alpha = 0$, the elements are fixed in their wells and the material behaves as a perfectly elastic solid with stiffness. As α increases, the system becomes more disordered until reaching the state of a pure Newtonian liquid ($\alpha = 1$). Many mechanical features of cells are captured and explained by the SGR model, whereas the microscopic explanation of the model parameters is lack.

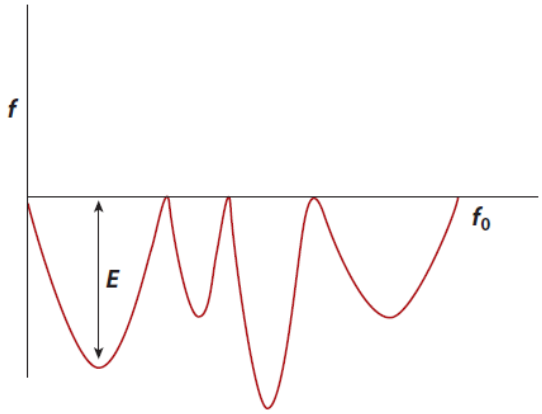

Figure 1.16 Energy landscape, showing different metastable states. Here, f_0 is the energy level below which the states are disconnected. It is the minimum energy required to hop between any two states. It is assumed here that the dynamics between the traps is very fast and that the probability to find the system between two metastable states is negligible. The depth of a trap is $E = f_0, f_0 > 0$. Figure adapted from [70].

1.5 Aim of This Study

From previous studies as mentioned above, it is considered that cell mechanics plays a major role in cell functions [73-75]. For the mechanical identification of cancerous states with different cell functions at cell population [35] and tissue levels [36], the measurement of not only the mean value but also the standard deviation of the mechanical distribution is necessary [35,36]. However, detailed information about the standard deviation of cell stiffness or storage modulus has not been provided. Indeed, little is known about the frequency dependence of the standard deviation, and thus we have no analytical method to quantify the standard deviation of cell rheological properties.

The aim of this study is to investigate the frequency dependences of temporal and spatial dependent cell-to-cell (ensemble) variations in cell rheology. To realize this aim, I used atomic force microscopy (AFM) combined with a cell microarray technique to measure number (ensemble) distribution in cell rheology with the measurement location

and the actin-myosin complex structure modifications and the temporal distribution with the actin filaments structure modification of single mouse fibroblast cells cultured in the wells of microarray.

1.6 Outline of This Dissertation

The research described in this dissertation mainly focuses on the frequency dependences of temporal and spatial dependent cell-to-cell variations in cell rheology with CSK structure modification. I concentrated on measuring number (ensemble) distribution in cell rheology with the measurement location and the actin-myosin complex structure modifications and the temporal distribution with the actin filaments structure modification.

In **Chapter 2**, the experimental principle including experimental material, method and model is introduced.

In **Chapter 3**, to quantify the cell-to-cell variation in cell rheology, the changes in cell-to-cell variation by the modifications of the measurement location and actin filaments structure in cells were investigated. The frequency-dependent component of cell-to-cell variation of cell rheology was estimated from cell-to-cell variation in term of SGR. The results showed that the frequency-dependent component of cell-to-cell variation can be reduced greatly by disrupting actin filaments networks, by probing at locations, and by measuring at high loading frequencies.

In **Chapter 4**, to quantify the precision of the spatial dependence of the cell-to-cell variation in power-law rheology, the relationships among power-law parameters for cell-to-cell variations in the storage modulus G' were clarified by investigating the cell-to-cell variations of single cells in different microarray samples. The results showed

that the spatial dependence of the frequency-dependent component of the cell-to-cell variation is preserved even if the spatial heterogeneities of G' are changed depending on the cell samples. The invariance in the frequency-dependent cell-to-cell variation indicates the robustness of AFM for the mechanical diagnosis of single cells.

In **Chapter 5,** to investigate the role of the actin-myosin interaction in cell-to-cell variation in cell rheology, I investigated how the cell-to-cell variation in cell rheology changes by the enhancement of myosin or the inhibition of myosin. The results indicated that the interaction between actin filaments and myosin regulates the heterogeneities of CSK structure that enhance the cell-to-cell variation in cell rheology.

In **Chapter 6,** to elucidate the temporal variation in cell rheology, a long-time evolution of the rheological properties of single mouse fibroblast cell was traced under a confined condition at the same location. The result suggests that rheological properties of single cell in the confined condition follows an ergodicity condition, in which cell mechanical state transits in all possible states where cell size and shape are unchanged. Furthermore, it is found that the rheological properties evolve in their possible states with a relaxation time of several and tens of minutes.

Concluding remarks are summarized in **Chapter 7**.

1.7 References

1. Stamenovic, D., S. M. Mijailovich, I. M. Tolic-Norrelykke, J. Chen, and N. Wang. 2002. Cell prestress. II. Contribution of microtubules. Am. J. Physiol. Cell Physiol. 282:C617–C624.
2. Alberts, B., A. Johnson, J. Lewis, M. Raff, K. Roberts, and P. Walter. 2008. Molecular biology of the cell. 5th Edition. Garland Science, New York, NY.
3. Nagayama, M., H. Haga, M. Takahashi, T. Saitoh, and K. Kawabata. 2004. Contribution of cellular contractility to spatial and temporal variations in cellular stiffness. Exp. Cell Res. 300:396-405.
4. Pullarkat, P. A., P. A. Fernandez, and A. Ott. 2007. Rheological properties of the eukaryotic cell cytoskeleton. Phys. Rep. 449:29-53.
5. Fabry, B., G. N. Maksym, J. Butle, M. Glogauer, D. Navajas, and J. J. Fredberg. 2001. Scaling the microrheology of living cells. Phys. Rev. Lett. 87:148102-148105.
6. Fabry, B., G. N. Maksym, J. P. Butler, M. Glogauer, D. Navajas, N. A. Taback, E. J. Millet, and J. J. Fredberg. 2003. Time scale and other invariants of integrative mechanical behavior in living cells. Phys. Rev. E 68:041914-1-041914-18.
7. Rotsch, C. and M. Radmacher. 2000. Drug-induced changes of cytoskeletal structure and mechanics in fibroblasts: an atomic force microscopy study. Biophys. J. 78:520-535.
8. Smith, B. A., B. Tolloczko, J. G. Martin, and P. Grutter. 2005. Probing the viscoelastic behavior of cultured airway smooth muscle cells with atomic force microscopy: stiffening induced by contractile agonist. Biophys. J. 88:2994-3007.
9. Charras, G. T. and M. A. Horton. 2002. Single cell mechanotransduction and its modulation analyzed by atomic force microscope indentation. Biophys. J.

82:2970-2981.

10. Puig-de-Morales, M., E. Millet, B. Fabry, D. Navajas, N. Wang, J. P. Butler, and J. J. Fredberg. 2004. Cytoskeletal mechanics in adherent human airway smooth muscle cells: probe specificity and scaling of protein-protein dynamics. Am. J. Physiol. Cell Physiol. 287:C643-C654.
11. Van Citters, K. M., B. D. Hoffman, G. Massiera, and J. C. Crocker. 2006. The role of F-Actin and myosin in epithelial cell rheology. Biophys. J. 91:3946-3956.
12. Hemmer J. D., J. Nagatomi, S. T. Wood, A. A. Vertegel, D. Dean, and M. Laberge. 2009. Role of cytoskeletal components in stress-relaxation behavior of adherent vascular smooth muscle cells. J. Biomech. Eng. 131:041001-1-041001-9.
13. Stamenovic, D.. 2005. Microtubules may harden or soften cells, depending of the extent of cell distension. J. Biomech. 38:1728-1732.
14. Tsai, M. A., R. E. Waugh, and P. C. Keng. 1998. Passive mechanical behavior of human neutrophils: effects of colchicines and paclitaxel. Biophys. J. 74:3282-3291.
15. Kollmannsberger, P. and B. Fabry. 2011. Linear and nonlinear rheology of living cells. Annu. Rev. Mater. Res. 41:75-97.
16. Vaziri, A., A. Gopinath, and V. S. Deshpande. 2007. Continuum-based computational models for cell and nuclear mechanics. J. Mech. Mater. Struct. 2:1169-1191.
17. Binng, G., C. F. Quate, and Ch. Gerber. 1986. Atomic Force Microscope. Phys. Rev. Lett. 56:930-933.
18. Radmacher, M., R. W. Tillamnn, M. Fritz, and H. E. Gaub. 1992. From molecules to cells: imaging soft samples with the atomic force microscope. Science 257:1900-1905.

19. Henderson, E., P. G. Haydon, and D. S. Sakaguchi. 1992. Actin filament dynamics in living glial cells imaged by atomic force microscopy. Science 257:1944-1946.
20. Tao, N. J., S. M. Lindsay, and S. Lees. 1992. Measuring the microelastic properties of biological-material. Biophys. J. 63:1165-1169.
21. Hoh, J. H. and C. A. Schoenenberger. 1994. Surface morphology and mechanical properties of MDCK monolayers by atomic force microscopy. J. Cell Sci. 107:1105-1114.
22. Mahaffy, R. E., S. Park, E. Gerde, J. Kas, and C. K. Shih. 2004. Quantitative analysis of the viscoelastic properties of thin regions of fibroblasts using atomic force microscopy. Biophys. J. 86:1777-1793.
23. Hiratsuka, S., Y. Mizutani, M. Tsuchiya, K. Kawahara, H. Tokumoto, and T. Okajima. 2009. The number distribution of complex shear modulus of single cells measured by atomic force microscopy. Ultramicroscopy 109:937-941.
24. Hiratsuka, S., Y. Mizutani, A. Toda, N. Fukushima, K. Kawahara, H. Tokumoto, and T. Okajima. 2009. Power-law stress and creep relaxations of single cells measured by colloidal probe atomic force microscopy. Jpn. J. Appl. Phys. 48:08JB17-1-08JB17-4.
25. Miyaoka, A., Y. Mizutani, M. Tsuchiya, K. Kawahara, and T. Okajima. 2011. Rheological properties of growth-arrested fibroblast cells under serum starvation measured by atomic force microscopy. Jpn. J. Appl. Phys. 50:08LB16-1-08LB16-4.
26. Mizutani, Y., M. Tsuchiya, S. Hiratsuka, K. Kawahara, H. Tokumot, and T. Okajima. 2008. Elasticity of living cells on a microarray during the early stages of adhesion measured by atomic force microscopy. Jpn. J. Appl. Phys. 47:6177-6180.
27. Guck, J., S. Schinkinger, B. Lincoln, F. Wottawah, S. Ebert, M. Romeyke, D. Lenz,

H. M. Erickson, R. Ananthakrishnan, D. Mitchell, and J. Käs. 2005. Optical deformability as an inherent cell marker for testing malignant transformation and metastatic competence. Biophys. J. 88:3689-3698.

28. Sleep, J., D. Wilson, R. Simmons, and W. Gratzer. 1999. Elasticity of the red cell membrane and its relation to hemolytic disorders: an optical tweezers study. Biophys. J. 77:3085–3095.
29. Thoumine, O. and A. Ott. 1997. Comparison of the mechanical properties of normal and transformed fibroblasts. Biorheology 34:309–326.
30. Lau, A. W. C., B. D. Hoffman, A. Davies, J. C. Crocker, and T. C. Lubensky. 2003. Microrheology, stress fluctuations, and active behvior of living cells. Phys. Rev. Lett. 91:198101-1-198101-4.
31. Crocker, J. C., M. T. Valentine, E. R. Weeks, T. Gisler, P. D. Kaplan, A. G. Yodh, and D. A. Weitz. 2000. Two-point microrheology of inhomogeneous soft materials. Phys. Rev. Lett. 85:888-891.
32. Jonas, M., H. Huang, R. D. Kamm, and P. T. C. So. 2008. Fast fluorescence laser tracking microrheometry, I: Instrument development. Biophys. J. 94:1459-1469.
33. Butcher, D. T., T. Alliston, and V. M. Weaver. 2009. A tense situation: forcing tumor progression. Nature Rev. Cancer 9:108-122.
34. Suresh, S.. 2007. Elastic clues in cancer detection. Nature Nanotech. 2:748-749.
35. Cross, S. E., Y. S. Jin, J .Y. Rao, and J. K. Gimzewski. 2007. Nanomechanical analysis of cells from cancer patients. Nature Nanotech. 2:780-783.
36. Plodinec, M., M. Loparic, C. A. Monnier, and E. C. Obermann. 2012. The nanomechanical signature of breast cancer. Nature Nanotech. 7:757-765.
37. Yamada, S., D. Wirtz, and S. C. Kuo. 2000. Mechanics of living cells measured by

laser tracking microrheology. Biophys. J. 78:1736-1747.

38. Laudadio, R. E., E. J. Millet, B. Fabry, S. S. An, J. P. Butler, and J. J. Fredberg. 2005. Rat airway smooth muscle cell during actin modulation: rheology and glassy dynamics. Am. J. Physiol. Cell Physiol. 289:C1388-C1395.
39. Dahl, K. N., A. J. Engler, J. D. Pajerowski, and D. E. Discher. 2005. Power-law rheology of isolated nuclei with deformation mapping of nuclear substructures. Biophys. J. 89:2855-2864.
40. Desprat, N., A. Richert, J. Simeon, and A. Asnacios. 2005. Creep function of a single living cell. Biophys. J. 88:2224-2233.
41. Alcaraz, J., L. Buscemi, M. Grabulosa, X. Trepat, B. Fabry, R. Farre, and D. Navajas. 2003. Microrheology of human lung epithelial cells measured by atomic force microscopy. Biophys. J. 84:2071-2079.
42. Smith, B. A., B. Tolloczko, J. G. Martin, and P. Grutter. 2005. Probing the viscoelastic behavior of cultured airway smooth muscle cells with atomic force microscopy: stiffening induced by contractile agonist. Biophys. J. 88:2994-3007.
43. Roca-Cusachs, P., I. Almendros, R. Sunyer, N. Gavara, R. Farre, and D. Navajas. 2006. Rheology of passive and adhesion-activated neutrophils probed by atomic force microscopy. Biophys. J. 91:3508-3518.
44. Deng, L. H., X. Trepat, J. P. Butler, E. Millet, K. G. Morgan, D. A. Weitz, and J. J. Fredberg. 2006. Fast and slow dynamics of the cytoskeleton. Nat. Mater. 5:636-640.
45. Balland, M., N. Desprat, D. Icard, S. Fereol, A. Asnacios, J. Browaeys, S. Henon, and F. Gallet. 2006. Power laws in microrheology experiments on living cells: Comparative analysis and modeling. Phys. Rev. E Stat. Nonlin. Soft Matter Phys. 74:021911-1-021911-17.

46. Kollmannsberger, P. and B. Fabry. 2009. Active soft glassy rheology of adherent cells. Soft Matter 5:1771-1774.

47. Massiera, G., K. M. Van Citters, P. L. Biancaniello, and J. C. Crocker. 2007. Mechanics of single cells: rheology, time depndence, and fluctuations. Biophys. J. 93:3703-3713.

48. Hoffman, B., G. Massiera, K. M. V. Citters, and J. C. Crocker. 2006. The consensus mechanics of cultured mammalian cells. Proc. Natl. Acad. Sci. USA 103:10259-10264.

49. Maksym, G. N., B. Fabry, J. P. Butler, D. Navajs, D. J. Tshumperlin, J. D. Laporte, and J. J. Fredberg. 2000. Mechanical properties of cultured human airway smooth muscle cells from 0.05 to 0.4 Hz. J. Appl. Physiol. 89:1619-1632.

50. Puig-de-Morales, M., E. Millet, B. Fabry, D. Navajas, N. Wang, J. P. Butler, and J. J. Fredberg. 2004. Cytoskeletal mechanics in adherent human airway smooth muscle cells: probe specificity and scaling of protein-protein dynamics. Am. J. Physiol. Cell. Physiol. 287:C643-C654.

51. Hoffman, B. D. and J. C. Crocker. 2009. Cell mechanics: dissecting the physical responses of cells to force. Annu. Rev. Biomed. Eng. 11:259-288.

52. Park, C. Y., D. Tambe, A. M. Alencar, X. Trepat, E. H. Zhou, E. Millet, J. P. Butler, and J. J. Fredberg. 2010. Mapping the cytoskeletal prestress. Am. J. Physiol. Cell Physiol. 298:C1245-C1252.

53. Bursac, P., G. Lenormand, B. Fabry, M. Oliver, D. A. Weitz, V. Viasnoff, J. P. Butler, and J. J. Fredberg. 2005. Cytoskeletal remodelling and slow dynamics in the living cell. Nat. Mater. 4:557-561.

54. Bursac, P., B. Fabry, X. Trepat, G. Lenormad, J. P. Butler, N. Wang, J. J. Fredberg,

S. S. An. 2007. Cytoskeleton dynamics: fluctuations within the network. Biochem. Biopys. Res. Commun. 355:324-330.

55. Stamenovic, D., N. Rosenblatt, M. Montoya-Zavala, B. D. Matthews, S. H. Hu, B. Suki, N. Wang, and D. E. Ingber. 2007. Rheological behavior of living cells is timescale-dependent. Biophys. J. 93: L39-L41.
56. Chowdhury, F., S. Na, O. Collin, B. Tay, F. Li, T. Tanaka, D. E. Leckband, and N. Wang. 2008. Is cell rheoogy governed by nonequilibrium-to-equilibrium transition of noncovalent bonds? Biophy. J. 95:5719-5727.
57. Wang, N. and D. Stamenovic. 2002. Mechanics of vimentin intermediate filaments. J. Muscle Res. Cell Motil. 23:535-540.
58. Wang, N., K. Naruse, D. Stamenovic, J. J. Fredberg, S. M. Mijailovich, I. M. Tolic-Norrelykke, T. Polte, R. Mannix, and D. E. Ingber. 2001. Mechanical behavior in living cells consistent with the tensegrity model. Proc. Natl. Acad. Sci. 14:7765-7770.
59. Wang, N., I. M. Tolic-Norrelykke, J. X. Chen, S. M. Mijailovich, J. P. Butler, J. J. Fredberg, and D. Stamenovic. 2002. Cell prestress. I. Stiffness and prestress are closely associated in adherent contractile cells. Am. J. Physiol. Cell Physiol. 282:C606-C616.
60. Stamenovic, D. and D. E. Ingber. 2002. Models of cytoskletal mechanics of adherent cell. Biomech. Model. Mechanobiol. 1:95-108.
61. Trepat, X., M. Grabulosa, F. Puig, G. N. Maksym, D. Navajas, and R. Farre. 2004. Viscoelasticity of human alveolar epithelial cells subjected to stretch. Am. J. Physiol. –Lung cell. Mol. Physiol. 287:L1025-L1034.
62. Pourati, J., A. Maniotis, D. Spiegel, J. L. Schaffer, J. P. Butler, J. J. Fredberg, D. E.

Ingber, D. Stamenovic, and N. Wang. 1998. Is cytoskeletal tension a major determinant of cell deformability in adherent endothelial cells? Am. J. Physiol. 274: C1283-C1289.

63. Wang, N. and D. E. Ingber. 1994. Control of cytoskeletal mechanics by extracellular matrix, cell shape, and mechanical tension. Biophys. J. 66:2181-2189.
64. Bausch, A. R., F. Ziemann, A. A. Boulbitch, K. Jacobson, and E. Sackmann. 1998. Local measurements of viscoelastic parameters of adherent cell surfaces by magnetic bead microrheometry. Biophys. J. 75:2023-2049.
65. Laurent, V. M., R. Fodil, P. Canadas, S. Fereol, B. Louis, E. Planus, and D. Isabey. 2003. Partitioning of cortical and deep cytoskeleton responses from transient magnetic bead twisting. Ann. Biomed. Eng. 31:1263-1278.
66. Ingber, D. E.. 2003. Tensegrity. I. Cell structure and hierarchical systems biology. J. Cell Sci. 116:1157-1173.
67. Ingber, D. E.. 1993. Cellular tensegrity: defining new rules of biological design that govern the cytoskeleton. J. Cell Sci. 104:613-627.
68. Caspi, A., R. Granek, and M. Elabaum. 2000. Enhanced diffusion in active intracellular transport. Phys. Rev. Lett. 85:5655-5658.
69. Fredberg, J. J. and D. Stamenovic. 1989. On the imperfect elasticity of lung tissue. J. Appl. Physiol. 67:2408-2419.
70. Bouchaud, J.. 1992. Weak ergodicity breaking and aging in disordered systems. J. Phys. I (France) 2:1705-1713.
71. Mandadapu, K. K., S. Govindjee, and M. R. K. Mofrad. 2008. On the soft glassy rheology and sytoskeletal mechanics. J. Biomech. 41:1467-1478.
72. Mofrad, M. R. K.. 2009. Rheology of the cytoskeleton. Annu. Rev. Fluid Mech.

41:433-453.

73. Kasza, K. E., A. C. Rowat, J. Y. Liu, T. E. Angelini, C. P. Brangwynne, G. H. Koenderink, and D. A. Weitz. 2007. The cell as a material. Curr. Opin. Cell Biol. 19:101-107.

74. Fletcher, D. A. and D. Mullins. 2010. Cell mechanics and the cytoskeleton. Nature 463:485-492.

75. Heidemann, S. R. and D. Wirtz. 2004. Towards a regional approach to cell mechanics. Trends Cell Biol. 14:160-166.

Chapter 2: Experimental Principle

2.1 AFM

It has been shown in many experiments that the AFM can be used to both image living cells and study dynamic properties of living cells under physiological condition [1-13]. The AFM is usually built into an inverted optical microscope. The AFM providing the method for nanoindentations has advantages, such as adaptability to the liquid environment, ability to measure forces precisely in a localized region, and repeatability. However, the AFM technique has been challenged with the effects of the underlying substrate in the thin regions of the cell. Some progress has been achieved by modeling the commercial AFM tip as a polystyrene bead at the end of the AFM tip. A well-defined spherical probe allows us to model the mechanical behavior accurately by adopting suitable model.

2.1.1 Principle of AFM

In the AFM, the sample surface is scanned or probed by the cantilever tip by adding a force (Fig. 2.1). During scanning or probing, the force between the tip and the samples is measured by monitoring the deflection of the cantilever using the optical lever method [14,15]. A laser beam is reflected off the back side of the cantilever and detected using a segmented photodiode. The deflection is transformed into force according to the Hook's law using the spring constant of the cantilever. A topographic image of the sample is obtained by plotting the deflection of the cantilever versus its position on the sample at a fixed force. The maintenance of the force level can be achieved by using feedback electronics continuously correcting the vertical position of the cantilever as the input signal varies due to the change of topographic height. Apart from imaging purposes, the AFM is widely used to measure force as further interactions

between tip and sample. The force measurement can be used to investigate the properties of the sample.

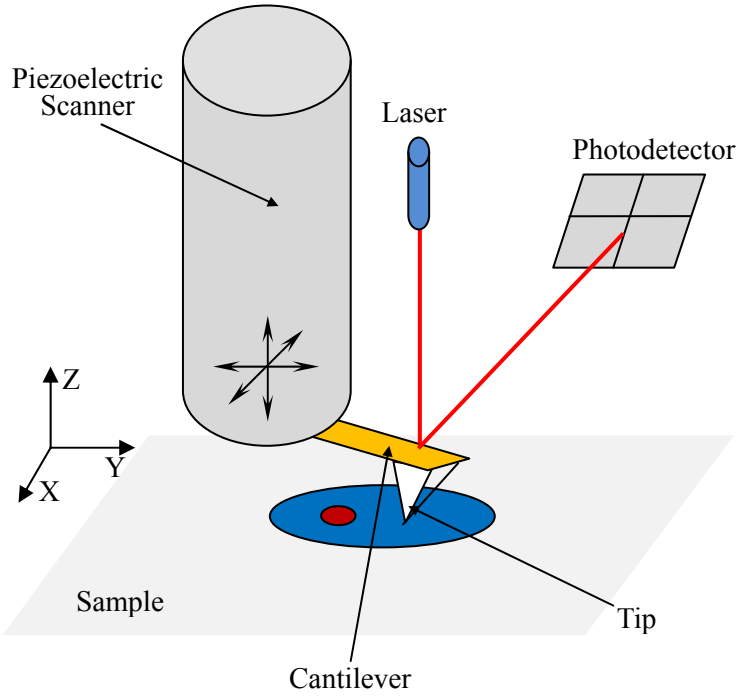

Figure 2.1 Schematic of an atomic force microscopy.

2.1.2 AFM force measurement for mechanical measurements

The AFM has high sensitivity of detecting forces ranging from tens of pNs to hundreds of nNs, which is the range involved in cell mechanics. The measurement of mechanical properties is realized by applying force on the cantilever in the vertical direction and monitoring the deflection of the cantilever tip. The vertical position of the tip and the defection of the cantilever are recorded and plotted as force-versus-distance curves, known as force-distance ($F - Z$) curves, or simply force curves (Fig. 2.2) [1,2]. Figure 2.2 shows the approaching and retracting curves obtained from living NIH3T3 cells under physiological condition by AFM. The information of the elastic and adhesion properties of the cell samples can be obtained by analyzing those approaching and the

retracting curves, respectively (Fig. 2.2). The common approach to obtain the elastic modulus (Young's modulus *E*) of living cells is described blow.

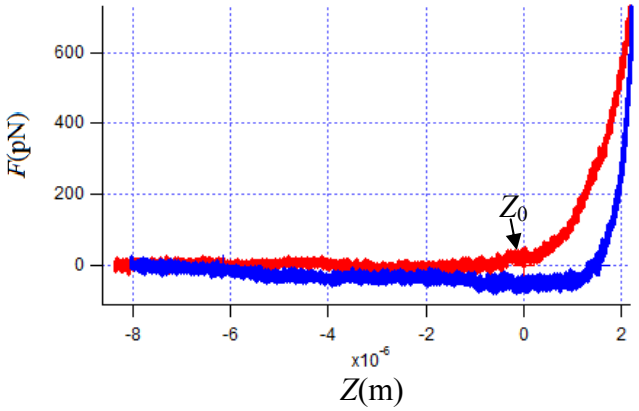

Figure 2.2 Force curve obtained from NIH3T3 cell by AFM in contact mode. Red and blue curves represent approaching and retracting curves, respectively. The tip of cantilever is artificial modified by polystyrene bead with spring constant 0.06 N/m. Z_0 represents the contact point.

2.1.3 Hertz model

The elastic deformation of the sample is related to its Young's modulus. The use of microspheres as cantilever tips allows the application of the simple 2-sphere Hertz contact model. In Hertz model, the adhesion of the sample is neglected. Hence, Hertz model can only be applied when the adhesion force is much smaller than the maximum load [14]. Firstly, the $F-Z$ curve is transformed into $F-\delta$ curve by computing the indentation δ of the tip into the sample. Under the compression by tip, the deflection of cantilever, *d*, is not proportional to the extension of cantilever, *Z*. The approaching curve is usually chosen to determine the contact point Z_0 in order to prevent from possible artifacts related to adhesion observed in the retracting curve. The contact point is Z_0 at which the cantilever starts to deflect (Fig. 2.2). The cell height can be evaluated

by determining and comparing the contact points obtained between the tip and the substrate and obtained between the tip and the cell surface. The difference between those two contact points is the cell height. Then, the indentation is obtained as $\delta = (Z - Z_0) - d$. The apparent Young's modulus E is determined by least squares fitting of the $F - \delta$ curve with small deformation as:

$$F = \frac{4R^{1/2}}{3(1-\nu^2)} E[(Z - Z_0) - d]^{3/2} = \frac{4R^{1/2}}{3(1-\nu^2)} E\delta^{3/2}, \quad (2.1)$$

Where ν is the Poisson ratio, assumed to be 0.5 and $1/R = 1/R_t + 1/R_s$, with R_t being the radius of the spherical cantilever tip and R_s being the radius of cell sample. Comparing to small indentation, R_s is usually assumed to infinite. Therefore, R_t is approximately used to calculate E instead of R. In the next, R is used to express the radius of the bead on the top of the cantilever.

2.1.4 AFM force modulation for cell rheology

Cell rheology is needed to describe the mechanical properties of such complex polymer system of cells in contrast to the static Young's modulus. Several researchers have measured the viscoelasticity of living cells by applying force steps for oscillations spanning a range of three frequency decades through monitoring the corresponding response as shown in Fig. 2.3 [2-4,7-13,16-18]. Therefore, the frequency-dependent viscoelastic behavior was obtained.

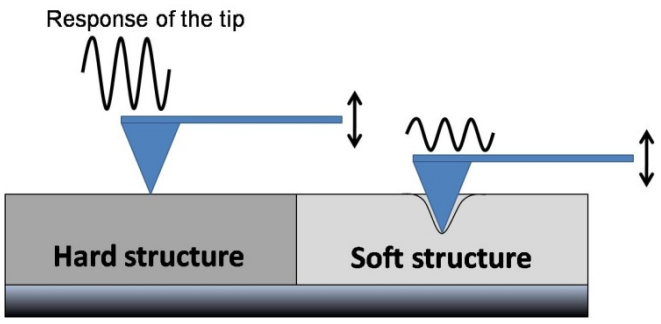

Figure 2.3 Schematic of force modulation to measure hard or soft structure of material.

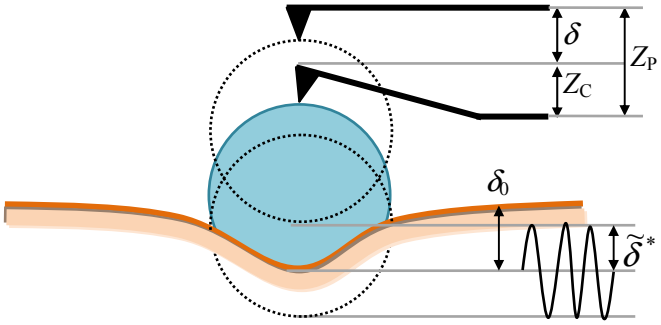

Figure 2.4 Schematic diagram representing a spherical AFM probe impacting sample surface. The indentation oscillation δ was calculated by subtracting the cantilever deflection, Z_C, from the cantilever piezo displacement, Z_P. The oscillating indentation, $\tilde{\delta}^*$, is superimposed on an offset indentation, δ_0.

The oscillatory technique used in AFM measurements on living cells consists in applying an oscillation introduced in the sample surface (drive oscillation) and then results in an oscillation of the cantilever resting on the sample surface with amplitude and phase differences that depend on the viscoelastic properties of the intervening sample (Figs. 2.3 and 2.4). In this case, the oscillating indentation, $\tilde{\delta}^*$, is superimposed on an offset indentation, δ_0, as shown in Fig. 2.4. $\tilde{\delta}^*$ is a complex as indicated by the asterisk. Thus, the corresponding total indentation, δ, is [17]

$$\delta = \delta_0 + \tilde{\delta}^* e^{i\omega t}, \tag{2.2}$$

where $\tilde{\delta}^*$ includes a real part and a imaginary part as $\tilde{\delta}^* = \delta' + i\delta''$ and ω is the frequency of driving oscillation. Under these conditions, the contact elastic Hertz model described by $F(\delta)$ can be approximated taking the first two terms of its Taylor expansion

$$F(\delta) = F(\delta_0) + \frac{\partial F}{\partial \delta}(\delta - \delta_0) + \cdots. \tag{2.3}$$

Inserting Eqs. 2.1 and 2.2 into Eq. 2.3, the loading force can be expressed as

$$F = \frac{4R^{1/2}}{3(1-\nu^2)}(E_0\delta_0^{3/2} + \frac{3}{2}E_1^*\delta_0^{1/2}\tilde{\delta}^*), \quad (2.4)$$

where E_0 is the Young's modulus at zero frequency obtained from the slow approach force curve. The frequency-dependent Young's modulus E_1^* is given by $2(1 + \nu)G^*$ [19]. While moving through a surrounding liquid, the probe is subject not only to the force applied to the cell, but also to a hydrodynamic drag forces F_d^* given by $F_d^*/\tilde{\delta}^* = ib(h)f$ [11,20], where $b(h)$ is a viscous drag factor that depends on the separation distance h between the cell surface and the probe [11,20]. Thus, G^* of cells is given by [11]:

$$G^* = G' + iG'' = \frac{1-\nu}{4(R\delta_0)^{1/2}}\left[\frac{F_1^*}{\tilde{\delta}^*} - ib(0)f\right], \quad (2.5)$$

where G' and G'' represent the storage and loss moduli of the cell, respectively, i is the imaginary unit, and $F_1^* = 2(R\delta)^{1/2}E_1^*\tilde{\delta}^*/(1-\nu^2)$. The value of $b(0)$ was determined by extrapolating value of $b(h)$ measured at various separation distance at f = 100 Hz.

2.1.5 Calculation method of G^* in the force modulation

Experimentally, the probe deforms the sample to a point δ_0 with a small additional oscillating signal $\tilde{\delta}^*$ and the cantilever responds with a phase-shifted signal ψ (Figs. 2.4 and 2.5). The changes in δ_0 were made extremely slow in comparison to the frequency of $\tilde{\delta}^*$, so δ_0 is essentially time independent. δ is calculated from the cantilever piezo displacement, Z_P, and the deflection of cantilever, Z_C as [17]

$$\delta = Z_P - Z_C. \quad (2.6)$$

The corresponding force is $F = KZ_C$, with the spring constant of the cantilever K. For the frequency-dependent modulus, the drive oscillation is added to the offset displacement. The exact displacement of Z-piezo and the deflection of cantilever are the

sum of the offset displacement and the added oscillation as (Fig. 2.4) [17]

$$Z_P = Z_0^p + \widetilde{Z}_p^* e^{iwt}, \tag{2.7}$$

$$Z_C = Z_0^c + \widetilde{Z}_c^* e^{iwt}, \tag{2.7′}$$

where Z_0^p is the offset displacement of the *Z*-piezo and Z_0^c is the offset displacement of the cantilever after the contact is made between the tip and the sample, thus there have the relations $Z_0^p = Z - Z_0$, $Z_0^c = d$ and $\delta_0 = Z_0^p - Z_0^c$ (see Section 2.1.3). Owing to the viscous properties of the sample, the oscillatory cantilever deflection, $\widetilde{Z}_c^*$, includes a phase factor, ψ, that differs from the oscillatory *Z*-piezo, $\widetilde{Z}_p^*$, as (Fig. 2.5) [17]

$$\widetilde{Z}_p^* e^{i\omega t} = A_{drive} e^{i\omega t}, \tag{2.8}$$

$$\widetilde{Z}_c^* e^{i\omega t} = A_{res}(\cos\psi - i\sin\psi) e^{i\omega t}, \tag{2.8′}$$

where A_{drive} is the amplitude of the oscillatory *Z*-piezo deflection and A_{res} is the amplitude of the oscillatory cantilever deflection. A_{drive} and A_{res} are monitored and obtained by a lock-in amplifier as driving signal and resulting (response) signal. Therefore, the oscillating indentation $\widetilde{\delta}^*$ equals $\widetilde{Z}_p^* - \widetilde{Z}_c^*$.

Inserting Eqs. 2.8 and 2.8′ into Eq. 2.5, the complex shear modulus can be obtained by the driving signal A_{drive} and the response signal A_{res} as

$$G^*(f) = \frac{1-\nu}{4(R\delta_0)^{1/2}} \left[\frac{KA_{res}(\cos\psi + i\sin\psi)}{A_{drive} - A_{res}(\cos\psi + i\sin\psi)} - ib(0)f \right], \tag{2.9}$$

where $b(0)$ is determined as described in Section 2.1.4, R is the radius of the microbead attached on the tip of cantilever.

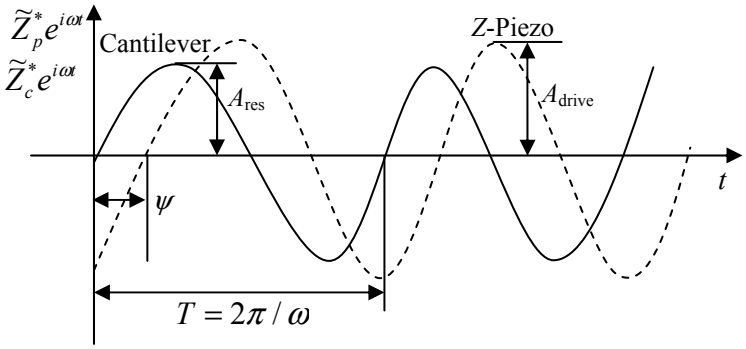

Figure 2.5 Schematic of the phase shift ψ between the driving signal $\tilde{Z}_p^* e^{i\omega t}$ of *Z*-piezo (dash line) and the response signal $\tilde{Z}_c^* e^{i\omega t}$ of cantilever (solid line).

2.2 Experimental Procedures

2.2.1 Microarray

A commercial cell microarray (LiveCell Array; Nunc, Penfield, NY) is used to culture cells. It comprises a hexagonal structure of microwells with a hexagonal shape and a width of 20 μm and depth of 8 μm fabricated on a glass substrate (Fig. 2.6).

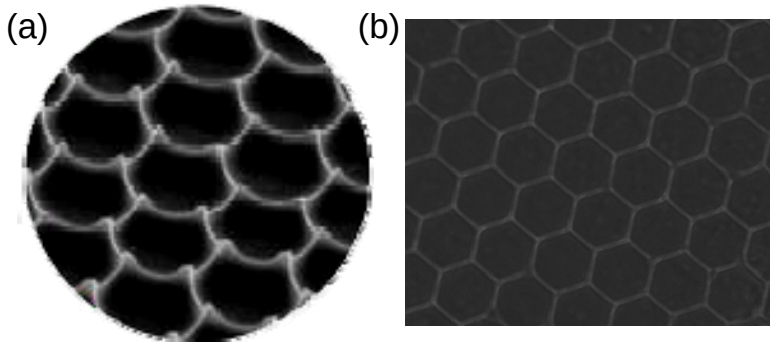

Figure 2.6 Imaging of microarray wells taken by scanning electron microscopy (a) and by microscopy (b).

2.2.2 Cell sample

Mouse fibroblast NIH3T3 cells (ATCC) were cultured at 37 °C and 5% CO_2 atmosphere

for 1–2 d in Dulbecco's modified Eagle's medium DMEM (Sigma-Aldrich, St. Louis, MO) containing penicillin (100 units/mL), streptomycin (100 mg/mL) (Sigma-Aldrich) and 10% fetal bovine serum (FBS; HyClone, Logan, UT). After suspension with trypsin (Sigma-Aldrich), cells were deposited in microarray wells, percolated with fibronectin (BD Biosciences, San Jose, CA), in complete medium (DMEM containing FBS) and immediately incubated for ca. 12 h under the same condition as described above. The cells were washed with CO_2-independent medium (Invitrogen, Carlsbad, CA), placed in the same medium and immediately used for AFM experiments.

2.2.3 Immunofluorescence observation

To visualize the nuclei and the actin filaments inside the cells, the staining was done as the procedure described blow [10]. Firstly, the medium was removed from cultured vessel, and then the cells were fixed with 4% formalin in phosphate buffed saline (PBS; PH 7.2) for 30 min. After that, cells were rinsed three times with PBS, permeabilized in 0.01% Triton X-100 for 10 min, and rinsed three times with PBS. Next, rhodamine-phalloidin (Molecular Probes) in PBS was added for the actin filaments staining and the cells were incubated for 1 h at 37 °C. Excess dye was removed by rinsing the cells three times with PBS. Finally, VECTASHIELD® mounting medium containing DAPI (Vector Laboratories) was used to prevent rapid photobleaching and to stain the nuclei.

In the experiment, the immunofluorescence imaging of the nuclei and the actin filaments was performed by a confocal optical microscope (DIGITAL ECLIPSE C1; Nikon, Tokyo, Japan).

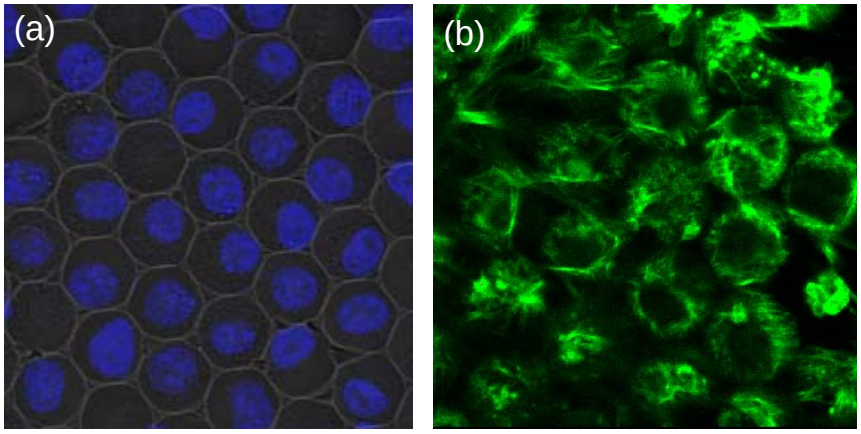

Figure 2.7 Fluorescence image of nuclei (a) and actin filaments (b) of NIH3T3 cells deposited in the wells of the microarray. After the Cells were cultured in the microarray for 12 h, the cells were tagged by staining their nuclei with DAPI and actin filaments with phalloidin.

Figure 2.7 shows the fluorescence image of the nuclei and the actin filaments cultured in the wells of microarray. I observed that cells were well cultured in the wells of the microarray with no detachment from the substrate and overlapping of nuclei through confirmed by changing the focal plane of the microscope in the Z-direction. The results revealed that the microarray was useful for retaining and culturing cells in the wells without loss of their adhesive function. The filling rate of cells in the wells was estimated to be > 98% from a fluorescence image of the nuclei on a large scale [Fig. 2.7 (a)]. Moreover, the structure of actin filaments was clearly visible in Fig. 2.7 (b). The configuration of the actin filaments was high restricted by the wells of the microarray.

To confirm the configuration of cells in the microarray, I statistically analyzed the distribution of the diameter and position of nuclei in the microarray wells. Figure 2.8 (a) shows the schematic diagram of a single cell with a nucleus diameter of D μm placed in a microarray well where the two boundaries of the well were coordinated as the x-axis from 0 to $10\sqrt{3}$ μm. The distribution of the position of cell nuclei to the wells was shown in Fig. 2.8 (b), and the average value was 8.8 μm in the x-axis and the deviation

was 2.9 μm. The results indicate that most of the cells fluctuated around the centers of wells. Furthermore, the average diameter of nucleus is 10.7 μm as shown in the distribution of *D* [Fig. 2.8 (c)].

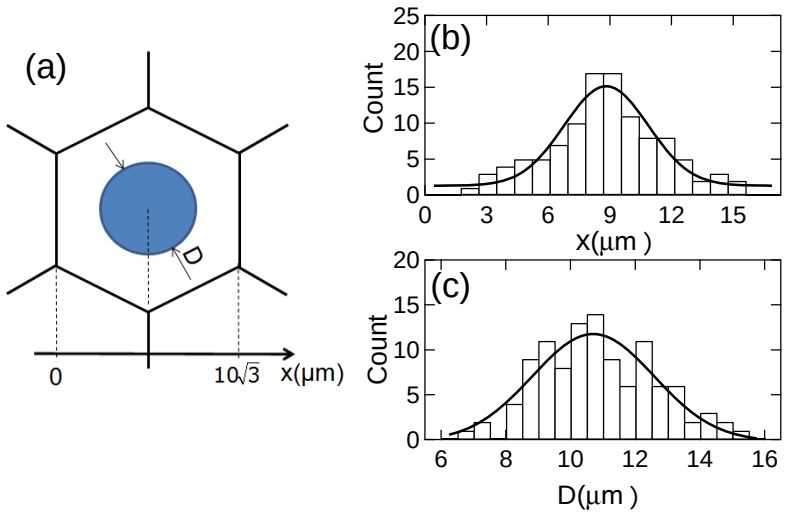

Figure 2.8 (a) Schematic of the cell nucleus in the well. The *x*-axis represents the relative positions between two boundaries of the well. (b) A histogram showing the distribution of the center of cell nuclei in the wells. (c) A histogram showing the distribution of the diameter of the cell nuclei.

In order to investigate the effect of actin filaments modification on cell rheology, cytochalasin D (cytoD) (Sigma-Aldrich) is used to disrupt the actin filaments in which cytoD inhibits actin filament polymerization. The effect of cytoD on actin filaments polymerization has been confirmed by comparing fluorescence images between untreated (control) and cytoD treated cells (Fig. 2.9). Figure 2.9 (a) showed the highly organized structure of actin filaments for control cell. After 20 min treatment with cytoD, the actin filaments were disrupted and scattered inside the cell [Fig. 2.9 (b)]. The results confirmed that cytoD could be used to modify the actin filaments structure in the cell rheological measurement.

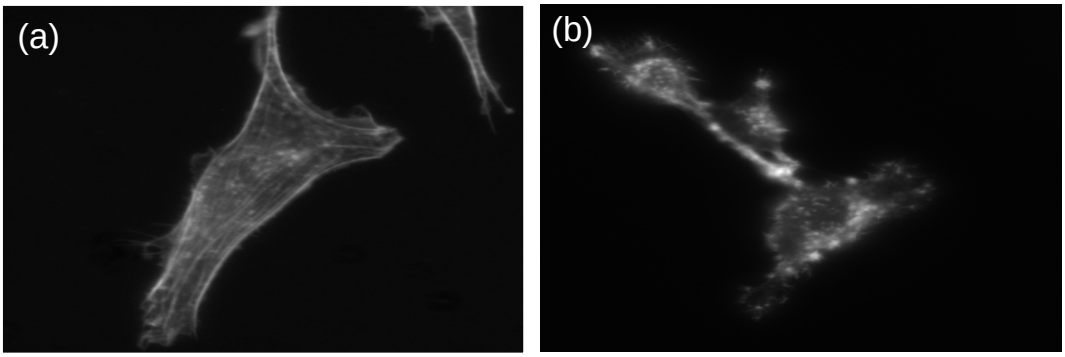

Figure 2.9 Fluorescence images of actin filaments for control cell (a) and cytoD-treated cell with 20 min (b).

2.2.4 Measurements of cell rheology by AFM

A commercial AFM (MFP-3D AFM; Asylum Research, Santa Barbara, CA) mounted in an inverted optical microscope (TE-2000E; Nikon, Tokyo, Japan) was employed to examine the rheological properties of NIH3T3 cells (Fig. 2.10). A small rectangular cantilever (BL-AC40TS; Olympus, Tokyo, Japan) with a nominal spring constant of less than 0.1 N/m was used. A colloidal silica bead with a radius, R, of ca. 2.5 μm (Funakoshi, Tokyo, Japan) was attached to the apex of the AFM tip using epoxy glue to measure the mechanics of single cell with well-defined contact geometry [7,9-10,21]. Prior to cell experiments, the spring constant of the cantilever was determined using the thermal fluctuation method built in the AFM. The loading force was determined by multiplying the calibrated cantilever spring constant by its deflection on the basis of Hooke's law.

The force modulation measurements were examined by indenting cells in the wells for 30–40 s at an initial loading force of less than 650 pN, which corresponded to the indentation of around 1 μm in the present cell samples. During the indentation, a reference signal of sinusoidal oscillation with an amplitude of 10 nm and several

frequencies in the range of f ~ 2–200 Hz was added to Z-piezo for moving the cantilever vertically. The amplitude and phase shift of the cantilever displacement with respect to the reference signal were measured using an external digital lock-in amplifier (7260, SEIKO EG&G Co, Tokyo, Japan) with a time constant of ~0.5 s. The amplitude and phase responses of the instrument including mechanics and electronics whose resonance was higher than the frequencies applied to cells were calibrated at different frequencies using a stiff cantilever in contact with a clean glass coverslip in air, and cell measurements were corrected accordingly.

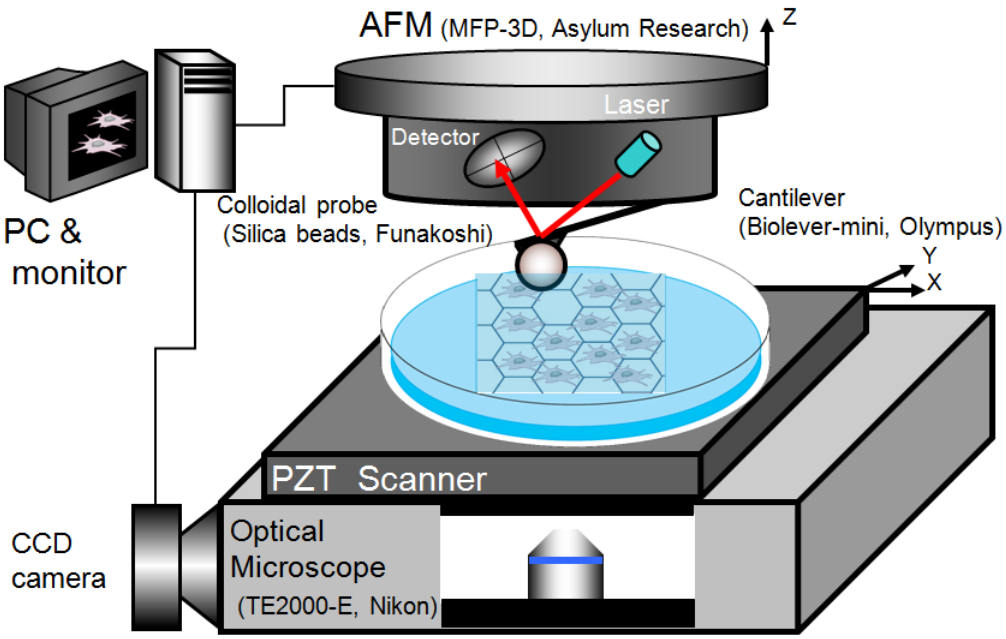

Figure 2.10 Experimental setup of the AFM force modulation with a microarray substrate used to obtain the viscoelastic data. Living cells were arranged and cultured in the microarray wells.

2.3 Data Analysis

The data are visualized under Igor Pro software (WaveMetrics, Lake Oswego, OR). In the first stage, the phase shift and amplitude of cantilever from the experiment are collected. Subsequent stages for rheological analysis are necessarily specific to the

applied force protocol. The collected AFM data are analyzed using the Igor Pro software with a built-in global fitting procedure. The G' and G'' were calculated by Eq. 2.9 for different frequencies. Then the G' and G'' as a function of f were fitted to the power-law structural damping model with additional Newtonian viscosity by Eq. 1.1.

The standard deviation σ_X of quantity X with normal Gaussian is expressed by

$$\sigma_X = \left[\frac{1}{n-1} \sum_{i=1}^{n} \left(X_i - \langle X \rangle \right)^2 \right]^{1/2}, \tag{2.10}$$

where n is the number of data, X_i, which is the i-th data, and $\langle X \rangle$ is arithmetic mean of X. Hereafter, $\overline{X}$ is denoted as the geometric mean of X. Student's t-test and Pearson correlation were used to estimate the significant differences of the parameters of the power-law rheology, and the correlation between G^*'s for different conditions, respectively.

2.4 References

1. Rotsch, C. and M. Radmacher. 2000. Drug-induced changes of cytoskeletal structure and mechanics in fibroblasts: an atomic force microscopy study. Biophys. J. 78:520-535.
2. Smith, B. A., B. Tolloczko, J. G. Martin, and P. Grutter. 2005. Probing the viscoelastic behavior of cultured airway smooth muscle cells with atomic force microscopy: stiffening induced by contractile agonist. Biophys. J. 88:2994-3007.
3. Van Citters K. M., B. D. Hoffman, G. Massiera, and J. C. Crocker. 2006. The role of F-Actin and myosin in epithelial cell rheology. Biophys. J. 91:3946-3956.
4. Radmacher, M., R. W. Tillamnn, M. Fritz, and H. E. Gaub. 1992. From molecules to cells: imaging soft samples with the atomic force microscope. Science 257:1900-1905.
5. Henderson, E., P. G. Haydon, and D. S. Sakaguchi. 1992. Actin filament dynamics in living glial cells imaged by atomic force microscopy. Science 257:1944-1946.
6. Tao, N. J., S. M. Lindsay, and S. Lees. 1992. Measuring the microelastic properties of biological-material. Biophys. J. 63:1165-1169.
7. Hiratsuka, S., Y. Mizutani, M. Tsuchiya, K. Kawahara, H. Tokumoto, and T. Okajima. 2009. The number distribution of complex shear modulus of single cells measured by atomic force microscopy. Ultramicroscopy 109:937-941.
8. Hiratsuka, S., Y. Mizutani, A. Toda, N. Fukushima, K. Kawahara, H. Tokumoto, and T. Okajima. 2009. Power-law stress and creep relaxations of single cells measured by colloidal probe atomic force microscopy. Jpn. J. Appl. Phys. 48:08JB17-1-08JB17-4.
9. Miyaoka, A., Y. Mizutani, M. Tsuchiya, K. Kawahara, and T. Okajima. 2011.

Rheological properties of growth-arrested fibroblast cells under serum starvation measured by atomic force microscopy. Jpn. J. Appl. Phys. 50:08LB16-1-08LB16-4.

10. Mizutani, Y., M. Tsuchiya, S. Hiratsuka, K. Kawahara, H. Tokumot, and T. Okajima. 2008. Elasticity of living cells on a microarray during the early stages of adhesion measured by atomic force microscopy. Jpn. J. Appl. Phys. 47:6177-6180.
11. Alcaraz, J., L. Buscemi, M. Grabulosa, X. Trepat, B. Fabry, R. Farre, and D. Navajas. 2003. Microrheology of human lung epithelial cells measured by atomic force microscopy. Biophys. J. 84:2071-2079.
12. Smith, B. A., B. Tolloczko, J. G. Martin, and P. Grutter. 2005. Probing the viscoelastic behavior of cultured airway smooth muscle cells with atomic force microscopy: stiffening induced by contractile agonist. Biophys. J. 88:2994-3007.
13. Roca-Cusachs, P., I. Almendros, R. Sunyer, N. Gavara, R. Farre, and D. Navajas. 2006. Rheology of passive and adhesion-activated neutrophils probed by atomic force microscopy. Biophys. J. 91:3508-3518.
14. Butt, H. J., B. Cappella, and M. Kappl. 2005. Force measurements with the atomic force microscope: technique, interpretation and applications. Surf. Sci. Rep. 59:1-152.
15. Hansma, P. K., B. Drake, D. Grigg, C. B. Prater, F. Yashar, G. Gurley, S. V. Eling, S. Feinstein, and R. Lal. 1994. A new, optical-lever based atomic-force microscope. J. Appl. Phys. 76:796–799.
16. Roca-Causachs, P., I. Almendros, R. Sunyer, N. Gavara, R. Farré, and D. Navajsa. 2006. Rheology of passive and adhesion-activated neutrophils probed by atomic force microscopy. Biophys. J. 91:3508-3518.
17. Mahaffy, R. E., S. Park, E. Gerde, J. Käs, and C. K. Shih. 2004. Quantitative

analysis of the viscoelastic properties of thin regions of fibroblasts using atomic force microscopy. Biophys. J. 86:1777-1793.

18. Mahaffy, R. E., C. K. Shih, F. C. MacKintosh, and J. Käs. 2000. Scanning probe-based frequency-dependent microrheology of polymer gels and biological cells. Phys. Rev. Lett. 85:880-883.
19. Landau, L. and E. M. Lifshitz. 1986. Theory of elasticity. Pergamon Press, Oxford.
20. Alcaraz, J., L. Buscemi, M. Puig-de-Morales, J. Colchero, A. Baró, and D. Navajs. 2002. Correction of microrheological measurements of soft samples with atomic force microscopy for the hydrodynamic drag on the cantilever. Langmuir. 18:716-721.
21. Ducker, W. A., T. J. Senden, and R. M. Pashley. 1991. Direct measurement of colloidal forces using an atomic force microscope. Nature 353:239-241.

Chapter 3: Quantifying Cell-to-Cell Variation in Power-Law Rheology

Among individual cells of the same source and type, the complex shear modulus G^* exhibits a large log-normal distribution. However, it has not quantified the frequency-dependent properties of cell-to-cell variation in cell rheology. It is important for the statistical evaluation of pharmacological treatments and the comparison of different cell states. In this chapter, the frequency-dependent properties of cell-to-cell variation were investigated with the modifications of the spatial location within the cells and the actin filaments structure, by mechanically probing fibroblasts arranged on a microarray via AFM. The results showed that the standard deviation σ of G^* was significantly reduced among cells in which actin filaments were depolymerized and also exhibited a subcellular spatial dependence. Based on the findings regarding the frequency dependence of σ of the storage modulus G', the two types of cell-to-cell variation in G' were proposed in which one arises from the purely elastic component and the other is the frequency-dependent component in terms of the soft glassy rheology model of cell deformability. It is concluded that the frequency-dependent component of the cell-to-cell variation can be reduced greatly by disrupting actin networks, by probing at locations within the cell nucleus boundaries distant from the cell center, and by measuring at high loading frequencies.

3.1 Introduction

The living cell is a compliant, viscoelastic material with a highly dynamic cytoskeleton (CSK) that is continuously remodeling [1-4]. The rheological properties of adherent cells are mainly attributed to the CSK and are related to various cell functions [5-9]. Studies have revealed that rheological parameters as the creep compliance and the complex shear modulus, G^*, which were measured at arbitrarily positions of cells and/or spatially averaged, follow single [10-24] or multiple [25-29] power-law behaviors over multiple decades around 10 Hz (see Section 1.3).

On the other hand, the inherently heterogeneous CSK structure results in spatial variation in cell elasticity [30,31] and rheology [32] measurements (see Section 1.3). Park *et al.* [33] investigated the local heterogeneity of the ensemble-averaged shear modulus G^* by measuring a large number of single cells that were cultured on micropatterned substrates. Using a single power-law rheology model [15,16,34], they showed that in addition to the stiffness, the power-law exponent and the Newtonian viscosity also depend on the choice of subcellular region probed [33]. Moreover, previous studies have revealed universal features of cell-to-cell variation in cell rheology: the number (ensemble) distribution of G^* exhibits a log-normal distribution, whereas the power-law exponent exhibits a normal, or Gaussian, distribution [23-26,35]. Furthermore, the distribution of G^* narrows as the frequency increases [35]. Phenomenological models to explain such a log-normal distribution and/or a frequency-dependent distribution have been proposed [23,36], but the frequency-dependent cell-to-cell variation in cell rheology remains poorly understood.

To address these questions, the ensemble distribution of G^* versus frequency f was investigated by using AFM-enabled loading of individual mouse fibroblast cells

arranged on a microarray substrate [35,37]. Actin filament structures were found to play a strong role in changing the frequency dependence of the ensemble distribution of G^*. Moreover, the standard deviation of the log-normal distribution varied depending on the measurement location on the cells. The frequency-dependent component of the cell-to-cell variation of the cell samples observed by AFM was discussed in terms of power-law rheology.

3.2 Materials and Methods

3.2.1 Cell samples

Detailed preparation procedures for cells arranged on a microarray substrate have been described in Section 2.2.2. Briefly, mouse fibroblast NIH3T3 cells (ATCC) were deposited in hexagonal microarray wells (LiveCell Array^{TM}; Nunc), and were immediately incubated for 12 h in complete medium (Dulbecco's modified Eagle's medium containing fetal bovine serum). For AFM measurements, the medium was replaced with a CO_2-independent medium (Invitrogen). A fluorescence image of the nuclei of NIH3T3 cells observed with a confocal optical microscope (DIGITAL ECLIPSE C1; Nikon, Tokyo, Japan) is shown in Fig. 3.1 (a). By staining nuclei with DAPI, the average nucleus diameter was 10.7 μm and that the center of the nucleus fluctuated from the center of the well with a standard deviation of 2.9 μm (see Fig. 2.8).

3.2.2 Measurements of cell rheology by AFM

An AFM (MFP-3D AFM; Asylum Research) was used to measure the complex shear modulus of NIH3T3 cells [Fig. 3.1 (b)]. Detailed measurement procedures of AFM force modulation for cell rheology have been described in Section 2.2.4. To achieve a well-defined contact geometry, a colloidal silica bead with a radius R of ~2.5 μm (Funakoshi) was attached to the apex of the AFM tip with epoxy [35,37,38]. Cells in the

microarray wells were indented for ~30 s at an initial loading force < 650 pN. The cantilever was then driven to oscillate with about 10 nm in amplitude at 2, 5, 10, 25, 50, 100 and 180 (or 200) Hz, in a stepwise fashion, while the amplitude and phase shift of the cantilever displacement were measured with a digital lock-in amplifier (7260; Seiko EG&G).

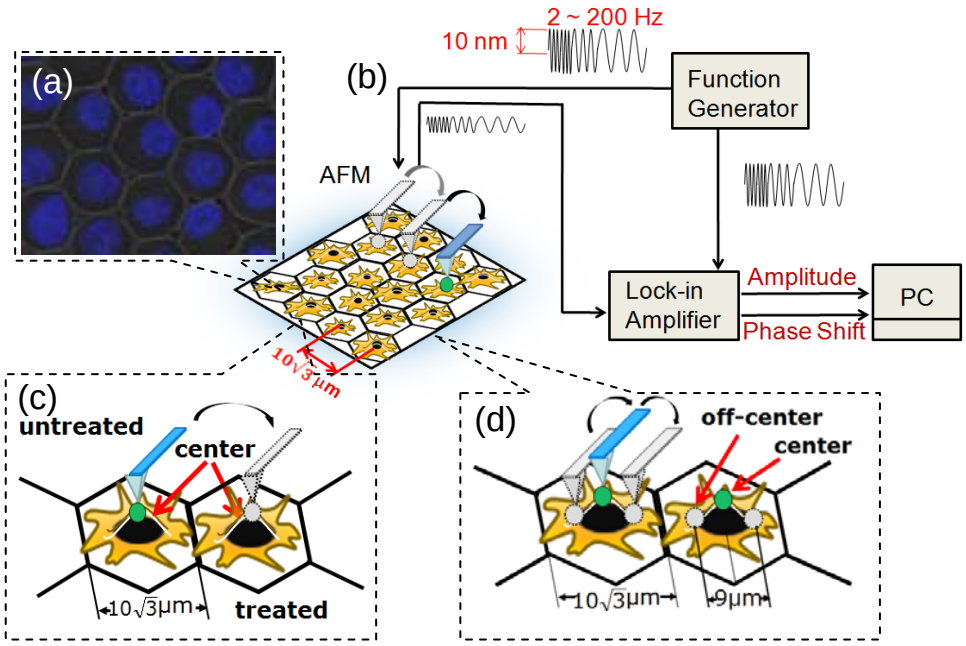

Figure 3.1 (a) Fluorescence image of nuclei of NIH3T3 cells deposited in microarray wells and cultured for 12 h using confocal microscopy. The cell nuclei were stained with DAPI. (b) Schematic of the AFM force modulation with a microarray substrate, on which living cells were arranged and cultured. (c) Measurements of the effect of cytoD on the G^* of cells. The untreated cells were measured at the center of wells and the same cells treated with cytoD were measured again at the same location. (d) Measurements of the spatial dependence of G^* of cells at different locations of the center and away from the center of wells.

To investigate the effects of cytochalasin D (cytoD) (Sigma-Aldrich) on cell rheology, which inhibits actin filaments polymerization, single cells were measured at the center of wells (essentially atop the nuclei), incubated in 2-μM cytoD for 20 min, and

measured again [Fig. 3.1 (c)]. The fluorescence image of actin filaments structure of control and cytoD-treated cells was shown in Fig. 2.9. To investigate the spatial dependence of cell rheology parameters, measurements were performed at the center and 4.5 μm from the center of wells for the same cells [Fig. 3.1 (d)]. The off-center position was closer to the periphery of the cell nucleus but still within the nucleus boundaries for most cells (see Fig. 2.8).

The complex shear modulus G^* is given by the Hertzian contact model [20,39-42] with a viscous drag factor F_d^* (see Section 2.1.4) [40,43]. The phase shift observed in the frequency range of 2–200 Hz mainly resulted from the mechanical response of AFM head and thus was calibrated at different frequencies using a stiff cantilever in contact with a clean glass cover slip in air.

3.2.2 Data analysis

AFM data were analyzed using the Igor Pro software (WaveMetrics, Lake Oswego, OR) with a built-in global fitting procedure. G' and G'' as a function of f were fitted to the power-law structural damping model with additional Newtonian viscosity (see Section 2.3) [15,16,34]. The parameters in power-law structural damping model are α with being the power-law exponent, G_0 with being a scale factor of the modulus at a scale factor of frequency f_0 (~1 Hz), and μ with being the Newtonian viscous damping coefficient. The standard deviations of G', G'', and the power-law parameters of the structural damping model were calculated by Eq. 2.10. Student's t-test was used to test statistically significant differences in the parameters of the structural damping model, and Pearson's correlation coefficient was used to characterize the correlation between G^* values measured at different subcellular locations.

3.3 Results

3.3.1 Influence of actin filaments

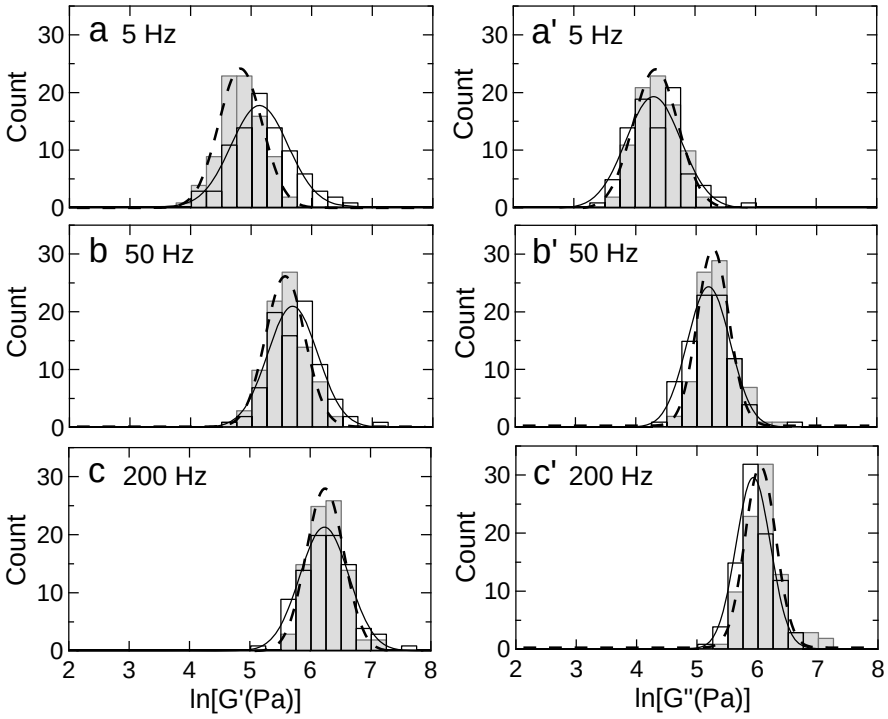

Figure 3.2 Distributions of the storage G' (left) and loss G'' (right) moduli of untreated cells (white, n = 87) and cytoD-treated cells (gray, n = 87) in microarray wells at different frequencies: (a) 5, (b) 50 and (c) 200 Hz. The solid and dashed lines represent the fitted results of untreated and treated cells, respectively, using a log-normal distribution function.

The stiffness of attached cells measured by AFM is strongly associated with the cytoskeletal actin network organization [30,31], which is spatially heterogeneous and changes over time. Therefore, G^* of cells was measured after actin filament polymerization was disrupted by cytoD (2-μM). Figure 3.2 shows the ensemble distribution of G^* of the treated and untreated cells measured at the center of wells by AFM at different frequencies. It is noted four observations. First, G^* consistently exhibited a log-normal distribution. Second, the geometric mean of G^* shifted to higher values with increasing f. Third, the distributions of G' became narrower with f,

and the distributions of G'' were narrower than those of G'. These features are consistent with those observed in previous studies [15,16,21-26,35]. Fourth, the distribution of G^* of the treated cells was narrower than that of the untreated cells.

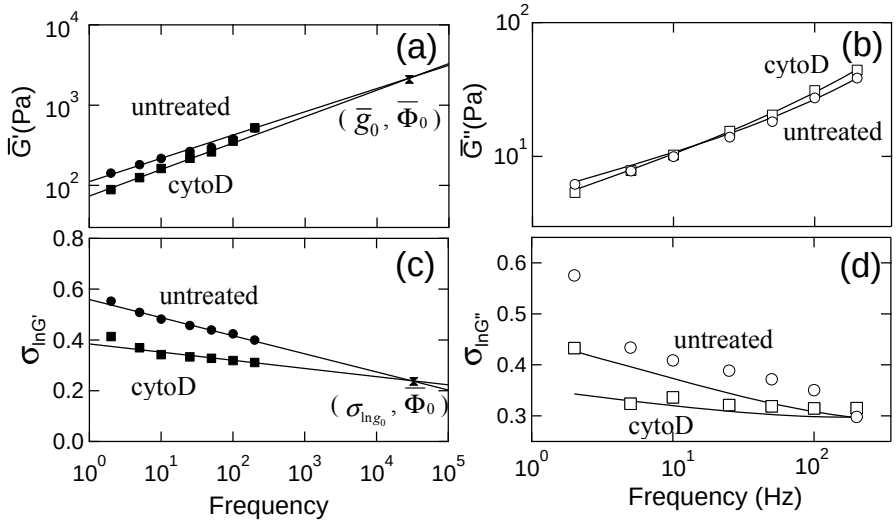

Figure 3.3 Frequency dependences of $\bar{G}^*$ [$\bar{G}'$ (a) and $\bar{G}''$ (b)] of untreated (circle) and treated (square) cells. Solid lines in (a) and (b) represent the fitted results to Eq. 1.1. The point where the curves of $\bar{G}'$ intersect is defined as $\bar{G}' = \bar{g}_0$ at $f = \bar{\Phi}_0$. Frequency dependence of $\sigma_{\ln G'}$ (c) and $\sigma_{\ln G''}$ (d) of untreated (circle) and treated (square) cells. Solid lines in (c) and (d) represent the fitted results using Eqs. 3.3 and A18, respectively (see Discussion). See Fig. A7 for fitted results of G' for each of single cells.

To clarify the effect of cytoD on G^*, I plotted the ensemble average $\bar{G}^*$ and the standard deviation of G^* distribution, $\sigma_{\ln G^*}$, versus frequency f (Fig. 3.3). As shown in Fig. 3.3 (a) and (b), $\bar{G}^*$ increased with f and closely followed the structural damping equation (Eq. 1.1). The disruption of actin filament polymerization resulted in a decrease in $\bar{G}_0$ by ~50% ($p < 10^{-5}$) and an increase in the average power-law exponent $\langle\alpha\rangle$ from 0.32 to 0.37 ($p < 10^{-5}$), which were similar behaviors to those

reported in previous studies [15-18]. As shown in Fig. 3.3 (a), the point at which the extrapolated lines of $\bar{G}'$ for the treated and untreated cells intersect was defined as $\bar{G}' = \bar{g}_0$ at $f = \bar{\Phi}_0$ [15,16].

	center		untreated	
	untreated (n = 87)	cytoD (n = 87)	center (n = 160)	off-center (n = 160)
$\bar{G}_0$ (Pa) [a]	95.58	51.41	54.60	66.02
$\langle\alpha\rangle$ [a]	0.32	0.37	0.29	0.28
$\bar{\mu}$ (Pa·s) [a]	0.75	0.70	0.62	0.64
$\sigma_{\ln G_0}$ [a]	0.62	0.41	0.82	0.72
σ_{α} [a]	0.08	0.05	0.09	0.08
$\sigma_{\ln \mu}$ [a]	0.65	0.61	0.59	0.41
$\bar{\Phi}_0$ (Hz) [b,c]	3.20×10^4	3.20×10^4	1.12×10^4	1.12×10^4
$\sigma_{\ln g_0}$ [c]	$0.24^{0.03}$	$0.24^{0.03}$	$0.38^{0.08}$	$0.38^{0.08}$
σ_{α} [c]	$0.031^{0.002}$	$0.014^{0.002}$	$0.042^{0.003}$	$0.029^{0.003}$
$\sigma_{\ln \mu}$ [c]	$0.35^{0.12}$	$0.37^{0.08}$	$0.62^{0.04}$	$0.44^{0.04}$

Table 3.1 Power-law rheological parameters (mean ± SD) of two kinds of cell experiments such as (1) untreated and cytoD-treated cells and (2) cells measured at the center and off-center of microarray wells. [a] represents estimates using Eq. 1.1, [b] represents estimates from the plot of ln $\bar{G}'$ vs. ln*f*, and [c] represents estimates from the plot of $\sigma_{\ln G^*}$ vs. ln*f*.

Figure 3.4 shows the ensemble distributions of the parameters of the power-law rheology of untreated and cytoD-treated cells, estimated from Eq. 1.1. G_0 displayed a log-normal behavior with a distribution that was narrower after cytoD treatment. Measurements of the power-law exponent α exhibited a Gaussian distribution that also became narrower after cytoD treatment, whereas μ exhibited a log-normal distribution (see Fig. A1), and its mean value did not change significantly ($p = 0.71$) after treatment.

The standard deviations of these parameters are listed in Table 3.1.

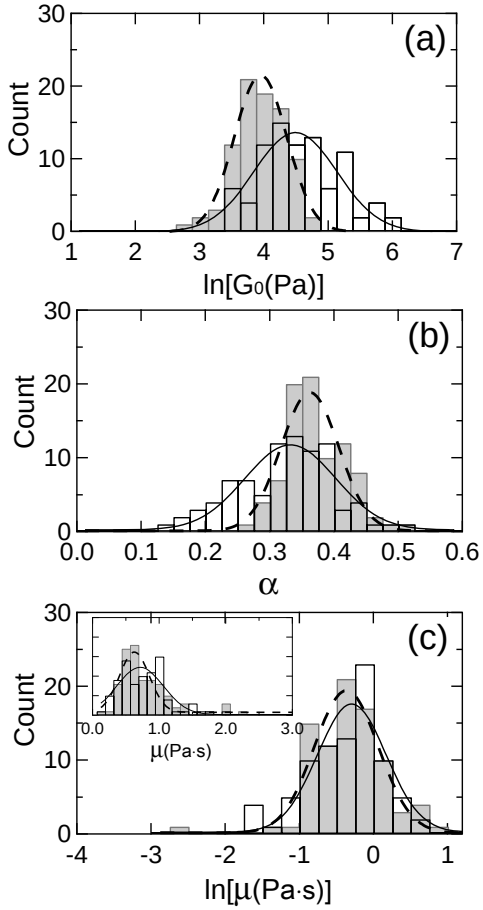

Figure 3.4 Distributions of (a) G_0 on a logarithmic scale, (b) α on a linear scale and (c) μ on a logarithmic scale of untreated (white) and treated (gray) cells. Inset in (c) shows the distribution of μ on a linear scale. Solid and dashed lines represent the fitted results of untreated and treated cells, respectively, using a log-normal distribution function (a and c) and to a normal distribution function (b and inset in c).

The standard deviation of the complex modulus $\sigma_{\ln G^*}$ was reduced in the treated cells [Fig. 3.3 (c) and (d)], and the reduction was larger than that expected from the change in $\ln \bar{G}^*$ (see Fig. A2). Moreover, $\sigma_{\ln G^*}$ of the treated cells was smaller than that of the untreated cells when both $\sigma_{\ln G^*}$ values were evaluated at the same $\bar{G}^*$ values but different frequencies [see Fig. A2 (a) and (b)]. The results indicate a strong

coupling between cell-to-cell variation and the cytoskeletal actin organization of cells.

3.3.2 Spatial dependence

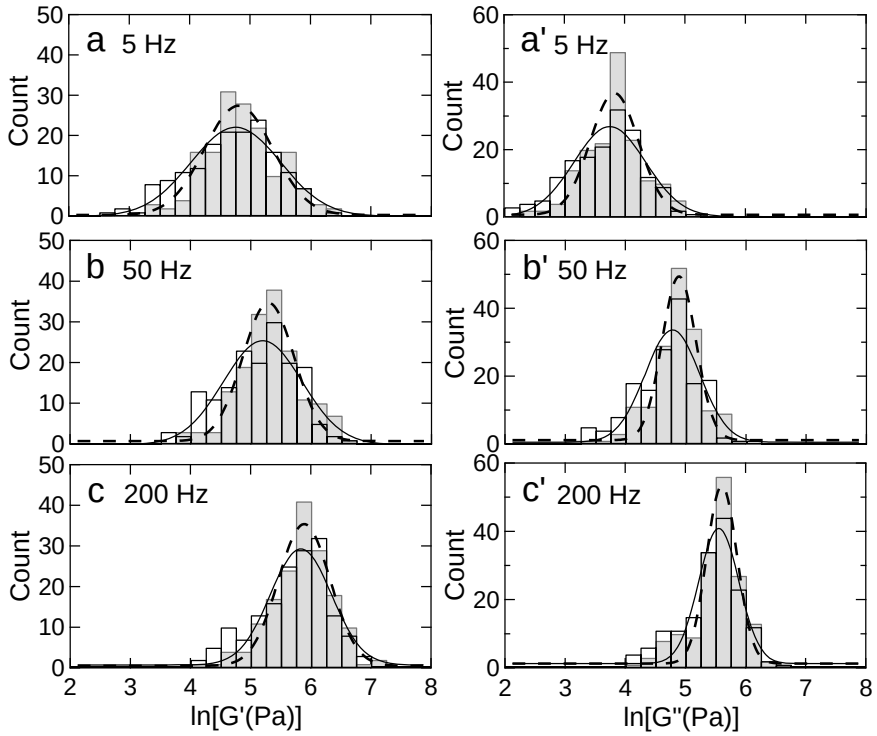

Figure 3.5 Distributions of G' (left) and G'' (right) moduli of cells measured at center (white, n = 160) and off-center (gray, n = 160) locations of microarray wells at different frequencies: (a) 5, (b) 50 and (c) 200 Hz. Solid and dashed lines represent fitted results of cells measured at center and off-center locations, respectively, using a log-normal distribution function.

Next, the ensemble distribution of cell rheology parameters was characterized at two different locations on the cells: the center and 4.5 μm away from the center of each microarray well. Measurement at both locations enables a comparison of mechanical response directly atop the cell nuclei with that measured toward the nuclear perimeter (see Methods in Section 3.2). Figure 3.5 shows the distribution of G^* for these two subcellular locations (center and off-center) at different frequencies. These distributions featured the same characteristic features as those observed in untreated and treated cells (see Fig. 3.2).

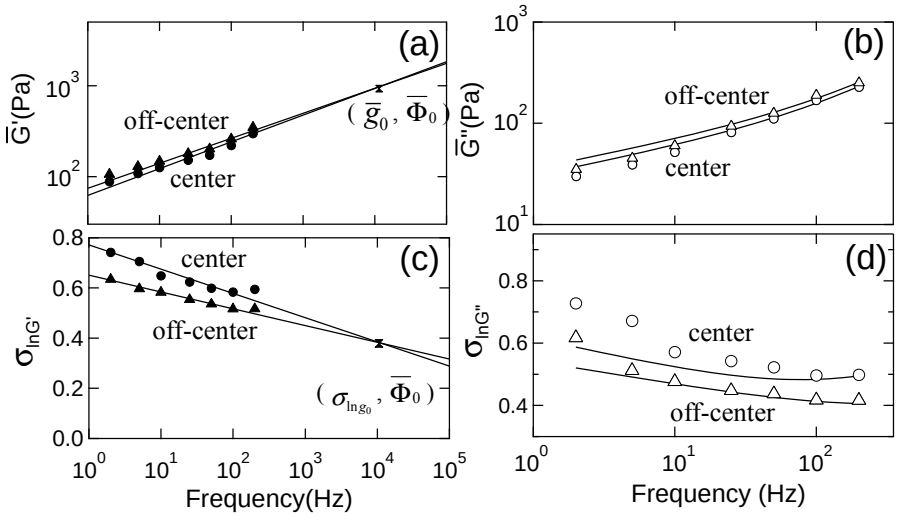

Figure 3.6 Frequency dependences of $\bar{G}^*$ [$\bar{G}'$ (a) and $\bar{G}''$ (b)] of cells measured at center (circle) and off-center (triangle) locations of wells. Solid lines in (a) and (b) represent the fitted results to Eq. 1.1. The point where the curves of $\bar{G}'$ intersect is defined as $\bar{G}' = \bar{g}_0$ at $f = \bar{\Phi}_0$. Frequency dependences of $\sigma_{\ln G'}$ (c) and $\sigma_{\ln G''}$ (d) of cells measured at center (circle) and off-center (triangle) locations of wells. Solid lines in (c) and (d) represent the fitted results using Eqs. 3.3 and A18, respectively (see Discussion in Section 3.4)

To quantify the distributions of G^*, $\bar{G}^*$ and $\sigma_{\ln G^*}$ is plotted as a function of f in Fig. 3.6. The $\bar{G}^*$ values, which fitted well to the model described in Eq. 1.1 [Fig. 3.6 (a) and (b)], did not differ considerably between center and off-center locations. However, for all frequencies considered, the distribution of G^* measured at off-center locations was remarkably narrower than that measured at the well center [Fig. 3.6 (c) and (d)]. Indeed, plotting $\sigma_{\ln G^*}$ vs. $\ln \bar{G}^*$ showed that $\sigma_{\ln G^*}$ for cells measured at the off-center location was smaller than that at the center for the same $\bar{G}^*$ values [see Fig. A3 (c) and (d)]. These results suggest that differences in rheological response among individual cells are reduced when mechanical loading occurs at locations beyond the cell center.

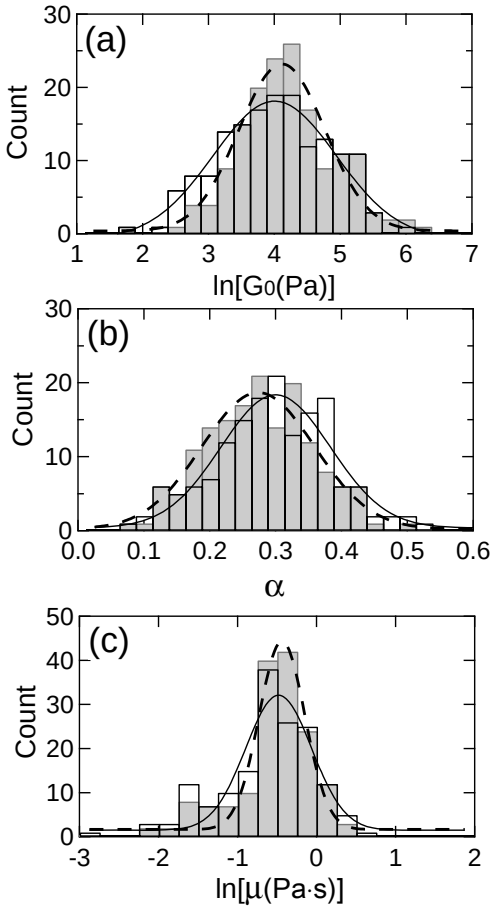

Figure 3.7 Distributions of (a) lnG_0, (b) α and (c) lnμ of cells measured at center (white) and off-center (gray) locations of wells. Solid and dashed lines represent the fitted results of cells measured at center and off-center locations, respectively, using a log-normal distribution function (a and c) and a normal distribution function (b).

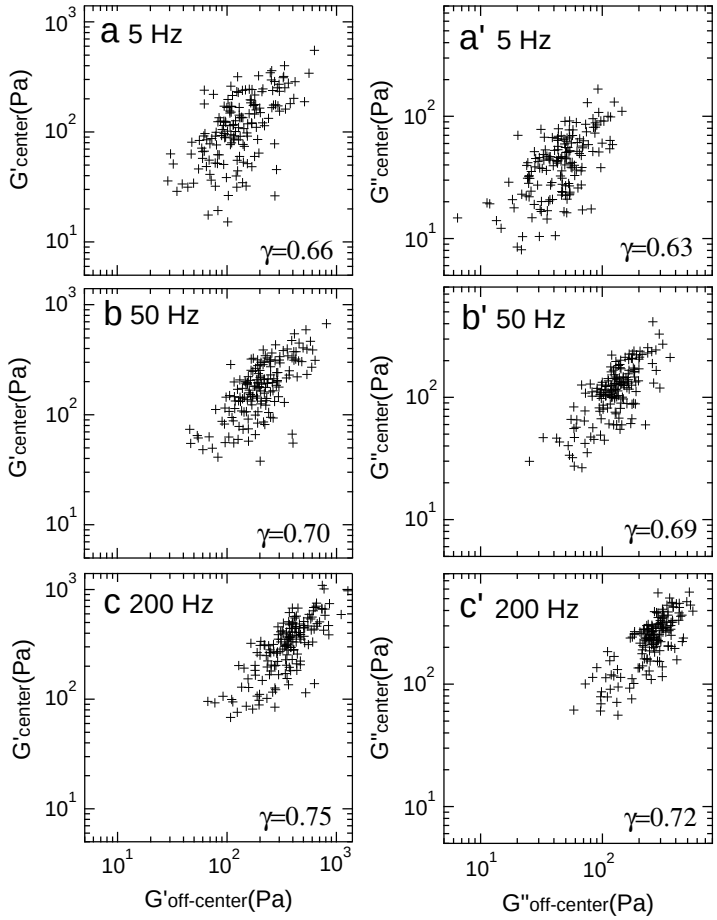

Figure 3.8 G' measured at the center of wells, G'_{center}, vs. G' measured away from the center of wells, $G'_{\text{off-center}}$ (left) and G'' measured at the center of wells, G''_{center}, vs. G'' measured away from the center of wells, $G''_{\text{off-center}}$ (right), at different frequencies: (a) 5, (b) 50 and (c) 200 Hz. The data are the same as those shown in Figs. 3.5–3.7.

Figure 3.7 shows the ensemble distributions of the parameters of the power-law rheology of cells, estimated from Eq. 1.1, at different subcellular locations. The shape of the distributions was unchanged, regardless of cell location; that is, G_0 and μ displayed a log-normal distribution, whereas α exhibited a Gaussian distribution. Moreover, on every distribution of $\ln G_0$, α and $\ln\mu$, the standard deviation measured at the center of wells was broader when compared with the corresponding value off-center (Table 3.1). Measurements of $\ln G_0$ were different between cells measured at the center and away

from the center of wells (p = 0.026), consistent with previous reports [30,31,33,44], which showed that cell stiffness measured near the nucleus was relatively low and gradually increased toward the peripheral regions. Conversely, I found no such obvious difference for $\ln\mu$ (p = 0.17) or α (p = 0.042). The results imply that cells have a similar fluidity, intermediate between elastic solids and viscous liquids [10-14], even in different subcellular locations within the nucleus boundaries.

Figure 3.8 shows the relation between G^* of cells measured at the center and away from the center of wells at different frequencies by replotting the data shown in Fig. 3.5. It was found that G^* of the cells measured at the center of wells were proportional to the corresponding magnitudes at the off-center, indicating that this intracellular rheological parameter, measured at different subcellular locations, is spatially correlated.

3.4 Discussion

3.4.1 Power-law rheology models

It has been commonly recognized that G' exhibits single power-law behavior in the range of 10^0-10^2 Hz. On the other hand, G' in other frequency ranges is still controversial, and there are mainly three types of power-law rheology models that have been proposed, i.e., one single [15,16] and two multiple [26,29] power-law rheology models. Fabry *et al.* [15,16] reported that regardless of the treatments applied to cells, $\bar{G}'$ of the cells as a function of f followed single power-law function in the frequency region of 10^{-2}-10^3 Hz and appeared to cross at $\bar{G}' = \bar{g}_0$ at a high frequency $f = \bar{\Phi}_0$. The behaviors have been observed in various types of cells and in different measurement techniques [15-17,45].

In the case of this study, $\bar{G}'$ was measured in only two decades of frequency range, i.e., 10^0-10^2 Hz. Nevertheless, as shown below, I found that the single power-law rheology model, which has the smallest number of fitting (rheological) parameters in power-law rheology models mentioned previously, allowed us to explain the frequency dependence of $\sigma_{\ln G'}$ and to quantify the cell-to-cell variations, which was invariant in different cell samples prepared under the same conditions.

3.4.2 Standard deviation of lnG'

A crucial problem to estimate the cell-to-cell variation from the experimental results is that the magnitude of $\sigma_{\ln G'}$ is largely varied in different sets of experiments. Namely, the magnitude of $\sigma_{\ln G'}$ is quite different for two different pairs of conditions (Fig. 3.3 showing the effects of cytoD, and Fig. 3.6 showing the effects of subcellular measurement location), even though the control conditions in both sets of experiments (untreated, in the well center) were ostensibly identical. This suggests that the parameter $\sigma_{\ln G'}$ observed experimentally in Figs. 3.3 (c) and 3.6 (c), is not an exact invariant quantity, and can vary with challenges to the cell. Therefore, I concluded that $\sigma_{\ln G'}$ obtained in the present AFM study contains experimental variation such as instrumental noise and day-to-day influences under in vitro culture that I cannot control and explain.

To quantify the cell-to-cell variation in different sets of experiments under the same conditions, I derive the relationship among fitting parameters of single power-law rheology model. I express G' for each cell as

$$G' = g_0\left(\frac{f}{\Phi_0}\right)^{\alpha}, \tag{3.1}$$

where Φ_0 of each cell can be estimated by extrapolating the G' vs. f curves measured under one pair of two conditions. Both sets of data, plotted on a log-log scale, form lines

that intersect at a point specified by (Φ_0, g_0) that varies considerably (see Fig. A4), showing that cells exhibit global mechanical variation that can be conceptualized to correspond to the variation in depth of the potential energy well that a cytoskeletal element must overcome to escape the glass transition, according to soft glassy rheology (SGR) [10-12]. Averaged over all cells, $\bar{g}_0$ and $\bar{\Phi}_0$ is obtained (Table 3.1).

The linear relation between lnG_0 and α for each cell is then given by (see Eq. A6)

$$\ln G_0 = \ln \bar{g}_0 - \left[\ln\left(\frac{\bar{\Phi}_0}{f_0}\right) + \frac{d \ln g(\alpha)}{d\alpha} \right] \alpha , \tag{3.2}$$

where ln$g(\alpha)$ is reasonably assumed to be approximately linear to α [see Fig. A6 (a)]. In Fig. 3.9 (a), I replot lnG_0 vs. α, measured at the center and off-center locations of wells, which are presented in Figs. 3.5-3.7. The result fits well to Eq. 3.2 with $\bar{g}_0$ and $\bar{\Phi}_0$. Moreover, the plot of lnG_0 vs. lnμ suggests a linear relationship [Fig. 3.9 (b)].

Thus, $\sigma_{\ln G'}$ of cells from Eq. 1.1 (or Eq. 3.1) can be expressed as (see Eq. A15)

$$\sigma_{\ln G'} = \sigma_{\ln g_0} + \left(\ln \bar{\Phi}_0 - \ln f\right) \sigma_\alpha , \tag{3.3}$$

showing that $\sigma_{\ln G'}$ is proportional to ln$f$ with a slope of $-\sigma_\alpha$ at $f < \bar{\Phi}_0$ [36], and that the variation, from all sources, in these cells' mechanical response is characterized by $\sigma_{\ln g_0}$ at $f = \bar{\Phi}_0$. Interestingly, I fitted $\sigma_{\ln G'}$ shown in Figs. 3.3 and 3.6 to Eq. 3.3 and found that the curves of $\sigma_{\ln G'}$ under one pair of two conditions can be crossed at the point $(\bar{\Phi}_0, \sigma_{\ln g_0})$ (Table 3.1).

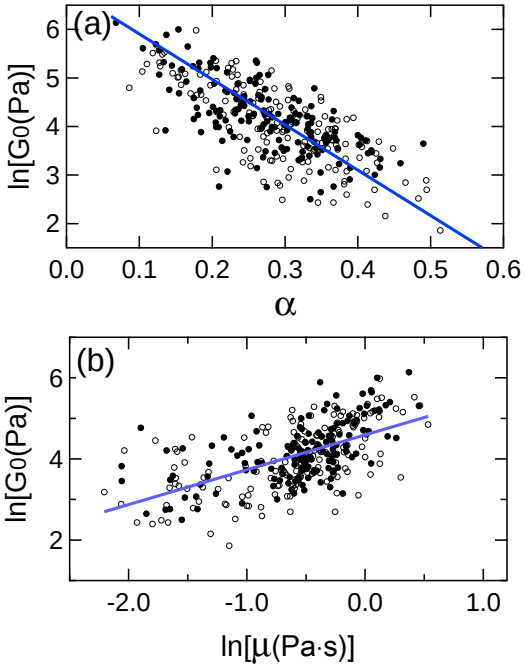

Figure 3.9 Plots of lnG_0 vs. α (a) and lnG_0 vs. lnμ (b) of cells measured at center (open circle) and off-center (closed circle) locations of cells, which are shown in Figs. 3.5–3.7. The solid lines in (a) and (b) represent the fitted results using Eq. 3.2 and a linear function, respectively.

Figure 3.10 shows $\tilde{\sigma}_{\ln G'}$, which is defined as $\sigma_{\ln G'} - \sigma_{\ln g_0}$, as a function of f estimated from Figs. 3.3 (c) and 3.6 (c). Importantly, the values of $\tilde{\sigma}_{\ln G'}$ for cells from control conditions in different experiments (i.e., untreated and measured at the center of wells in each experimental pairwise comparison) were similar even in different pairs of experimental conditions (e.g., control conditions in Figs. 3.3 and 3.6). Moreover, it was found that the features of $\tilde{\sigma}_{\ln G'}$ with f remained even after the definition of the standard deviation was changed from $\sigma_{\ln G'}$ to $\tilde{\sigma}_{\ln G'}$, i.e., (1) $\tilde{\sigma}_{\ln G'}$ of cells treated with cytoD was largely reduced compared with that of the control cells [see Fig. A3 (c)]; and (2) $\tilde{\sigma}_{\ln G'}$ away from the center of wells was smaller than the corresponding value at the center. Therefore, the frequency dependence of $\tilde{\sigma}_{\ln G'}$ apparently varies

with the integrity of the actin network, and the cell-to-cell mechanical variation exhibits a spatial dependence. The frequency-dependent component of the cell-to-cell variation of G' in the frequency domain was schematically shown in Fig. 3.11.

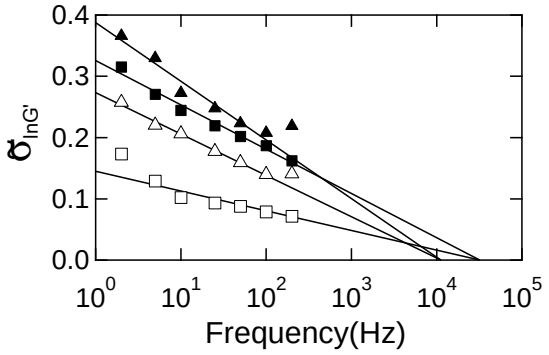

Figure 3.10 $\sigma_{\ln G'}$, which represents $\sigma_{\ln G'} - \sigma_{\ln g_0}$ as a function of ln$f$. The results obtained from two cell samples shown in Fig. 3.3 (c) and in Fig. 3.6 (c) are replotted: One sample is untreated (closed rectangle) and treated (open rectangle) cells measured at the center of wells, whereas the other is untreated cells measured at the center (closed triangle) and away from the center (open triangle) of wells. Solid lines represent the fitted results using Eq. 3.3.

The parameter $\sigma_{\ln G''}$ could not be analytically solved based on the power-law rheology model, and thus a first-order approximate formula of $\sigma_{\ln G''}$ was derived from Eq. 1.1 (details of deriving the formula of $\sigma_{\ln G''}$ are given in Eq. A19). We can see in Figs. 3.3 (d) and 3.6 (d) that Eq. A19 is semi-quantitatively valid for the observed $\sigma_{\ln G''}$; however, Eq. A19 remains only an approximation for this parameter.

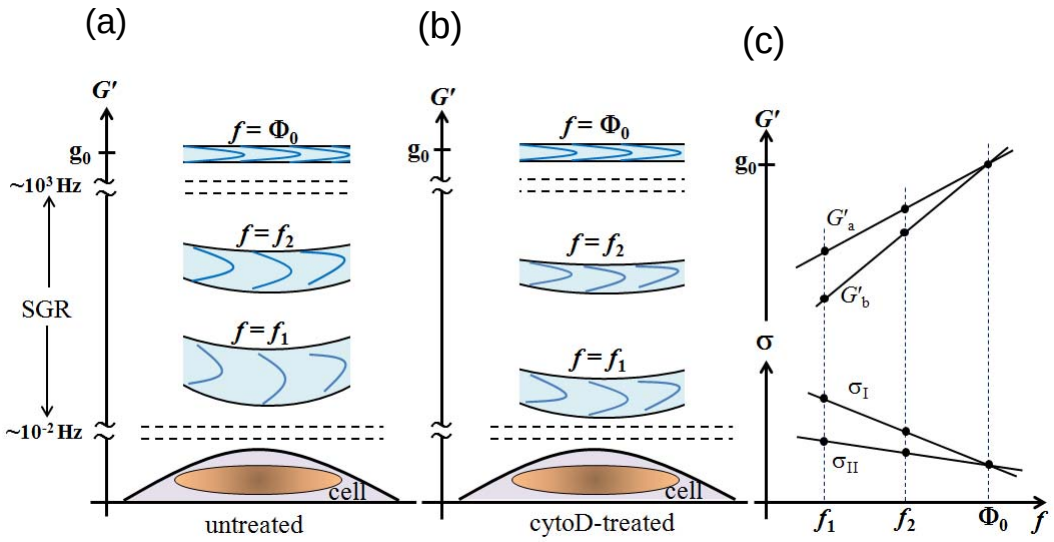

Figure 3.11 Schematic of G' of untreated cells (a) and cytoD-treated cells (b) at different frequencies. The cell-to-cell variation of G' varies depending on intracellular locations: the distribution narrows when changing from cell center to cell nucleus boundaries. The spatial component of cell-to-cell variation of G' between the untreated and treated cells decreases with increasing f, and consequently both cells become spatially homogeneous at $f = \bar{\Phi}_0$ beyond the SGR region (see Eq. 3.3), but the cell-to-cell variation still exists at $f = \bar{\Phi}_0$. The spatial variation of G' for the untreated cells in the SGR region is larger than that for the treated cells. One experimental condition is that G'_a (σ_{II}) and G'_b (σ_I) represent the values measured at off-center and center locations, respectively, while the other G'_a (σ_I) and G'_b (σ_{II}) are those of the untreated and treated cells, respectively (c).

3.4.3 Standard deviation of α

I observed that the σ_α values estimated from the slope of $\sigma_{\ln G'}$ in Figs. 3.3 (c) and 3.6 (c) were smaller than those obtained from the distribution of α shown in Figs. 3.4 (b) and 3.7 (b) (Table 3.1). This finding indicated that σ_α values' estimated from the frequency dependence of G^* in each cell group with Eq. 1.1 contain a substantial fitting error in addition to the frequency-dependent component of the cell-to-cell variation.

It is noted that $\sigma_{\ln G'}$ values measured under one pair of two conditions were

different even at the same value of $\overline{G}'$ (see Fig. A4), suggesting that the $\sigma_{\ln G'}$ value is not simply governed by the magnitude of $\overline{G}'$. The $\sigma_{\ln G'}$ as a function of $\ln \overline{G}'$ (Eq. A21) is also expressed as:

$$\sigma_{\ln G'} = \sigma_{\ln g_0} + \frac{\sigma_\alpha}{\langle \alpha \rangle} (\ln \overline{g}_0 - \ln \overline{G}'), \tag{3.4}$$

showing that $\sigma_{\ln G'}$ decreases with increasing $\ln \overline{G}'$ with a slope of $\sigma_\alpha / \langle \alpha \rangle$. The value of $\sigma_\alpha / \langle \alpha \rangle$ was 0.11 and 0.035 for the untreated and treated cells, respectively, although it is 0.15 and 0.11 for cells measured at center and off-center locations of the wells, respectively (Table 3.1). Using these values, I found that the plots of $\sigma_{\ln G'}$ vs. $\ln \overline{G}'$ fitted well to Eq. 3.4 [see Fig. A4 (a) and (c)]. Therefore, $\sigma_\alpha / \langle \alpha \rangle$ is interpreted as a measure of the variation in mechanical response of cell groups with the same $\ln \overline{G}'$ measured in different conditions.

In SGR, the power-law exponent of G' is related to the transition probability between the potential wells, i.e., the transition rate decreases with the decreasing exponent [10-12]. In the molecular points of view, the SGR elements and the energy wells can be identified with myosin motors and the binding energies between myosin and actin, respectively [12]. This model suggests that the depolymerization of actin filaments by cytoD leads to the reduction of the actin-myosin interactions and the enhancement of the spatial homogeneity of the interactions.

3.4.4 Sources of experimental uncertainty

It is noted that there are still at least three main sources of experimental uncertainty in this study. The first is the imperfection of call sample preparation, in which the cells are not perfectly centered within each well, so the exact location of the nucleus center and

perimeter vary correspondingly. To understand how such cell preparations influence the observed distribution of G', let us assume an ideal condition in which the subcellular mechanical heterogeneity of each cell measured by AFM is identical and fixed according to Fig. 3.11. When these identical cells are deposited with randomized locations of the cell center within the microarray wells, we must inevitably observe a distribution of G^* of cells in which variation arises due to the fluctuation of cell positions in the wells. It is noted that the distribution in G' for cells measured at the center is relatively large compared with corresponding distribution in G' away from the center because the spatial heterogeneities within cells increase toward the cell center [Fig. 3.11 (a)]. Moreover, the distribution width is reduced when cells are treated with cytoD because the spatial heterogeneity of treated cells is smaller than that of untreated ones [Fig. 3.11 (b)].

The second is the cell-cell contact of the cell sample. Cells on microwells have almost the same size and shape, which allows us to compare measurements at the same position between different cells, and to blindly touch down the AFM tip and still know exactly where I have probed the cell. This tremendously speeds up the measurements as we no longer need to visually search for cells. On the other hand, cells in the microarrays form cell-cell contacts on all six intersecting sides, and therefore I expect the cells to have both physical and chemical interactions, and furthermore I expect that these contacts influence cell-mechanical properties and their distributions (compared with isolated nonconfluent cells). It has been reported in a previous study [29] on human airway smooth muscle cells that cell-cell contacts play only a minor role. However, in most other studies of single cell rheology, cell-cell contacts are usually not well controlled or characterized, and thus the relationship between single cell rheology

and cell rheology in a sheet of cells is not well understood.

The third is related to the AFM experimental method, in which the AFM probe indents the cells by applying an initial force. This causes a change in the indentation depth among cells measured by AFM because the depth depends on the cell stiffness. It is known that the AFM is capable of detecting the mechanical properties of highly tensed deep cytoskeleton such as stress fibers, rather than the flexible cortical cytoskeleton [30,31]. Rheological measurements of cells depend to some degree on the complex modulus as a function of cell depth, which is not identical among the measured cells.

3.4.5 Variation in measured rheological properties of cells

Several techniques have been employed to measure the rheological properties of single cells. Previous studies have revealed that the value of α was in the range of 0.1–0.4, regardless of the techniques employed [10-13]. The results presented in Fig. 3.6 are in agreement with these previous results in which α is relatively insensitive to the subcellular measurement position. On the other hand, the mean G_0 value was dependent on the measurement position (Table 3.1). It has been reported that cell stiffness – as measured by AFM in terms of the apparent Young's modulus, which is related to G_0 (see Fig. A7) – is a useful indicator to distinguish normal and abnormal cells [46,47]. The results suggest that the precise control of the measurement position of cells is crucial to obtain clear correlations between the rheological properties and the biological states of the adherent cells.

3.5 Conclusions

The cell-to-cell variation in rheological parameters measured via AFM oscillatory loading was quantified as a standard deviation, $\tilde{\sigma}_{\ln G'}$, in which the contribution of the

variation at a crossover frequency $f = \bar{\Phi}_0$ containing experimental variation was subtracted from the variation measured by AFM. I found that $\tilde{\sigma}_{\ln G'}$ observed for different cell populations under the same conditions was almost identical. The value of $\tilde{\sigma}_{\ln G'}$ of cells treated with cytoD was significantly reduced, indicating that $\tilde{\sigma}_{\ln G'}$ can be varied by perturbing the cytoskeleton at least via altered actin polymerization. Moreover, $\tilde{\sigma}_{\ln G'}$ measured at the center of microarray wells containing single cells was larger than that measured within the cell nucleus boundaries away from the well centers, suggesting that cell-to-cell variation of G' also exhibits a subcellular spatial dependence related to cytoskeletal organization.

3.6 References

1. Schmidt, C. E., A. F. Horwitz, D. A. Lauffenburger, and M. P. Sheetz. 1993. Integrin-cytoskeletal interactions in migrating fibroblasts are dynamic, asymmetric, and regulated. J. Cell Biol. 123:977-991.
2. Bursac, P., G. Lenormand, B. Fabry, M. Oliver, D. A. Weitz, V. Viasnoff, J. P. Butler, and J. J. Fredberg. 2005. Cytoskeletal remodelling and slow dynamics in the living cell. Nat. Mater. 4:557-561.
3. Kasza, K. E., A. C. Rowat, J. Y. Liu, T. E. Angelini, C. P. Brangwynne, G. H. Koenderink, and D. A. Weitz. 2007. The cell as a material. Curr. Opin. Cell Biol. 19:101-107.
4. Fletcher, D. A. and D. Mullins. 2010. Cell mechanics and the cytoskeleton. Nature 463:485-492.
5. Ingber, D. E. 2003. Tensegrity I. Cell structure and hierarchical systems biology. J. Cell Sci. 116:1157-1173.
6. Discher, D. E., P. Janmey, and Y. L. Wang. 2005. Tissue cells feel and respond to the stiffness of their substrate. Science 310:1139-1143.
7. Janmey, P. A. and C. A. McCulloch. 2007. Cell mechanics: integrating cell responses to mechanical stimuli. Ann. Rev. Biomed. Eng. 9:1-34.
8. Janmey, P. A. and D. A. Weitz. 2004. Dealing with mechanics: mechanisms of force transduction in cells. Trends Biochem. Sci 29:364-370.
9. Vogel, V. and M. Sheetz. 2006. Local force and geometry sensing regulate cell functions. Nat. Rev. Mol. Cell Biol. 7:265-275.
10. Trepat, X., G. Lenormand, and J. J. Fredberg. 2008. Universality in cell mechanics. Soft Matter 4:1750-1759.

11. Kollmannsberger, P. and B. Fabry. 2009. Active soft glassy rheology of adherent cells. Soft Matter 5:1771-1774.
12. Kollmannsberger, P. and B. Fabry. 2011. Linear and nonlinear rheology of living cells. Annu. Rev. Mater. Res. 41:75-97.
13. Hoffman, B. D. and J. C. Crocker. 2009. Cell mechanics: dissecting the physical responses of cells to force. Ann. Rev. Biomed. Eng. 11:259-288.
14. Yamada, S., D. Wirtz, and S. C. Kuo. 2000. Mechanics of living cells measured by laser tracking microrheology. Biophys. J. 78:1736-1747.
15. Fabry, B., G. N. Maksym, J. P. Butler, M. Glogauer, D. Navajas, and J. J. Fredberg. 2001. Scaling the microrheology of living cells. Phys. Rev. Lett. 87:148102-1-148102-4.
16. Fabry, B., G. N. Maksym, J. P. Butler, M. Glogauer, D. Navajas, N. A. Taback, E. J. Millet, and J. J. Fredberg. 2003. Time scale and other invariants of integrative mechanical behavior in living cells. Phys. Rev. E 68:041914-1-041914-18.
17. Puig-de-Morales, M., E. Millet, B. Fabry, D. Navajas, N. Wang, J. P. Butler, and J. J. Fredberg. 2004. Cytoskeletal mechanics in adherent human airway smooth muscle cells: probe specificity and scaling of protein-protein dynamics. Am. J. Physiol. Cell Physiol. 287:C643-C654.
18. Laudadio, R. E., E. J. Millet, B. Fabry, S. S. An, J. P. Butler, and J. J. Fredberg. 2005. Rat airway smooth muscle cell during actin modulation: rheology and glassy dynamics. Am. J. Physiol. Cell Physiol. 289:C1388-C1395.
19. Dahl, K. N., A. J. Engler, J. D. Pajerowski, and D. E. Discher. 2005. Power-law rheology of isolated nuclei with deformation mapping of nuclear substructures. Biophys. J. 89:2855-2864.

20. Alcaraz, J., L. Buscemi, M. Grabulosa, X. Trepat, B. Fabry, R. Farre, and D. Navajas. 2003. Microrheology of human lung epithelial cells measured by atomic force microscopy. Biophys. J. 84:2071-2079.
21. Hoffman, B. D., G. Massiera, K. M. Van Citters, and J. C. Crocker. 2006. The consensus mechanics of cultured mammalian cells. Proc. Natl. Acad. Sci. USA 103:10259-10264.
22. Van Citters, K. M., B. D. Hoffman, G. Massiera, and J. C. Crocker. 2006. The role of F-actin and myosin in epithelial cell rheology. Biophys. J. 91:3946-3956.
23. Balland, M., N. Desprat, D. Icard, S. Fereol, A. Asnacios, J. Browaeys, S. Henon, and F. Gallet. 2006. Power laws in microrheology experiments on living cells: comparative analysis and modeling. Phys. Rev. E 74:021911-1-021911-17.
24. Massiera, G., K. M. Van Citters, P. L. Biancaniello, and J. C. Crocker. 2007. Mechanics of single cells: rheology, time depndence, and fluctuations. Biophys. J. 93:3703-3713.
25. Desprat, N., A. Richert, J. Simeon, and A. Asnacios. 2005. Creep function of a single living cell. Biophys. J. 88:2224-2233.
26. Deng, L. H., X. Trepat, J. P. Butler, E. Millet, K. G. Morgan, D. A. Weitz, and J. J. Fredberg. 2006. Fast and slow dynamics of the cytoskeleton. Nat. Mater. 5:636-640.
27. Overby, D. R., B. D. Matthews, E. Alsberg, and D. E. Ingber. 2005. Novel dynamic rheological behavior of individual focal adhesions measured within single cells using electromagnetic pulling cytometry. Acta Biomater. 1:295-303.
28. Stamenovic, D., N. Rosenblatt, M. Montoya-Zavala, B. D. Matthews, S. Hu, B. Suki, N. Wang, and D. E. Ingber. 2007. Rheological Behavior of living cells is timescale-dependent. Biophys. J. 93:L39-L41.

29. Chowdhury, F., S. Na, O. Collin, B. Tay, F. Li, T. Tanaka, D. E. Leckband, and N. Wang. 2008. Is cell rheology governed by nonequilibrium-to-equilibrium transition of noncovalent bonds? Biophys. J. 95:5719-5727.

30. Rotsch, C. and M. Radmacher. 2000. Drug-induced changes of cytoskeletal structure and mechanics in fibroblasts: an atomic force microscopy study. Biophys. J. 78:520-535.

31. Haga, H., S. Sasaki, K. Kawabata, E. Ito, T. Ushiki, and T. Sambongi. 2000. Elasticity mapping of living fibroblasts by AFM and immunofluorescence observation of the cytoskeleton. Ultramicroscopy 82:253-258.

32. Heidemann, S. R. and D. Wirtz. 2004. Towards a regional approach to cell mechanics. Trends Cell Biol. 14:160-166.

33. Park, C. Y., D. Tambe, A. M. Alencar, X. Trepat, E. H. Zhou, E. Millet, J. P. Butler, and J. J. Fredberg. 2010. Mapping the cytoskeletal prestress. Am. J. Physiol. Cell Physiol. 298:C1245-C1252.

34. Fredberg, J. J. and D. Stamenovic. 1989. On the imperfect elasticity of lung-tissue. J. Appl. Physiol. 67:2408-2419.

35. Hiratsuka, S., Y. Mizutani, M. Tsuchiya, K. Kawahara, H. Tokumoto, and T. Okajima. 2009. The number distribution of complex shear modulus of single cells measured by atomic force microscopy. Ultramicroscopy 109:937-941.

36. Maloney, J. M. and K. J. Van Vliet. 2011. On the origin and extent of mechanical variation among cells. arXiv:1104.0702v2.

37. Mizutani, Y., M. Tsuchiya, S. Hiratsuka, K. Kawahara, H. Tokumot, and T. Okajima. 2008. Elasticity of living cells on a microarray during the early stages of adhesion measured by atomic force microscopy. Jpn. J. Appl. Phys. 47:6177-6180.

38. Ducker, W. A., T. J. Senden, and R. M. Pashley. 1991. Direst measurement of colloidal forces using an atomic force microscope. Nature 353:239-241.

39. Radmacher, M., R. W. Tillmann, M. Fritz, and H. E. Gaub. 1992. From molecules to cells: imaging soft samples with the atomic force microscope. Science 257:1900-1905.

40. Radmacher, M., R. W. Tilmann, and H. E. Gaub. 1993. Imaging viscoelasticity by force modulation with the atomic force microscope. Biophys. J. 64:735-742.

41. Mahaffy, R. E., S. Park, E. Gerde, J. Kas, and C. K. Shih. 2004. Quantitative analysis of the viscoelastic properties of thin regions of fibroblasts using atomic force microscopy. Biophys. J. 86:1777-1793.

42. Landau, L. and E. M. Lifshitz. 1986. Theory of elasticity. Oxford: Pergamon Press.

43. Alcaraz, J., L. Buscemi, M. Puig-de-Morales, J. Colchero, A. Baro, and D. Navajas. 2002. Correction of microrheological measurements of soft samples with atomic force microscopy for the hydrodynamic drag on the cantilever. Langmuir 18:716-721.

44. Nagayama, M., H. Haga, and K. Kawabata. 2001. Drastic change of local stiffness distribution correlating to cell migration in living fibroblasts. Cell Motil. Cytoskel. 50:173-179.

45. Djordjevic, V. D., J. Jaric, B. Fabry, J. J. Fredberg, and D. Stamenovic. 2003. Fractional derivatives embody essential features of cell rheological behavior. Ann. Biomed. Eng. 31:692-699.

46. Lekka, M., P. Laidler, D. Gil, J. Lekki, Z. Stachura, and A. Z. Hrynkiewicz. 1999. Elasticity of normal and cancerous human bladder cells studied by scanning force microscopy. Eur. Biophys. J. Biophys. Lett. 28:312-316.

47. Cross, S. E., Y. S. Jin, J. Rao, and J. K. Gimzewski. 2007. Nanomechanical analysis of cells from cancer patients. Nat. Nanotechnol. 2:780-783.

Chapter 4: Precision of Spatial Dependence of Cell-to-Cell Variation in Power-Law Rheology

The frequency-dependent component of cell-to-cell variation in cell rheology was quantified in Chapter 3. However, less is known about how precisely and routinely the spatial dependent cell-to-cell variation is obtained when the complex moduli vary substantially in different cell samples. In this chapter, the storage modulus G' for single cells was measured at controlled positions by AFM. It is found that the spatial dependence of the frequency-dependent component of the cell-to-cell variation is preserved even if the spatial heterogeneity of G' is changed with the cell sample. The invariance of the frequency-dependent cell-to-cell variation indicates the robustness of AFM for the mechanical diagnosis of single cells.

4.1 Introduction

The mechanical properties of single cells have been extensively investigated by measuring not only the static elastic moduli, but also the complex moduli as a function of time or frequency (see Section 1.3) [1-3]. Recent studies revealed that the mechanical properties, such as Young's modulus [4-6], deformability [7,8], and relaxation process [9,10] of cells are critical indicators that facilitate the identification and sorting of cells. As a compliant material, the complex modulus of a cell is an intrinsic mechanical coefficient, in contrast to the static Young's modulus and the cell deformability [1-3,11-13]. Thus, the quantitative measurement of the complex modulus of cells is necessary for further improvement of the mechanical identification and sorting of cells.

The rheological properties of single cells, such as the complex shear modulus are known to be strongly associated with the CSK filamentous structures that are widely distributed in the cell cytoplasm [1,12-17]. Despite the complex CSK network, the storage modulus G' of cells commonly follows a single power-law function over the frequency range of 10^0–10^2 Hz. That is, G' increases in a single power-law manner with increasing frequency f of the loading force (see Section 1.3) [1,12,13,18-22]. The power-law curves of the ensemble-averaged G' of cells exhibit a universal behavior, that is, the curves for cells, whose CSK of which is modified with different types of drugs, when extrapolated toward higher frequency, consistently cross at single point of $G' = \bar{g}_0$ at a high frequency limit $f = \bar{\Phi}_0$ where g_0 and Φ_0 are the storage modulus and the frequency for each cell, respectively, at the crossing point [1,12,13,23]. This suggests the existence of a point where $\bar{g}_0$ and $\bar{\Phi}_0$ correspond to the invariant modulus and frequency, respectively, with respect to any modification of CSK structures.

For a more detailed understanding of single cell rheology, I used AFM combined with a cell microarray technique, which allows us to reduce the variation in cell shape and improve the precision of measurement position, to investigate the cell-to-cell variation in G' [23]. Such a variation is important for the statistical evaluation of pharmacological treatments and different cell states. By assuming that the point ($\bar{\Phi}_0$, $\bar{g}_0$) obtained from cells in a microarray sample is invariant to measurement positions within cells in Chapter 3, where the complex modulus does not markedly vary, I found that the frequency-dependent components of the cell-to-cell variation in G' defined at $f < \bar{\Phi}_0$ can be quantified for cell microarray samples [23]. However, it is not known how precisely and routinely the frequency-dependent component of the cell-to-cell variation can be obtained when the complex modulus varies substantially in different cell samples. Here, I investigate G' of single cells in different microarray samples by AFM to clarify the relationship between $G' = \bar{g}_0$ at $f = \bar{\Phi}_0$ and other rheological parameters for $f < \bar{\Phi}_0$. The latter determines the mechanical properties of cells over the frequency range of 10^0–10^2 Hz.

4.2 Methods

4.2.1 Cell samples

Detailed preparation procedures for cells arranged on a microarray substrate have been described in Section 2.2.2. Briefly, mouse fibroblast NIH3T3 cells (ATCC) were deposited in hexagonal microarray wells (LiveCell Array^{TM}; Nunc), and were immediately incubated for 12 h in complete medium (Dulbecco's modified Eagle's medium containing fetal bovine serum). For AFM measurements, the medium was replaced with a CO_2-independent medium (Invitrogen).

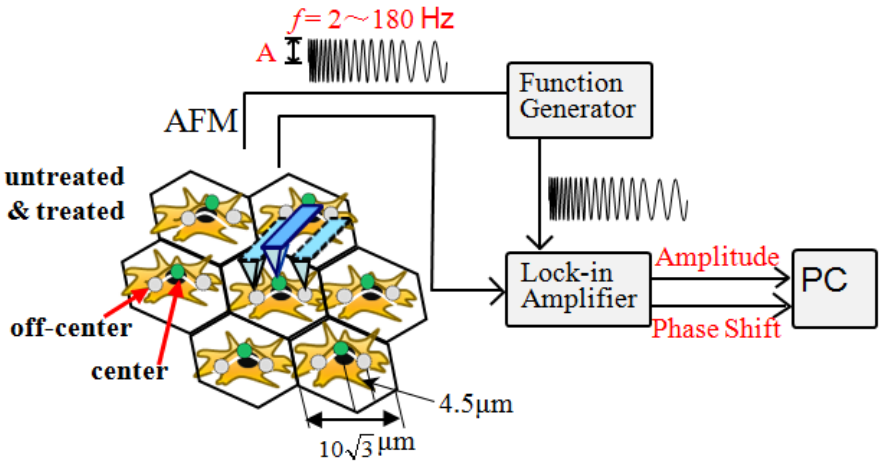

Figure 4.1 Schematic of AFM force modulation measurements on cells cultured on a microarray substrate. The measurements were conducted at the center of wells and 4.5 μm away from the center. After the measurements, the cells (n > 80) were treated with cytoD to depolymerize the actin filaments and then measured again at the same two locations. The storage modulus of the cells was estimated from the amplitude and phase shift of the cantilever displacement at different frequencies.

4.2.2 AFM measurements

An AFM (MFP-3D AFM; Asylum Research) was used to measure the complex shear modulus of NIH3T3 cells (Fig. 4.1). Detailed AFM procedure was described in Section 2.2.4. To achieve a well-defined contact geometry, a colloidal silica bead with a radius R of ~2.5 μm (Funakoshi) was attached to the apex of the AFM tip with epoxy [23-25]. Cells in the microarray wells were indented for ~30 s at an initial loading force < 650 pN. The cantilever was then driven to oscillate with about 10 nm in amplitude at 2, 5, 10, 25, 50, 100 and 180 Hz, in a stepwise fashion, while the amplitude and phase shift of the cantilever displacement were measured with a digital lock-in amplifier (7260; Seiko EG&G). The measurements were performed at the center of each well, which is located on cell nucleus, and at the off-center which is a distance of 4.5 μm away from the center

at the locations within the cell nucleus boundaries [23]. The cells were then incubated for 20 min in 2-μM cytochalasin D (cytoD) (Sigma–Aldrich), which depolymerizes actin filaments, and the same cells were measured again (Fig. 4.1). For each microarray, at least 80 cells were measured before and after the cytoD treatment. The effect of cytoD on actin filaments structure was shown in Fig. 2.9.

The complex shear modulus G^* is given by the Hertzian contact model [22,27-29] with a viscous drag factor F_d^* (see Section 2.1.4) [22,28]. The phase shift observed in the frequency range of 2–180 Hz mainly resulted from the mechanical response of AFM head and thus was calibrated at different frequencies using a stiff cantilever in contact with a clean glass cover slip in air.

4.2.3 Data analysis

The G' for cells obtained with AFM was analyzed using Igor Pro software (WaveMetrics), with a built-in global fitting procedure. Detailed method of data analysis was described in Section 2.3. G' and G'' as a function of f were fitted to the power-law structural damping model with additional Newtonian viscosity as given by Eq. 1.1. The parameters in power-law structural damping model are α with being the power-law exponent, G_0 with being a scale factor of the modulus at a scale factor of frequency f_0 (~1 Hz), and μ with being the Newtonian viscous damping coefficient. The standard deviations of G', G'', and the corresponding power-law parameters were calculated by Eq. 2.10. Pearson's coefficient γ is used to characterize the correlation between the cellular storage moduli measured at center and off-center locations of microarray wells.

4.2.4 SGR model of cells

G' as a function of f is assumed to follow the power-law structural damping model

[12,13,30]:

$$G' = G_0 g(\alpha)\left(\frac{f}{f_0}\right)^{\alpha}, \tag{4.1}$$

where α is the power-law exponent and $g(\alpha)$ is $\Gamma(1-\alpha)\cdot\cos(\pi\alpha/2)$, in which Γ is the gamma function. G_0 is a scale factor of the modulus at frequency f_0, which was arbitrarily set to 1 Hz. It is assumed that G' of each cell can be expressed as [23]:

$$G' = g_0\left(\frac{f}{\Phi_0}\right)^{\alpha}. \tag{4.2}$$

The point (Φ_0, g_0) for each cell can be estimated by extrapolating the G' vs. f curves measured under untreated (control) and treated conditions with different types of drugs at the same positions. The geometric mean of G' is also expressed as [1,12,13]:

$$\overline{G}' = \overline{g}_0\left(\frac{f}{\overline{\Phi}_0}\right)^{\alpha}. \tag{4.2′}$$

Such a power-law behavior of G' has often been explained in terms of a soft glassy rheology (SGR) model of cell deformability [1,2,11-13]. In this SGR model, the cellular mechanical state on average evolves on an energy landscape with a high number of local minima. The typical depth of these minima is much larger than the thermal noise, and thus the temporal evolution in this energy landscape proceeds because of activation energy, such as a loading force in micro-rheological measurements. As the frequency of the loading force increases, G' increases in a power-law manner where the exponent corresponds to the degree that the mechanical state of cell is suffering from hopping among local minima. At the higher frequency limit of $f = \overline{\Phi}_0$ where $G' = \overline{g}_0$ is unchanged, the cell mechanical state can no longer escape from the trapping local

minima [1,2,12,13,23].

According to the SGR model (Eq.4.2), $\sigma_{\log G'}$ is approximately proportional to $\log f$, which is given by [23,31]:

$$\sigma_{\log G'} = \sigma_{\log g_0} + (\log \bar{\Phi}_0 - \log f)\sigma_\alpha . \tag{4.3}$$

The first term $\sigma_{\log g_0}$ on the right-hand side is the standard deviation of g_0, which is independent of f; whereas the second term is the frequency-dependent component of the standard deviation of G', which is expressed as [23]:

$$\tilde{\sigma}_{\log G'} = (\log \bar{\Phi}_0 - \log f)\sigma_\alpha , \tag{4.4}$$

where σ_α is the standard deviation for power-law exponents for different cells.

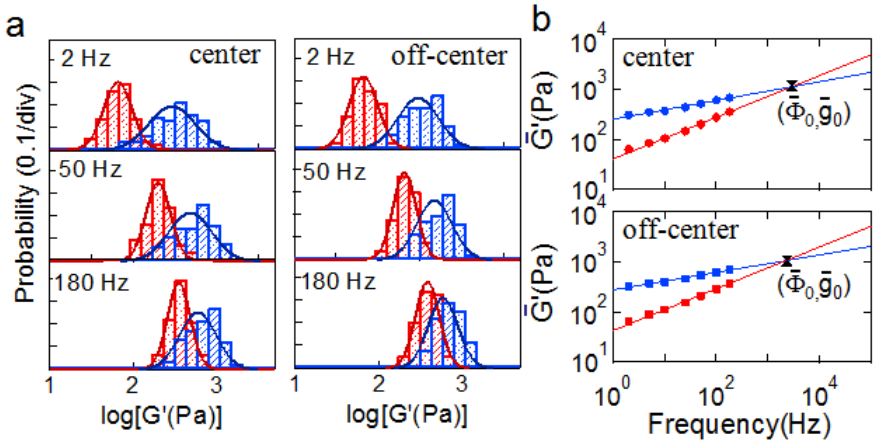

Figure 4.2 (a) Typical ensemble distributions of G' for untreated (blue) and cytoD-treated (red) cells measured at the well centers (left) and off-center (right) at 2 Hz, 50 Hz, and 180 Hz. Solid lines in (a) represent the fitted results with a log-normal distribution. (b) The geometric mean of G' for untreated (blue) and cytoD-treated (red) conditions at the center (upper) and the off-center (lower) locations of wells. Solid lines in (b) represent fits with Eq. 4.2′.

4.3 Results and Discussion

Figure 4.2 (a) shows the distribution of G' of the untreated and cytoD-treated cells

measured at center and off-center locations. The distribution of G' exhibited log-normal behavior regardless of measurement position and whether it had cytoD treatment. The corresponding ensemble average $\bar{G}'$ is plotted as a function of f in Fig. 4.2 (b). $\bar{G}'$ increases with f and can be fitted well with Eq. 4.2′.

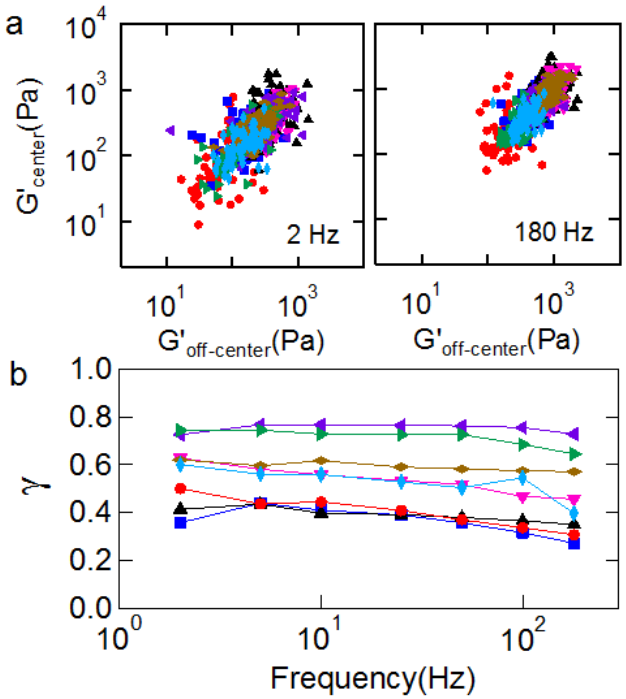

Figure 4.3 Relation between $\log G'_{\text{center}}$ and $\log G'_{\text{off-center}}$ for untreated cells at 2 Hz and 180 Hz (a) and frequency-dependent correlation coefficient between $\log G'_{\text{center}}$ and $\log G'_{\text{off-center}}$ (b). The different colors represent different cell samples in (a) and (b).

To estimate the spatial heterogeneity of the CSK structures, the relationship between the values of G' of untreated cells measured at center and off-center locations was plotted for different frequencies [Fig. 4.3 (a)]. A positive correlation was clearly seen at every frequency, but γ varied between 0.4 and 0.8 for different cell microarray samples

(N = 8) [Fig. 4.3 (b)]. This result indicates that cells have heterogeneous structures that vary even if the same protocol is used for the preparation of cell microarray samples. Such day-to-day variability is inevitable in measuring the mechanical properties of cells.

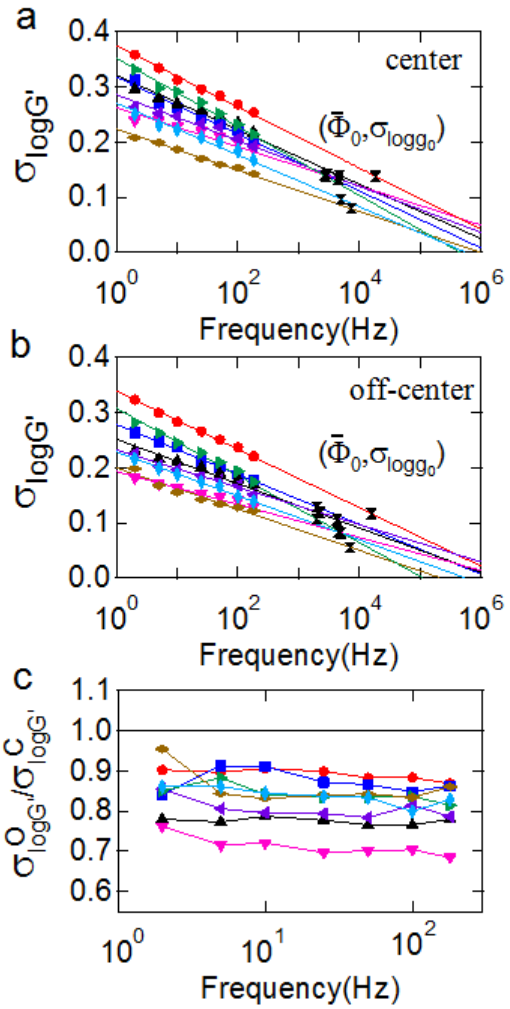

Figure 4.4 Frequency dependence of $\sigma_{\log G'}$ (a, center and b, off-center). The point $(\bar{\Phi}_0, \sigma_{\log g_0})$ is where the curves of $\sigma_{\log G'}$ for untreated and cytoD-treated cells cross. The color represents the cell sample. (c) Frequency-dependent $\sigma^{\mathrm{O}}_{\log G'} / \sigma^{\mathrm{C}}_{\log G'}$. The superscript C and O respectively represent center and off-center. The solid line in (c) represents a constant 1.

Next, the influence of the day-to-day variability in cell samples on the cell-to-cell variation in the power-law rheology was investigated. Figure 4.4 (a) and (b) shows the

standard deviation of the log-normal distribution of G', $\sigma_{\log G'}$, as a function of f, measured at center and off-center locations, respectively, for different cell microarray samples. Similar to the variation in γseen in Fig. 4.3 (b), $\sigma_{\log G'}$ largely varied from 0.2 to 0.4 in the cell microarray samples at lower frequencies.

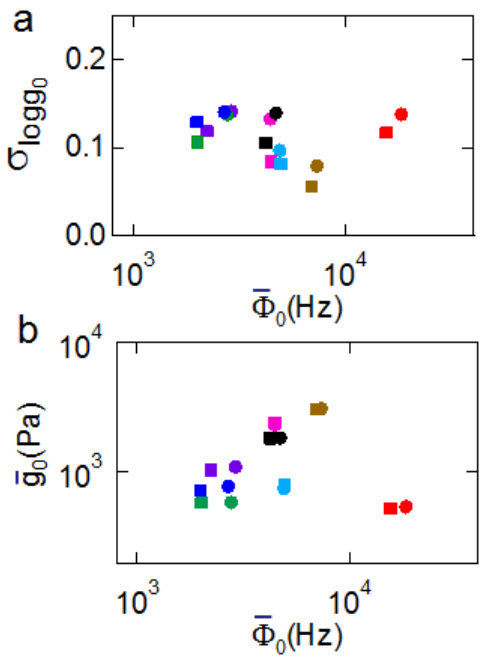

Figure 4.5 (a) Relation between $\sigma_{\log g_0}$ and $\bar{\Phi}_0$, and (b) a set of $(\bar{\Phi}_0, \bar{g}_0)$ estimated at the center (circle) and the off-center (rectangle) for different cell samples (colors).

On the other hand, a common feature was noticed in which $\sigma_{\log G'}$ decreased monotonically with increasing f and is likely to have followed the functional form $\sigma_{\log G'} \sim \log f$. This suggests that the observed cell-to-cell variation of G' is consistent with the SGR model (Eq. 4.3), irrespective of its magnitude. Also, it was observed that

$\sigma_{\log G'}$ at the off-center location was smaller than that at the center location [Fig. 4.4 (c)], indicating that $\sigma_{\log G'}$ has a spatial dependence.

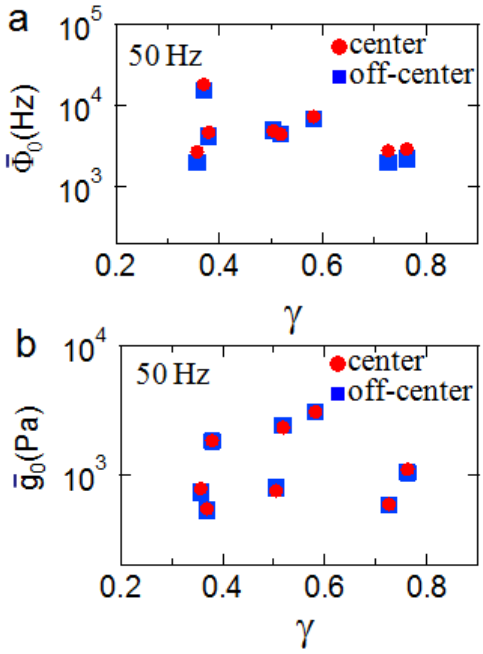

Figure 4.6 Plots of power-law parameters $\bar{\Phi}_0$ (a) and $\bar{g}_0$ (b) for center (circle) and off-center (rectangle) as a function of γ at f = 50 Hz.

According to the SGR model (Eq. 4.3), $\sigma_{\log G'}$ is related to the three parameters, namely, $\sigma_{\log g_0}$, $\bar{\Phi}_0$, and σ_α. Thus, it is important to know to what degree these parameters change among different cell microarray samples. Figure 4.5 (a) shows the relation between $\sigma_{\log g_0}$ and $\bar{\Phi}_0$ in different cell microarray samples. For the same cell sample, the point $(\bar{\Phi}_0, \sigma_{\log g_0})$ had almost the same value at center and off-center locations, although it was largely scattered among cell samples. Similar behavior was also found for $\bar{\Phi}_0$ and $\bar{g}_0$, whose values were identical at center and off-center

locations in the same cell sample [Fig. 4.5 (b)]. These results indicate that $\bar{\Phi}_0$ and $\bar{g}_0$ are invariant to measurement positions. It was noted that $\bar{\Phi}_0$ and $\bar{g}_0$ were independent of γ, as shown in Fig. 4.6 (a) and (b), suggesting that the variation in the point ($\bar{\Phi}_0$, $\bar{g}_0$) is not associated with the heterogeneities of actin filaments structures. Indeed, $\sigma_{\log g_0}$ was not related to the standard deviation of G_0 and α (Fig. 4.7), which are strongly associated with the actin filament networks where the disruption of the actin filaments decreases G_0 and increases α [12,13,23].

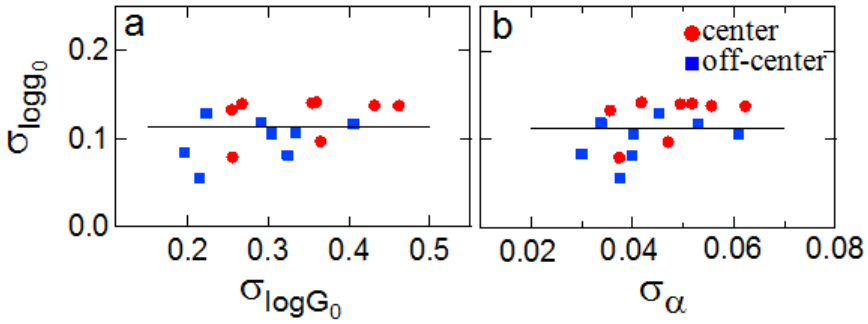

Figure 4.7 Plots of $\sigma_{\log g_0}$ vs. $\sigma_{\log G_0}$ (a) and σ_α (b) at center (circle) and off-center (rectangle) for eight cell samples. The solid line represents a fit to a constant.

In contrast, σ_α, which is the slope of $\sigma_{\log G'}$ plotted against $\log f$, exhibited spatial dependence, where σ_α at the off-center was smaller than that at the center (Fig. 4.8). Thus, it is concluded that the spatial dependence of $\sigma_{\log G'}$ shown in Fig. 4.4 (c) is derived from that of σ_α. As a consequence, the frequency-dependent component of the cell-to-cell variation in G', $\tilde{\sigma}_{\log G'}$, measured at the center was larger than that at the

off-center (see Fig. 4.9). This characteristic feature is consistent with the results found in Chapter 3.

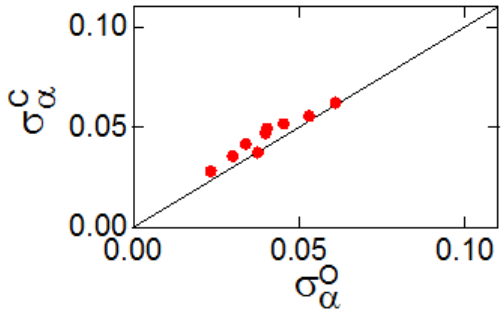

Figure 4.8 Relation between σ_α^C and σ_α^O estimated from the slopes in Fig. 4.4 (a) and (b). The solid line is linear with a slope of 1 through the origin.

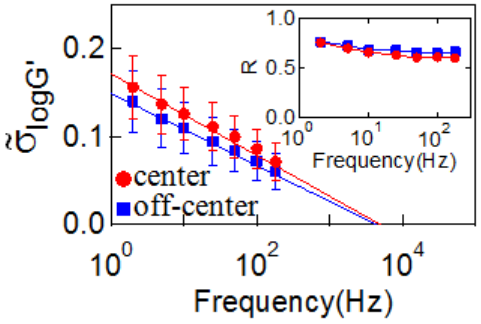

Figure 4.9 Sample-averaged frequency-dependent component of the cell-to-cell variation in logG', $\tilde{\sigma}_{\log G'}$, of center (circle) and off-center (rectangle) within cells (N = 8). The inset shows the ratio of the variation of $\tilde{\sigma}_{\log G'}$ to the variation of $\sigma_{\log G'}$, R, at center (circle) and off-center (rectangle) locations as a function of f.

It was observed that the variation in $\tilde{\sigma}_{\log G'}$ was 35% less than that of $\sigma_{\log G'}$ (the inset of Fig. 4.9). Recent studies reported that the variation of mechanical properties was dependent on the cancerous states of cells [4,7,32]. Thus, the quantification of the frequency-dependent component of the cell-to-cell variation by controlling the

measurement position may be useful for the mechanical identification and sorting of various cell states at the single cell level.

As mentioned previously in Chapter 3, the observed cell-to-cell variation is subjected to at least three main sources of experimental uncertainty. The first is the imperfection of cell sample preparation where the cells are not perfectly centered in the microarray wells. The second is the cell-cell contact of the cell sample, in which cells are in contact on all six intersecting sides. Previous studies showed that cell-cell contact plays a minor role in determining the power-law behavior [33-35]. The effect of cell-cell contact on cell-to-cell variation was, however, ignored in the most of previous studies and thus is yet to be determined in detail. The third is related to the AFM method, in which the indentation is directly associated with the initial and instantaneous stiffness of cells. This manifests that the observed cell-to-cell variation involves a degree of inhomogeneity as a function of cell depth. Furthermore, the instantaneous stiffness of cells exhibits a spatial dependence [28]. Therefore, controlling of the measurement location within the cells is essential to quantify the cell-to-cell variation of cell mechanics and minimize the experimental error by AFM.

In cells adhered to substrates, actin filaments are formed within cells by anchoring adhesion points, and then a large-scale network of actin filaments is stabilized in an apical region over a cell nucleus [36]. The observation shown in Fig. 4.4 (c) that spatial dependence of variation measured within the cell nucleus is preserved, in contrast to the spatial heterogeneities of G' which depends on the cell samples indicates that remodeling of a large-scale actin filament network in cells arranged on the microarray wells is spatially synchronized.

4.4 Conclusion

The cell-to-cell variation in the storage modulus G' measured with AFM was investigated at different locations, such as the center and off-center locations of microarray wells. It was found that ($\bar{\Phi}_0$, $\bar{g}_0$), defined as the point at which the curves of the untreated cells and the actin-disrupted cells cross for a cell microarray sample, was almost the same in the center and off-center locations. Moreover, it was found that the spatial dependence of the frequency-dependent component of the cell-to-cell variation in G' determined from the SGR model was preserved even if the spatial heterogeneities of G' largely varied among cell samples. Therefore, AFM can be used to precisely estimate the frequency-dependent component of the cell-to-cell variation and may be used in the future to mechanically identify and sort cell states. The measurement locations as well as the regulation of the cell shape are crucially important for quantitatively estimating the magnitude of both the complex modulus and the cell-to-cell variation.

4.5 References

1. Kollmannsberger, P. and B. Fabry. 2011. Linear and nonlinear rheology of living cells. Annu. Rev. Mater. Res. 41:75-97.
2. Trepat, X., G. Lenormand, and J. J. Fredberg. 2008. Universality in cell mechanics. Soft Matter 4:1750-1759.
3. Hoffman, B. D. and J. C. Crocker. 2009. Cell mechanics: dissecting the physical responses of cells to force. Ann. Rev. Biomed. Eng. 11:259-288.
4. Cross, S. E., Y. S. Jin, J. Rao, and J. K. Gimzewski. 2007. Nanomechanical analysis of cells from cancer patients. Nat. Nanotechnol. 2:780-783.
5. Lekka, M., P. Laidler, D. Gil, J. Lekki, Z. Stachura, and A. Z. Hrynkiewicz. 1999. Elasticity of normal and cancerous human bladder cells studied by scanning force microscopy. Eur. Biophys. J. Biophys. Lett. 28:312-316.
6. Lekka, M., D. Gil, K. Pogoda, J. Dulinska-Litewka, R. Jach, J. Gostek, O. Klymenko, S. Prauzner-Bechcicki, Z. Stachura, J. Wiltowska-Zuber, K. Okon, and P. Laidler. 2012. Cancer cell detection in tissue sections using AFM. Arch. Biochem. Biophys. 518:151-156.
7. Guck, J., S. Schinkinger, B. Lincoln, F. Wottawah, S. Ebert, M. Romeyke, D. Lenz, H. M. Erickson, R. Ananthakrishnan, D. Mitchell, J. Kas, S. Ulvick, and C. Bilby. 2005. Optical deformability as an inherent cell marker for testing malignant transformation and metastatic competence. Biophys. J. 88:3689-3698.
8. Gossett, D. R., H. T. Tse, S. A. Lee, Y. Ying, A. G. Lindgren, O. O. Yang, J. Rao, A. T. Clark, and D. Di Carlo. 2012. Hydrodynamic stretching of single cells for large population mechanical phenotyping. Proc. Natl. Acad. Sci. USA 109:7630-7635.
9. Wottawah, F., S. Schinkinger, B. Lincoln, R. Ananthakrishnan, M. Romeyke, J.

Guck, and J. Kas. 2005. Optical rheology of biological cells. Phys. Rev. Lett. 94: 098103-1-098103-4.

10. Maloney, J. M., D. Nikova, F. Lautenschlager, E. Clarke, R. Langer, J. Guck, and K. J. Van Vliet. 2010. Mesenchymal stem cell mechanics from the attached to the suspended state. Biophys. J. 99: 2479-2487.
11. Kollmannsberger, P. and B. Fabry. 2009. Active soft glassy rheology of adherent cells. Soft Matter 5:1771-1774.
12. Fabry, B., G. N. Maksym, J. P. Butler, M. Glogauer, D. Navajas, N. A. Taback, E. J. Millet, and J. J. Fredberg. 2003. Time scale and other invariants of integrative mechanical behavior in living cells. Phys. Rev. E 68:041914-1-041914-18.
13. Fabry, B., G. N. Maksym, J. P. Butler, M. Glogauer, D. Navajas, and J. J. Fredberg. 2001. Scaling the microrheology of living cells. Phys. Rev. Lett. 87:148102-1-148102-4.
14. Fletcher, D. A. and D. Mullins. 2010. Cell mechanics and the cytoskeleton. Nature 463:485-492.
15. Kasza, K. E., A. C. Rowat, J. Y. Liu, T. E. Angelini, C. P. Brangwynne, G. H. Koenderink, and D. A. Weitz. 2007. The cell as a material. Curr. Opin. Cell Biol. 19:101-107.
16. Bursac, P., G. Lenormand, B. Fabry, M. Oliver, D. A. Weitz, V. Viasnoff, J. P. Butler, and J. J. Fredberg. 2005. Cytoskeletal remodelling and slow dynamics in the living cell. Nat. Mater. 4:557-561.
17. Schmidt, C. E., A. F. Horwitz, D. A. Lauffenburger, and M. P. Sheetz. 1993. Integrin-cytoskeletal interactions in migrating fibroblasts are dynamic, asymmetric, and regulated. J. Cell Biol. 123:977-991.

18. Hoffman, B. D., G. Massiera, K. M. Van Citters, and J. C. Crocker. 2006. The consensus mechanics of cultured mammalian cells. Proc. Natl. Acad. Sci. USA 103:10259-10264.

19. Balland, M., N. Desprat, D. Icard, S. Fereol, A. Asnacios, J. Browaeys, S. Henon, and F. Gallet. 2006. Power laws in microrheology experiments on living cells: comparative analysis and modeling. Phys. Rev. E 74:021911-1-021911-17.

20. Laudadio, R. E., E. J. Millet, B. Fabry, S. S. An, J. P. Butler, and J. J. Fredberg. 2005. Rat airway smooth muscle cell during actin modulation: rheology and glassy dynamics. Am. J. Physiol. Cell Physiol. 289:C1388-C1395.

21. Puig-de-Morales, M., E. Millet, B. Fabry, D. Navajas, N. Wang, J. P. Butler, and J. J. Fredberg. 2004. Cytoskeletal mechanics in adherent human airway smooth muscle cells: probe specificity and scaling of protein-protein dynamics. Am. J. Physiol. Cell Physiol. 287:C643-C654.

22. Alcaraz, J., L. Buscemi, M. Grabulosa, X. Trepat, B. Fabry, R. Farre, and D. Navajas. 2003. Microrheology of human lung epithelial cells measured by atomic force microscopy. Biophys. J. 84:2071-2079.

23. Cai, P. G., Y. Mizutani, M. Tsuchiya, J. M. Maloney, B. Fabry, K. J. Van Vliet, and T. Okajima. 2013. Quantifying cell-to-cell variation in power-law rheology. Biophys. J. 105:1093-1102.

24. Hiratsuka, S., Y. Mizutani, M. Tsuchiya, K. Kawahara, H. Tokumoto, and T. Okajima. 2009. The number distribution of complex shear modulus of single cells measured by atomic force microscopy. Ultramicroscopy 109:937-941.

25. Miyaoka, A., Y. Mizutani, M. Tsuchiya, K. Kawahara, and T. Okajima. 2011. Rheological properties of growth-arrested fibroblast cells under serum starvation

measured by atomic force microscopy. Jpn. J. Appl. Phys. 50:08LB16-1-08LB16-4.

26. Mizutani, Y., M. Tsuchiya, S. Hiratsuka, K. Kawahara, H. Tokumot, and T. Okajima. 2008. Elasticity of living cells on a microarray during the early stages of adhesion measured by atomic force microscopy. Jpn. J. Appl. Phys. 47:6177-6180.
27. Mahaffy, R. E., S. Park, E. Gerde, J. Kas, and C. K. Shih. 2004. Quantitative analysis of the viscoelastic properties of thin regions of fibroblasts using atomic force microscopy. Biophys. J. 86:1777-1793.
28. Radmacher, M., R. W. Tillmann, M. Fritz, and H. E. Gaub. 1992. From molecules to cells: imaging soft samples with the atomic force microscope. Science 257:1900-1905.
29. Landau, L. and E. M. Lifshitz. 1986. Theory of elasticity. Oxford: Pergamon Press.
30. Fredberg, J. J. and D. Stamenovic. 1989. On the imperfect elasticity of lung-tissue. J. Appl. Physiol. 67:2408-2419.
31. Maloney, J. M. and K. J. Van Vliet. 2011. On the origin and extent of mechanical variation among cells. arXiv:1104.0702v2.
32. Plodinec, M., M. Loparic, C. A. Monnier, E. C. Obermann, R. Zanetti-Dallenbach, P. Oertle, J. T. Hyotyla, U. Aebi, M. Bentires-Alj, R. Y. Lim, and C. A. Schoenenberger. 2012. The nanomechanical signature of breast cancer. Nat. Nanotechnol. **7**:757-765.
33. Chowdhury, F., S. Na, O. Collin, B. Tay, F. Li, T. Tanaka, D. E. Leckband, and N. Wang. 2008. Is cell rheology governed by nonequilibrium-to-equilibrium transition of noncovalent bonds? Biophys. J. 95:5719-5727.
34. Takahashi, R., S. Ichikawa, A. Subagyo, K. Sueoka, and T. Okajima. 2014. Atomic force microscopy measurements of mechanical properties of single cells patterned by microcontact printing. Adv. Robot. 28:449-455.

35. Bursac, P., B. Fabry, X. Trepat, G. Lenormand, J. P. Butler, N. Wang, J. J. Fredberg, and S. S. An. 2007. Cytoskeleton dynamics: fluctuations within the network. Biochem. Bioph. Res. Co. 355:324-330.

36. Khatau, S. B., C. M. Hale, P. J. Stewart-Hutchinson, M. S. Patel, C. L. Stewart, P. C. Searson, D. Hodzic, and D. Wirtz. 2009. A perinuclear actin cap regulates nuclear shape. Proc. Natl. Acad. Sci. USA 106:19017-19022.

Chapter 5: Role of Actin-Myosin Interaction in Cell-to-Cell Variation in Power-Law Rheology

Rheological property of cell is directly associated with the structure of stress fibers, in which individual actin filaments are organized into networks and bundles through myosin. In Chapters 3 and 4, it is known that one source of the frequency-dependent component of cell-to-cell variation arises from the actin filaments organization. However, it is little known how the interaction between actin and myosin influences the cell-to-cell variation. In this chapter, the effect of the interaction between actin and myosin on the cell-to-cell variation in cell rheology was investigated. It was found that the enhancement of myosin with calyculin A had no distinct change in the ensemble-averaged G^*, but led to an apparent increase in the cell-to-cell variation of G^*, $\sigma_{\log G^*}$, showing that the calyculin A-treated cells had more heterogeneous CSK structures rather than the untreated ones. Moreover, the inhibition of myosin with blebbistatin led to a significant decrease in both the ensemble averaged G^* and $\sigma_{\log G^*}$, showing that blebbistatin-treated cells had more homogenous CSK structures rather than the untreated ones. These results indicate that the interaction between actin and myosin regulates the heterogeneities of CSK structures and enhances the cell-to-cell variation in cell rheology.

5.1 Introduction

Cytoskeleton in living cell is a heterogeneous polymer network composed of protein filaments and crosslinker and regulates various cellular processes such as cell shape, motility, and division [1-4]. It is recognized that the rheology of living cells is one of the most important physical properties to understand cell functions [5-9]. In order to explore the mechanical contribution of the molecular mechanism, the cytoskeletal meshwork is modeled as a "soft glassy material", which is appropriate to describe out-of-equilibrium systems [10-15]. The dynamics and rheological properties of this soft glassy material have been reasonably well studied [10-32]. In particular, ensemble measurement revealed that complex shear modulus G^* followed power-law behavior [10-32] and the populations of "seemingly identical" cells exhibited heterogeneity, that is, cell-to-cell variation [15-21].

The structural origin for cell rheology is widely believed to originate in the integrity stress fibers (SFs) structure which is composed of the individual actin filaments and their organization into networks and bundles through myosin [33-36]. Thus, it is crucial to identify the respective contribution of the different constituents of SFs to the mechanical response including cell-to-cell variation. Indeed, many results focused on the mechanical behavior of the actin filaments meshwork revealed an important role of actin filaments in ensemble averaged G^*, which was made possible by the specific drugs to alter the structure of actin filaments [12,13,18,23,29,30,33]. Moreover, the results in Chapters 3 and 4 showed that the cell-to-cell variation of cell rheology was strongly associated with the actin filamentous structures [18]. On the other hand, the promotion and depromotion drugs of myosin were also used to investigate the roles of myosin in cell mechanical properties [29,33-36]. Van Citters *et al*. investigated the contributions of

actin and myosin in the mechanical response from the epithelial cell interior and cortex by several pharmacological interventions using either active or passive driving forces [33]. They revealed that myosins do not contribute significantly to cell rheology. Moreover, Lu *et al*. explored the mechanical properties of individual SFs in living endothelial cells through increasing or decreasing contractile level by myosin drugs calyculin A and blebbistatin using an atomic force microscope, demonstrating that the SFs actomyosin contractile level plays a pivotal role on mechanical properties in living cells [36]. To my knowledge, a central challenge is to process the information of individual cells because the averaged ensemble behavior may not sufficiently capture the information of the difference behavior of any individual cell. Although previous studies provided useful information about the myosin mechanical roles in the complex shear modulus, however, there has no information about the correspondingly detailed roles in the cell-to-cell variation.

My major purpose in this chapter is to characterize the contribution of the interaction between actin and myosin to frequency-dependent cell-to-cell variation of ensemble distributions G^*. To accomplish this goal, the effect of the interaction between actin and myosin on the ensemble distributions of G^* of single mouse fibroblast cells was measured as a function of frequency, in which myosin drugs, including calyculin A and blebbistatin, were used to alter the interaction between actin and myosin of single cells. As a consequence, the ensemble-averaged G^* and cell-to-cell variation of untreated cells exhibited similar frequency-dependent features as ensemble distribution of control cells whereas their values are regulated by myosin drugs. The results provide the physical and critical insight into the mechanisms responsible for cell-to-cell variation of cell rheology by myosin II.

5.2 Materials and Methods

5.2.1 Cell samples

Detailed preparation procedures for cells arranged on a microarray substrate have been described in Section 2.2.2. Briefly, mouse fibroblast NIH3T3 cells (ATCC) were deposited in hexagonal microarray wells having a width of 20 μm (LiveCell Array^{TM}; Nunc), and were immediately incubated for 12 h in complete medium (Dulbecco's modified Eagle's medium containing fetal bovine serum). For AFM measurements, the medium was replaced with a CO_2-independent medium (Invitrogen).

5.2.2 Alteration of actin-myosin interaction

To assess the role of the interaction between actin and myosin in the distribution, cells were treated with either 2-nM calyculin A (Sigma-Aldrich) or 2-μM blebbistatin (Sigma-Aldrich) at 37 °C for at least 20 min prior to induce myosin hyperpolymerization or depolymerization, respectively. Calyculin A inhibits myosin-light-chain phosphatase from dephosphorylating myosin, thus myosin is hyperactivated [36]. Blebbistatin inhibits both the cross-linking and motor properties of myosin II by inhibiting its binding of actin filaments [29,33]. Concentrations of cytoskeletal drugs were chosen based on published research [33,36] or based on my own experience and tests, where I chose the maximum concentration that can be used without inducing cell detachment from the well. Calyculin A and blebbistatin were dissolved in DMSO carrier before adding to the cells.

5.2.3 Measurements of the cell rheology by AFM

An AFM (MFP-3D AFM; Asylum Research) was used to measure the complex shear modulus of NIH3T3 cells (Fig. 5.1). Detailed AFM procedure was described in Section 2.2.4. To achieve a well-defined contact geometry, a colloidal silica bead with a radius R of ~2.5 μm (Funakoshi) was attached to the apex of the AFM tip with epoxy

[18,20,21,37]. Cells in the microarray wells were indented for ~30 s at an initial loading force < 650 pN. The cantilever was then driven to oscillate with about 10 nm in amplitude at 2, 5, 10, 25, 50, 100 and 180 Hz, in a stepwise fashion, while the amplitude and phase shift of the cantilever displacement were measured with a digital lock-in amplifier (7260; Seiko EG&G). The measurements were performed at the center of each well.

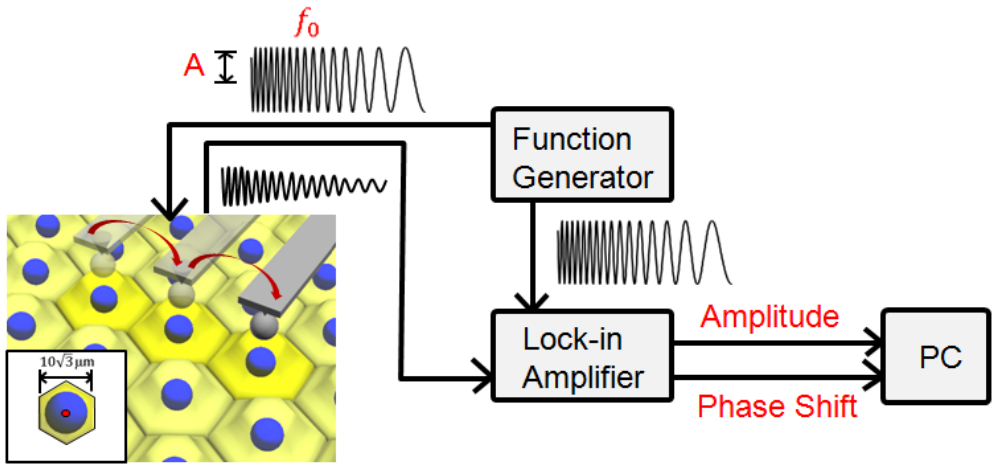

Figure 5.1 Schematic of the AFM force modulation with a microarray substrate, on which living cells were arranged and cultured. The effects of myosin drugs on the G^* of cells were measured. The untreated cells were measured at the center of wells and the same cells treated with drugs were measured again at the same locations.

The complex shear modulus G^* is given by the Hertzian contact model [27,38-40] with a viscous drag factor F_d^* (see Section 2.1.4) [27,41]. The phase shift was observed in the frequency range of 2–180 Hz resulted from the mechanical response of AFM head and thus was calibrated at different frequencies using a stiff cantilever in contact with a clean glass cover slip in air.

5.2.4 Data analysis

The G' for cells obtained with AFM was analyzed using Igor Pro software (WaveMetrics), with a built-in global fitting procedure. Detailed method of data analysis was described in Section 2.3. G' and G'' as a function of f were fitted to the power-law structural damping model with additional Newtonian viscosity as given by Eq. 1.1. The parameters in power-law structural damping model are α with being the power-law exponent, G_0 with being a scale factor of the modulus at frequency f_0 (~1 Hz), and μ with being the Newtonian viscous damping coefficient. The standard deviations of G', G'', and the corresponding power-law parameters were calculated by Eq. 2.10.

5.2.5 Soft glassy rheology

In soft glass rheology (SGR) theory, individual elements of matrix such as CSK are trapped within an energy landscape containing wells with different energies and transit from one energy well to another. Fabry *et al.* reported that $\overline{G}'$ of the cells as a function of f appeared to cross at $\overline{G}' = \overline{g}_0$ at a high frequency $f = \overline{\Phi}_0$, in which the $\overline{g}_0$ and $\overline{\Phi}_0$ values are respectively identified as being the intrinsic stiffness of the cytoskeleton at the glass transition ($\alpha = 0$) and the intrinsic maximum rate at which the cytoskeletal elements can rearrange [12,13]. The geometric mean of G' is also expressed as [1,12,13]:

$$\overline{G}' = \overline{g}_0 \left(\frac{f}{\overline{\Phi}_0} \right)^{\alpha} . \tag{5.1}$$

Hence, each cell complex shear modulus can be expressed as [18] :

$$G' = g_0 \left(\frac{f}{\Phi_0} \right)^{\alpha} , \tag{5.1′}$$

in which the point (Φ_0 , g_0) can be estimated by extrapolating the G' vs. f curves

measured under one pair of two conditions. Therefore, ($\bar{\Phi}_0$, $\bar{g}_0$) can also be obtained by averaging a series of points (Φ_0, g_0). Furthermore, the standard deviation of G', $\sigma_{\log G'}$, can be expressed as[18]

$$\sigma_{\log G'} = \sigma_{\log g_0} + (\log \bar{\Phi}_0 - \log f)\sigma_\alpha , \tag{5.2}$$

in which $\sigma_{\log g_0}$ is the standard deviation for the intrinsic stiffness $\bar{g}_0$ at $f = \bar{\Phi}_0$ and σ_α is the standard deviation of power-law exponents for different cells. Additionally, $\sigma_{\log G'}$ can also be rewritten as a function of $\log G'$ [18]:

$$\sigma_{\log G'} = \sigma_{\log g_0} + \frac{\sigma_\alpha}{\langle \alpha \rangle}(\log \bar{g}_0 - \log \bar{G}') , \tag{5.3}$$

where $\langle \alpha \rangle$ is the ensemble mean of power-law exponents for different cells.

5.3 Results

5.3.1 Promotion of myosin II activity

Myosin II in cells plays two structural roles: one is the actin filament cross-linkers; the other is motor proteins. The role of myosin II activity in the ensemble distribution of cell rheology was investigated by myosin II-polymerizing drug calyculin A. Figure 5.2 shows the ensemble distribution (N = 98) of G^* of the untreated and calyculin A-treated cells measured at the center of wells by AFM at different frequencies. The calyculin A-treated cells exhibited similar features as untreated cells, displaying a log-normal distribution with three frequency-dependent features (see Chapter 3) [18,20]. However, the distribution of G^* of treated cells broadened compared with the untreated cells.

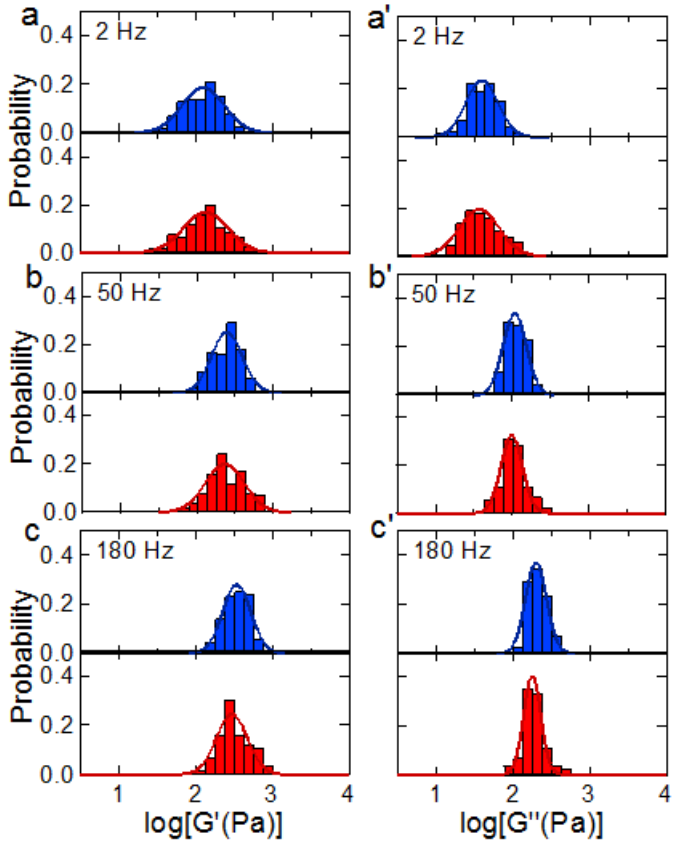

Figure 5.2 Distributions of the storage G' (left) and loss G'' (right) moduli of untreated cells (blue, n = 98) and calyculin A-treated cells (red, n = 98) in microarray wells at different frequencies: (a) 2, (b) 50 and (c) 180 Hz. The solid lines represent the fitted results of untreated and calyculin A-treated cells using a log-normal distribution function.

To further clarify the effect of calyculin A on G^*, the ensemble-averaged $\overline{G}^*$ and standard deviation of the log-normal distribution of G^*, $\sigma_{\log G*}$, were plotted as a function of f in Fig. 5.3. $\overline{G}^*$ increased with f and was fitted well to the power-law model described in Eq. 5.1, as shown in Fig. 5.3 (a) and (b) (Table 5.1). No discernible changes were observed in $\overline{G}^*$ via the polymerization of myosin II. Interestingly, $\sigma_{\log G*}$ of the calyculin A-treated cells was significantly increased and changed quickly with f compared with the results of the untreated cells. These findings are consistent with the notion that the polymerization of myosin has no effect on cell stiffness, but

yields an enhancement in the cell-to-cell variation. It is in agreement with previous result that the mechanical properties of SFs became much more heterogeneous after actomyosin contractile level was increased by calyculin A [36].

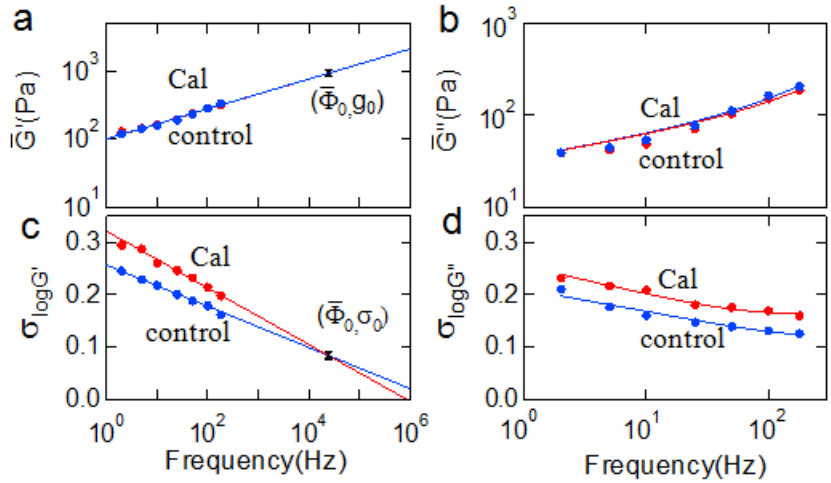

Figure 5.3 Frequency dependence of $\bar{G}'$ (a) and $\bar{G}''$ (b) of untreated (blue) and calyculin A (Cal)-treated (red) cells. Solid lines in (a) and (b) represent the fitted results to Eq. 5.1. The fitting lines cross at the coordinate close to $(\bar{\Phi}_0, \bar{g}_0)$. Frequency dependence of σ of $\log G'$, $\sigma_{\log G'}$, (c) and $\log G''$, $\sigma_{\log G''}$ (d) of untreated (blue) and calyculin A-treated (red) cells. Solid lines in (c) and (d) represent the fitted results using Eqs. 5.2 and A18, respectively.

The frequency-dependent component of the cell-to-cell variation $\tilde{\sigma}_{\log G'}$ was obtained by subtracting $\sigma_{\log g_0}$ from $\sigma_{\log G'}$. Figure 5.4 showed a plot of $\tilde{\sigma}_{\log G'}$ vs. log*f* which was well fitted by Eq. 5.2 (Table 5.1). $\tilde{\sigma}_{\log G'}$ was proportional to log*f* with a slope of $-\sigma_\alpha$ regardless of treatment. $\tilde{\sigma}_{\log G'}$ for treated cell was markedly larger than that of untreated cell at each frequency. $\tilde{\sigma}_{\log G'}$ also exhibited a decay dependent function with $\log \bar{G}$ with a slope of $-\sigma_\alpha / \langle \alpha \rangle$ which was well fitted by Eq.5.3, as shown in the inset

of Fig. 5.4.

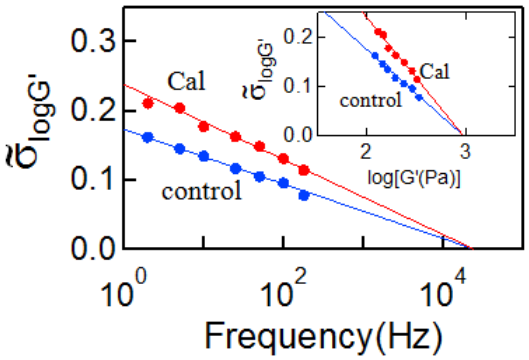

Figure 5.4 Plots of $\tilde{\sigma}_{\log G'}$, which represents $\sigma_{\log G'} - \sigma_{\log g_0}$, as a function of *f*: (1) untreated condition (blue); (2) calyculin A (Cal)-treated condition (red). The inset represents the plot of $\sigma_{\log G'}$ vs. $\log \overline{G'}$. Solid lines represent the fitted results using Eq. 5.2 in main figure and Eq. 5.3 in the inset.

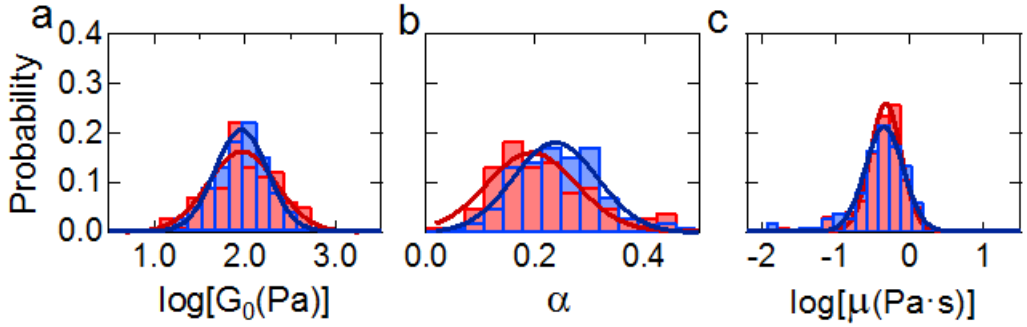

Figure 5.5 Distributions of (a) G_0 as a logarithmic scale, (b) α as a linear scale and (c) μ as a logarithmic scale of untreated (blue) and calyculin A-treated (red) cells. Solid lines represent the fitted results of untreated and calyculin A-treated cells using a log-normal distribution function (a and c) and a normal distribution function (b).

G_0 and the power-law exponent α respectively displayed a log-normal and a normal Gaussian behavior with distributions, in which their distributions broadened after calyculin A treatment, whereas no significant change in mean value of G_0 ($P = 0.43$) and α ($P = 0.14$) was found (Table 5.1, Fig. 5.5). Furthermore, μ exhibited a log-normal

distribution, and its mean value did not change significantly (p = 0.23) after treatment. The results indicate that the polymerization of myosin has no detectable effect on the ensemble mean stiffness but remarkable effect on the cell-to-cell variations. In Fig. 5.6 (a), logG_0 was replotted as a function of α, measured for untreated and calyculin A-treated cells, which were presented in Figs. 5.2-5.5. Owing to the same value of crosspoint ($\overline{\Phi}_0$, $\overline{g}_0$), thus two conditions were well fitted as the same slope by Eq. 3.2 [18]. Moreover, the plot of logG_0 vs. logμ suggests a linear relationship in two conditions [Fig. 5.6 (b)].

	Pair 1		Pair 2	
	untreated (n = 98)	calyculin A (n = 98)	untreated (n = 96)	blebbistatin (n = 96)
$\overline{G}_0$ (Pa) [a]	83.1	90.9	60.9	45.6
$\langle\alpha\rangle$ [a]	0.24	0.22	0.27	0.29
$\overline{\mu}$ (Pa·s) [a]	0.33	0.39	0.34	0.38
$\sigma_{\log G_0}$ [a]	0.29	0.35	0.30	0.24
σ_α [a]	0.08	0.09	0.07	0.07
$\sigma_{\log\mu}$ [a]	0.47	0.33	0.41	0.25
$\overline{\Phi}_0$ (Hz) [b,c]	2.41×10^4	2.41×10^4	1.11×10^4	1.11×10^4
$\sigma_{\log g_0}$ [c]	$0.084^{0.072}$	$0.084^{0.072}$	$0.082^{0.080}$	$0.082^{0.080}$
σ_α [c]	$0.039^{0.002}$	$0.054^{0.002}$	$0.047^{0.003}$	$0.035^{0.003}$
$\sigma_{\log\mu}$ [c]	$0.12^{0.01}$	$0.21^{0.01}$	$0.20^{0.02}$	$0.16^{0.02}$

Table 5.1 Parameter values (mean ± SD) of the power-law rheology of two pairs of cells: (1) untreated and calyculin A-treated cells and (2) untreated and blebbistatin-treated cells. [a] estimates using Eq. 1.1, [b] estimates from the plot of log G' vs. log f using Eq. 5.1 and [c] estimates from the plot of σ vs. log f using Eq. 5.2.

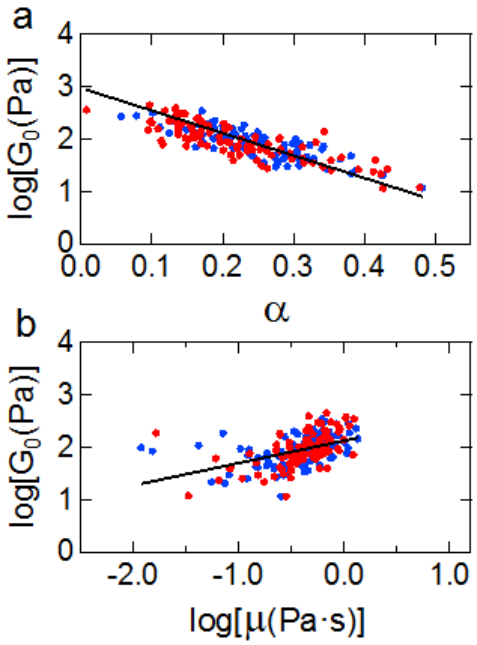

Figure 5.6 Plots of logG_0 vs. α (a) and logG_0 vs. logμ (b) of untreated (blue) and calyculin A-treated (red) cells. Solid lines represent a linear fitting.

5.3.2 Inhibition of myosin II motors

For a deeper understanding the relative contribution of myosin II to cell-to-cell variation in cell rheology, myosin II is inhibited using the specific drug blebbistatin (2-μM). Previous studies reported that blebbistatin inhibits both the cross-linking and motor properties of myosin II by inhibiting its binding of actin filaments [29,36]. Figure 5.7 shows the ensemble distribution (N = 96) of G^* of the blebbistatin-treated and untreated cells measured at the center of wells by AFM at different frequencies. The distribution of G^* of the treated cells appeared to be narrower than that of the untreated cells. To clarify the effect of blebbistatin on G^*, the $\overline{G}^*$ and $\sigma_{\log G*}$ were plotted as a function of f in Fig. 5.8. As shown in Fig. 5.8 (a) and (b), $\overline{G}^*$ was fitted well to the power-law model described in Eq. 5.1 (Table 5.1). Contractile deactivation by blebbistatin caused a greater decrease in $\overline{G}'$ than in $\overline{G}''$. This is consistent with an inhibition of ATPase and reduction of the gliding mobility of myosin II on actin filaments [29]. Interestingly,

as shown in Fig. 5.8 (c) and (d), $\sigma_{\log G*}$ was well fitted by Eq. 5.2 (Table 5.1). $\sigma_{\log G*}$ of the treated cells was significantly reduced and changed less with f compared with the untreated cells. The results showed that depolymerizing myosin II as well as decreasing actin polymerization led to a reduction in the cell-to-cell variation in cell rheology (see Chapters 3 and 4) [18].

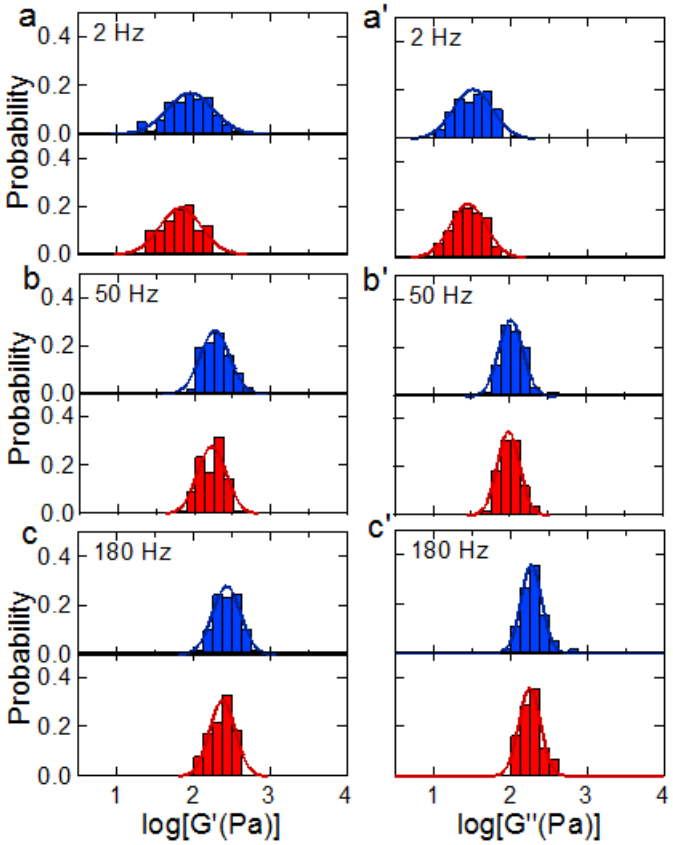

Figure 5.7 Distributions of the storage G' (left) and loss G'' (right) moduli of untreated cells (blue, n = 96) and blebbistatin-treated cells (red, n = 96) in microarray wells at different frequencies: (a) 2, (b) 50 and (c) 180 Hz. The solid lines represent the fitted results of untreated and blebbistatin-treated cells using a log-normal distribution function.

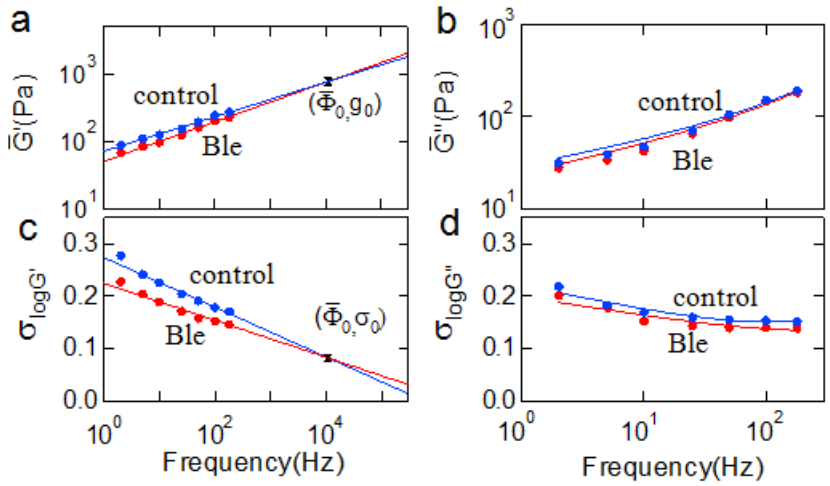

Figure 5.8 Frequency dependence of $\bar{G}'$ (a) and $\bar{G}''$ (b) of untreated (blue) and blebbistatin (Ble)-treated (red) cells. Solid lines represent the fitted results to Eq. 5.1. The fitting lines cross at the coordinate close to $(\bar{\Phi}_0, \bar{g}_0)$. Frequency dependence of $\sigma_{\log G'}$ (c) and $\sigma_{\log G''}$ (d) of untreated (blue) and blebbistatin-treated (red) cells. Solid lines in (c) and (d) represent the fitted results using Eqs. 5.2 and A18, respectively.

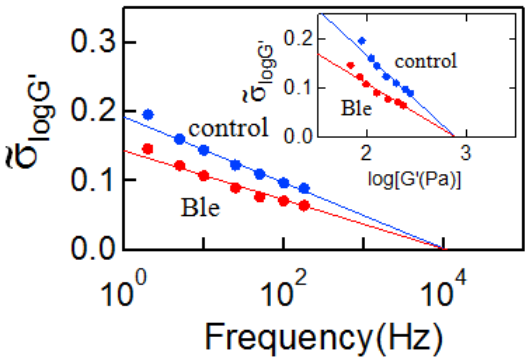

Figure 5.9 Plots of $\tilde{\sigma}_{\log G'}$, which represents $\sigma_{\log G'} - \sigma_{\log g_0}$, as a function of *f*: (1) untreated condition (blue); (2) Blebbistatin-treated condition (red). The inset represents the plot of $\sigma_{\log G'}$ vs. $\log \bar{G}'$. Solid lines represent the fitted results using Eq. 5.2 in main figure and Eq. 5.3 in the inset.

Furthermore, the $\tilde{\sigma}_{\log G'}$ as a function of log*f* was shown in Fig. 5.9. The inset showed the plot of $\tilde{\sigma}_{\log G'}$ vs. $\log \bar{G}'$. After the inhibition of myosin II activity, the frequency and

$\log\overline{G'}$ dependencies of $\tilde{\sigma}_{\log G'}$ were also well fitted by Eqs. 5.2 and 5.3 (Table 5.1), respectively. $\tilde{\sigma}_{\log G'}$ for treated cell was markedly smaller than that of untreated cell at the same frequency or the same magnitude of $\log\overline{G'}$.

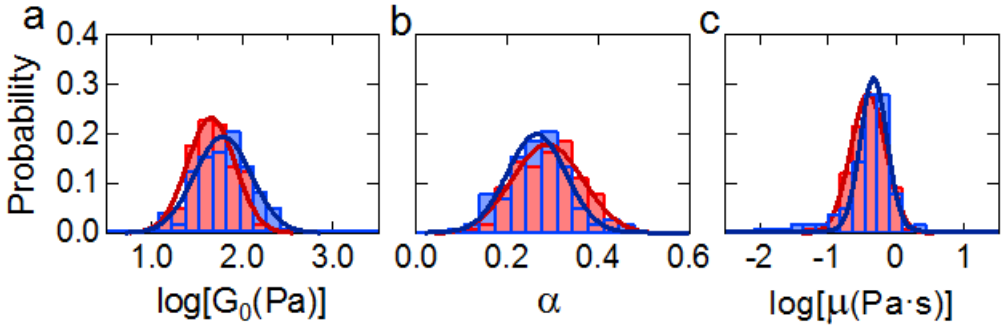

Figure 5.10 Distributions of (a) G_0 as a logarithmic scale, (b) α as a linear scale and (c) μ as a logarithmic scale of untreated (blue) and blebbistatin-treated (red) cells. Solid lines represent the fitted results of untreated and blebbistatin-treated cells using a log-normal distribution function (a and c) and a normal distribution function (b).

After treatment with blebbistatin, G_0 and μ exhibited a log-normal distribution, whereas α was a normal Gaussian distribution (Fig. 5.10). The depolymerization of myosin II in cells resulted in a decrease in G_0 by approximately 25% ($p < 0.01$) and an increase in α ($p = 0.08$) (Table 5.1). I replot $\log G_0$ vs. α, and $\log G_0$ vs. $\log\mu$, measured for untreated and blebbistatin-treated cells, as shown in Fig. 5.11. The results indicate that the depolymerization of myosin II has remarkable effect on the ensemble mean stiffness and the cell-to-cell variation.

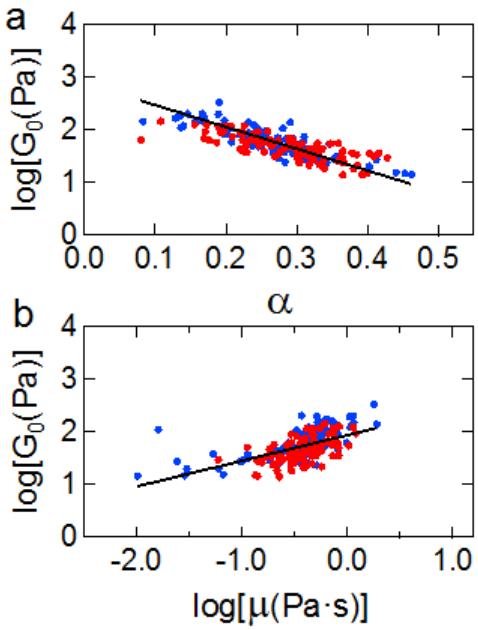

Figure 5.11 Plots of logG_0 vs. α (a) and logG_0 vs. logμ (b) of untreated cell (blue) and blebbistatin A-treated cell (red). Solid lines represent a linear fitting.

5.4 Discussion

5.4.1 Comparison of the frequency-dependent component of cell-to-cell variation

As shown in Figs. 5.3 and 5.8, the complex shear modulus $\overline{G}^*$ and its corresponding standard deviation $\sigma_{\log G*}$ were respectively well fitted by power-law equation and its derivative Equations. Both the curves of $\overline{G'}$ and $\sigma_{\log G*}$ crossed at $f = \bar{\Phi}_0$ with $\bar{g}_0$ and $\sigma_{\log g_0}$, respectively. It has become clear that $\sigma_{\log g_0}$ and $\bar{\Phi}_0$ always present to some fluctuation in any cell population, depending on various experimental errors and the AFM probe indentation. Therefore, $\tilde{\sigma}_{\log G'}$ that represent the variation related to the interaction between actin and myosin is used to compare among different experimental conditions. Figure 5.12 shows $\tilde{\sigma}_{\log G'}$ as a function of f for two pairs of drugs' treatment experiments (Figs. 5.4 and 5.9). Importantly, $\tilde{\sigma}_{\log G'}$'s of untreated cells were

almost same even in different cell samples. The result further supports the notion that $\tilde{\sigma}_{\log G'}$ is invariant in consistent with the results in Chapters 3 and 4 [18]. Moreover, it was found about other relations of $\tilde{\sigma}_{\log G'}$ with f via drugs treatment: (1) $\tilde{\sigma}_{\log G'}$ of calyculin A-treated cells was largely enhanced compared with $\tilde{\sigma}_{\log G'}$ of the control cells; and (2) $\tilde{\sigma}_{\log G'}$ of blebbistatin-treated cells was markedly reduced compared with that of the control cells. Therefore, it is concluded that the frequency dependence of $\tilde{\sigma}_{\log G'}$ originates mainly not only from actin but also myosin, probably their complex heterogeneous structures.

5.4.2 Role of myosin in cell-to-cell variation

The effects of myosin drugs on cell rheology including complex shear modulus G^* and cell-to-cell variation were evaluated. Data from this study provided evidence for the important role of myosin II in cell-to-cell variation. Actin disruption with cytoD greatly altered the rheological behavior of NIH3T3 cells. With the actin largely disassembled, the more fluidlike cytoplasm dominates rheological behavior. The more homogeneity structure of cell cytoskeleton caused a reduction of cell-to-cell variation [18]. The role of myosin II in cell-to-cell variation is a manner similar to that of actin. Inhibiting the actomyosin complex by blebbistatin simultaneously induces a decrease in cell stiffness and cell-to-cell variation. This result shows that the myosin activity makes the meshwork more rigid and dissipative. This is in contrast to the result reported by Van Citters *et al*. that neither the cross-link nor sliding role of any myosin isoform plays a role in cell rheology [33]. However, the decreasing in G^* caused by blebbistatin in the result is consistent with the results of Balland *et al*., whereas the increasing in α is in contrast to the results of Balland *et al*. [29].

Contrarily, the enrichment of myosin enhanced the cell-to-cell variation. A major difference between findings is that the results of the ensemble mean complex shear modulus appear largely insensitive to myosin enrichment, whereas other MTC measurements are strongly affected by myosin perturbation. Actually, the result is consistent with the result of Lu *et al*. in which although the stiffness of the peripheral regions of stress fibers increased significantly, whereas stiffness in the center regions remained essentially unchanged [36]. Furthermore, their finding of the highly significant difference between the peripheral and central regions has further proven the result of the increment of the cell-to-cell variation. The interpretation of the result is that the drug calyculin A caused the spacing at the ends of the fibers to be smaller and those near the center of the stress fibers to be larger than the homogeneous spacing observed before calyculin A treatment. The two pharmacological interventions affect the roles differently, providing additional clues regarding myosin's effect on cell mechanics.

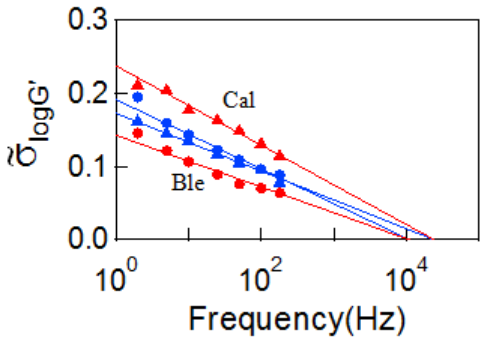

Figure 5.12 Plot of $\tilde{\sigma}_{\log G'}$ of $\log G'$ as a function of $\log f$. The results obtained from two cell samples in Figs. 5.4 and 5.9 are replotted: (a) one sample is untreated (triangle, blue) and calyculin A-treated (triangle, red); (b) the other is untreated (circle, blue) and blebbistatin-treated (circle, red) cells. Solid lines represent the fitted result to Eq. 5.2.

5.5 Conclusions

To my knowledge, the data presented herein is the first time to describe the role of

myosin II in governing cell-to-cell variation of cell rheology. Two pharmacological drugs affect the roles differently, providing additional clues regarding myosin effects on cell-to-cell variation in cell rheology. Based on the power-law model, I attempted to estimate the frequency-dependent component of the cell–to-cell variations, $\tilde{\sigma}_{\log G'}$, of different conditions, allowing us to distinguish actual changes in the cell-to-cell variation in the cytoskeleton rheology. $\tilde{\sigma}_{\log G'}$'s observed from different cell samples under the same conditions were almost identical and closed to zero at $f = \bar{\Phi}_0$. Moreover, $\tilde{\sigma}_{\log G'}$ of cells treated with calyculin A or blebbistatin was markedly increased or decreased, indicating that frequency-dependent $\tilde{\sigma}_{\log G'}$ was also strongly related to the myosin II. The approach provides a possible estimation for the variable mechanical properties of the cells and helps us to further understand the mechanical role of SFs under a variety of conditions.

5.6 References

1. Kollmannsberger, P. and B. Fabry. 2011. Linear and nonlinear rheology of living cells. Annu. Rev. Mater. Res. 41:75-97.
2. Alberts, B., A. Johnson, J. Lewis, M. Raff, K. Roberts, and P. Walter. 2008. Molecular biology of the cell. 5th Edition. Garland Science, New York, NY.
3. Pullarkat, P. A., P. A. Fernandez, and A. Ott. 2007. Rheological properties of the eukaryotic cell cytoskeleton. Phys. Rep. 449:29-53.
4. Chen, D. T. N., Q. Wen, P. A. Janmey, J. C. Crocker, and A. G. Yodh. 2010. Rheology of soft materials. Annu. Rev. Condens. Matter Phys. 1:301-322.
5. Ingber, D. E. 2003. Tensegrity I. Cell structure and hierarchical systems biology. J. Cell Sci. 116:1157-1173.
6. Discher, D. E., P. Janmey, and Y. L. Wang. 2005. Tissue cells feel and respond to the stiffness of their substrate. Science 310:1139-1143.
7. Janmey, P. A. and C. A. McCulloch. 2007. Cell mechanics: integrating cell responses to mechanical stimuli. Ann. Rev. Biomed. Eng. 9:1-34.
8. Janmey, P. A. and D. A. Weitz. 2004. Dealing with mechanics: mechanisms of force transduction in cells. Trends Biochem. Sci. 29:364-370.
9. Vogel, V. and M. Sheetz. 2006. Local force and geometry sensing regulate cell functions. Nat. Rev. Mol. Cell Biol. 7:265-275.
10. Trepat, X., G. Lenormand, and J. J. Fredberg. 2008. Universality in cell mechanics. Soft Matter 4:1750-1759.
11. Kollmannsberger, P. and B. Fabry. 2009. Active soft glassy rheology of adherent cells. Soft Matter 5:1771-1774.
12. Fabry, B., G. N. Maksym, J. P. Butler, M. Glogauer, D. Navajas, and J. J. Fredberg.

2001. Scaling the microrheology of living cells. Phys. Rev. Lett. 87:148102-1-148102-4.

13. Fabry, B., G. N. Maksym, J. P. Butler, M. Glogauer, D. Navajas, N. A. Taback, E. J. Millet, and J. J. Fredberg. 2003. Time scale and other invariants of integrative mechanical behavior in living cells. Phys. Rev. E 68:041914-1-041914-18.
14. Chowdhury, F., S. Na, O. Collin, B. Tay, F. Li, T. Tanaka, D. E. Leckband, and N. Wang. 2008. Is cell rheology governed by nonequilibrium-to-equilibrium transition of noncovalent bonds? Biophys. J. 95:5719-5727.
15. Deng, L. H., X. Trepat, J. P. Butler, E. Millet, K. G. Morgan, D. A. Weitz, and J. J. Fredberg. 2006. Fast and slow dynamics of the cytoskeleton. Nat. Mater. 5:636-640.
16. Balland, M., N. Desprat, D. Icard, S. Fereol, A. Asnacios, J. Browaeys, S. Henon, and F. Gallet. 2006. Power laws in microrheology experiments on living cells: comparative analysis and modeling. Phys. Rev. E 74:021911-1-021911-17.
17. Desprat, N., A. Richert, J. Simeon, and A. Asnacios. 2005. Creep function of a single living cell. Biophys. J. 88:2224-2233.
18. Cai, P. G., Y. Mizutani, M. Tsuchiya, J. M. Maloney, B. Fabry, K. J. Van Vliet, and T. Okajima. 2013. Quantifying cell-to-cell variation in power-law rheology. Biophys. J. 105:1093-1102.
19. Massiera, G., K. M. Van Citters, P. L. Biancaniello, and J. C. Crocker. 2007. Mechanics of single cells: rheology, time dependence, and fluctuations. Biophys. J. 93:3703-3713.
20. Hiratsuka, S., Y. Mizutani, M. Tsuchiya, K. Kawahara, H. Tokumoto, and T. Okajima. 2009. The number distribution of complex shear modulus of single cells

measured by atomic force microscopy. Ultramicroscopy 109:937-941.

21. Miyaoka, A., Y. Mizutani, M. Tsuchiya, K. Kawahara, and T. Okajima. 2011. Rheological properties of growth-arrested fibroblast cells under serum starvation measured by atomic force microscopy. Jpn. J. Appl. Phys. 50:08LB16-1-08LB16-4.
22. Hoffman, B. D. and J. C. Crocker. 2009. Cell mechanics: dissecting the physical responses of cells to force. Ann. Rev. Biomed. Eng. 11:259-288.
23. Yamada, S., D. Wirtz, and S. C. Kuo. 2000. Mechanics of living cells measured by laser tracking microrheology. Biophys. J. 78:1736-1747.
24. Puig-de-Morales, M., E. Millet, B. Fabry, D. Navajas, N. Wang, J. P. Butler, and J. J. Fredberg. 2004. Cytoskeletal mechanics in adherent human airway smooth muscle cells: probe specificity and scaling of protein-protein dynamics. Am. J. Physiol. Cell Physiol. 287:C643-C654.
25. Laudadio, R. E., E. J. Millet, B. Fabry, S. S. An, J. P. Butler, and J. J. Fredberg. 2005. Rat airway smooth muscle cell during actin modulation: rheology and glassy dynamics. Am. J. Physiol. Cell Physiol. 289:C1388-C1395.
26. Dahl, K. N., A. J. Engler, J. D. Pajerowski, and D. E. Discher. 2005. Power-law rheology of isolated nuclei with deformation mapping of nuclear substructures. Biophys. J. 89:2855-2864.
27. Alcaraz, J., L. Buscemi, M. Grabulosa, X. Trepat, B. Fabry, R. Farre, and D. Navajas. 2003. Microrheology of human lung epithelial cells measured by atomic force microscopy. Biophys. J. 84:2071-2079.
28. Hoffman, B. D., G. Massiera, K. M. Van Citters, and J. C. Crocker. 2006. The consensus mechanics of cultured mammalian cells. Proc. Natl. Acad. Sci. USA 103:10259-10264.

29. Balland, M., A. Richert, and F. Gallet. 2005. The dissipative contribution of myosin II in the cytoskeleton dynamics of myoblasts. Eur. Biophys. J. 34:255-261.

30. Smith, B. A., B. Tolloczko, J. G. Martin, and P. Grütter. 2005. Probing the viscoelastic behavior of cultured airway smooth muscle cells with atomic force microscopy: stiffening induced by contractile agonist. Biophys. J. 88:2994-3007.

31. Overby, D. R., B. D. Matthews, E. Alsberg, and D. E. Ingber. 2005. Novel dynamic rheological behavior of individual focal adhesions measured within single cells using electromagnetic pulling cytometry. Acta Biomater. 1:295-303.

32. Stamenovic, D., N. Rosenblatt, M. Montoya-Zavala, B. D. Matthews, S. Hu, B. Suki, N. Wang, and D. E. Ingber. 2007. Rheological behavior of living cells is timescale-dependent. Biophys. J. 93:L39-L41.

33. Van Citters, K. M., B. D. Hoffman, G. Massiera, and J. C. Crocker. 2006. The role of F-actin and myosin in epithelial cell rheology. Biophys. J. 91:3946-3956.

34. Lieleg, O., M. M. A. E. Claessens, Y. Luan, and A. R. Bausch. 2008. Transient binding and dissipation in cross-linked actin networks. Phys. Rev. Lett. 101:108101-1-108101-4.

35. Goff, L. L., F. Amblard, and E. M. Furst. 2002. Motor-driven dynamics in actin-myosin networks. Phys. Rev. Lett. 018101-1-018101-4.

36. Lu, L., S. J. Oswald, H. Ngu, and F. C. –P. Yin. 2008. Mechanical properties of actin stress fibers in living cells. 95:6060-6071.

37. Mizutani, Y., M. Tsuchiya, S. Hiratsuka, K. Kawahara, H. Tokumot, and T. Okajima. 2008. Elasticity of living cells on a microarray during the early stages of adhesion measured by atomic force microscopy. Jpn. J. Appl. Phys. 47:6177-6180.

38. Mahaffy, R. E., S. Park, E. Gerde, J. Kas, and C. K. Shih. 2004. Quantitative

analysis of the viscoelastic properties of thin regions of fibroblasts using atomic force microscopy. Biophys. J. 86:1777-1793.

39. Radmacher, M., R. W. Tillmann, M. Fritz, and H. E. Gaub. 1992. From molecules to cells: imaging soft samples with the atomic force microscope. Science 257:1900-1905.
40. Landau, L. and E. M. Lifshitz. 1986. Theory of elasticity. Oxford: Pergamon Press.
41. Alcaraz, J., L. Buscemi, M. Puig-de-Morales, J. Colchero, A. Baro, and D. Navajas. 2002. Correction of microrheological measurements of soft samples with atomic force microscopy for the hydrodynamic drag on the cantilever. Langmuir 18:716-721.

Chapter 6: Quantifying Temporal Variation of Single Cell in Power-Law Rheology

The spatial dependence of cell-to-cell variation and the role of the actin-myosin complex in cell-to-cell variation have been investigated in previous chapters. On the other hand, the temporal variation of G^* has not been fully understood. In this chapter, the temporal variation of rheological properties of single cells was investigated under a confined condition where cell migration was highly restricted and cell shape was unchanged. A long-time evolution of single cell rheology was probed at the same measurement location within the cell by atomic force microscopy. Based on a power-law rheology model, it is found that the temporal variation of adherent cells is quantitatively consistent with the ensemble variation, indicating that rheological properties of cells in the confined condition follow an ergodicity condition. The time correlation function of G^* shows that the fluctuations of cell rheological properties are not a random manner but transit from one small region to others with a characteristic time of about several to tens of minutes so that all the possible mechanical states of the ensemble one are traced.

6.1 Introduction

Cells have inherent heterogeneous network structures of cytoskeleton (CSK), which is organized with a complex network of three types of filaments such as actin filaments, microtubules, and intermediate filaments [1-4]. Among those filaments, actin filaments are the most essential component of CSK for determining rheological properties of adherent cells [5-13]. Indeed, actin filament networks formed in the cells [1-4,14] are dynamically remodeled and highly adapted according to the surrounding environments [15-17] and external stresses. A detailed knowledge of the temporal change in rheological properties of cells is crucial to understand how network-forming actin filaments in living cells are self-organized with fluctuations that retain an ability to remodel and adjust flexibly with respect to various external changes. Massiera *et al*. [18] succeeded to quantify the temporal variation of rheological properties of adherent singe cells cultured on a flat substrate by monitoring the motion of micro-beads attached to the actin filaments in the cells under external forces such as magnetic force and optical pressure. The experiments showed that the temporal distributions of cell mechanical parameters were consistent with those observed in the ensemble (number) distributions [8,18-22], that is, the frequency-dependent shear modulus exhibited a log-normal distribution while a power-law exponent characterizing the power-law behavior of the shear modulus was distributed in a normal distribution. Furthermore, the temporal variation during 30 min measurement was smaller than that observed among an ensemble one. They considered that single cell rheology was not statistically ergodic [18].

Such adherent cells cultured on flat substrates can migrate macroscopically. Remodeling of actin filaments causes a translational movement of cell, and the shape

and size of cell are changed accordingly. Thus, it is important to notice that the temporal fluctuations observed in cells on flat substrates include two types of time variations such as a fluctuation owing to the translational movement of the whole cell and an intrinsic fluctuation occurring in local regions of cells without changing the whole cell shape and size. In particular, the latter temporal fluctuation is deeply associated with the mechanism how the filament network in cell fluctuates arising from the biochemical and molecular events of actin filaments. In this context, Bursac *et al.*[15] reported that the fluctuation of microbeads attached on cell surface through CSK with a specific binding exhibited a super-diffusive motion, and the dynamic behavior of the remodeling of actin filaments was the same in both cases of cells cultured on a micro-patterned substrate with a confined condition and sub-confluent cells.

The aim of this study is to elucidate the frequency-dependent component of temporal variation of rheological properties of single mouse fibroblast cells under a confined condition where cell migration is highly restricted and cell shape is unchanged. By probing single cells placed in the wells of microarray with atomic force microscopy (AFM), a long-time evolution of single cell rheology was traced at the same location. The estimation suggests that rheological properties of cells in the confined condition follow an ergodicity condition, in which the cell mechanical state transits in all possible states where cell size and shape are unchanged. Furthermore, it is found that the rheological properties evolve in their possible states with a relaxation time of several and tens of minutes.

6.2 Materials and Methods

6.2.1 Cell samples

Detailed preparation procedures for cells arranged on a microarray substrate have been

described in Section 2.2.2. Briefly, mouse fibroblast NIH3T3 cells (ATCC) were deposited in hexagonal microarray wells having a width of 20 μm (LiveCell Array^{TM}; Nunc), and were immediately incubated for 12 h in complete medium (Dulbecco's modified Eagle's medium containing fetal bovine serum). For AFM measurements, the medium was replaced with a CO_2-independent medium (Invitrogen).

6.2.2 Measurements of cell rheology by AFM

A detailed setup of AFM system and the calibration have been described in Section 2.2.4. Briefly, a commercial AFM (MFP-3D AFM; Asylum Research, Santa Barbara, CA) was used to examine the rheology of NIH3T3 cells [Fig. 6.1 (a)]. A colloidal probe cantilever where a silica bead with a radius R of ~2.5 μm (Funakoshi, Tokyo, Japan) was attached to the apex of the AFM tip of cantilever (BioLever mini, BL-AC40TS-C2; Olympus, Tokyo, Japan) was used for the force modulation measurements [8,22-24]. The initial loading force was less than 650 pN, and the modulation frequency was changed in a stepwise manner as f = 2, 5, 10, 25, 50, 100, and 180 Hz with an amplitude of 10 nm. The amplitude and phase shift of the cantilever displacement with respect to the reference signal were detected with a lock-in amplifier (7260, SEIKO EG&G Co, Tokyo, Japan).

Firstly, a few of single cells were successively measured at the center of wells in cell microarray substrate (essentially atop the nuclei) for 160 min with an interval time 2 min [Fig. 6.1 (b)]. Next, the cells were incubated in 2-μM cytochalasin D (cytoD) for 20 min, and the same cells were measured again at the same positions by AFM. The fluorescence image of nuclei of untreated cells cultured in microarray wells was shown in Fig. 6.1 (c).

The complex shear modulus G^* is given by the Hertzian contact model [25-29] with a viscous drag factor F_d^* (see Section 2.1.4) [25,27]. The phase shift observed in the frequency range of 2–180 Hz mainly resulted from the mechanical response of AFM head and thus was calibrated at different frequencies using a stiff cantilever in contact with a clean glass cover slip in air.

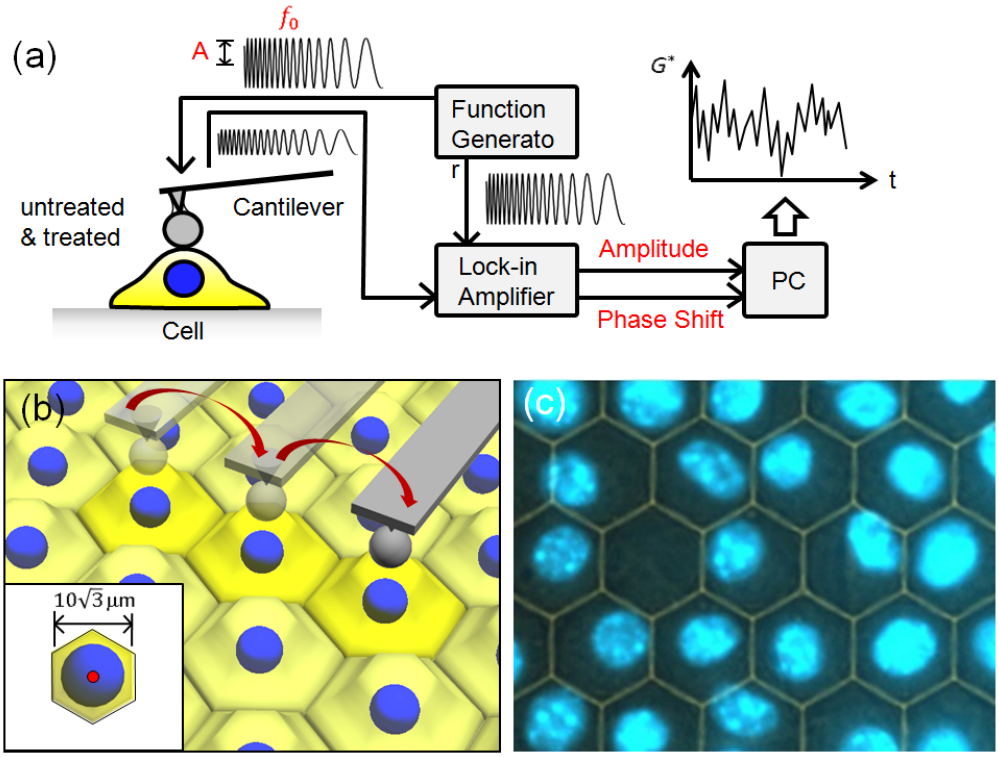

Figure 6.1 (a) Schematic of measurement of G^* by the AFM force modulation. G^* fluctuated with time lapse. (b) Measurements of G^* of single cell with a microarray substrate. (c) Fluorescence image of nuclei of cells cultured in microarray wells. The untreated cell was measured at the center of well and the same single cell treated with cytoD was measured again at the same location.

6.2.3 Data analysis

G' and G'' as a function of f obtained in time course was analyzed using the Igor Pro software (WaveMetrics, Lake Oswego, OR) with a built-in global fitting procedure. The

detailed method of data analysis was described in Section 2.3. G' and G'' as a function of f were fitted to the power-law structural damping model with additional Newtonian viscosity as given by Eq. 1.1 [6,7,30]. The parameters in power-law structural damping model are α with being the power-law exponent, G_0 with being a scale factor of the modulus at a scale factor of frequency f_0 (~1 Hz), and μ with being the Newtonian viscous damping coefficient. The standard deviations of G', G'', and the corresponding power-law parameters were calculated by Eq. 2.10.

6.2.4 Soft glassy rheology of cell deformability

According to Soft glassy rheology (SGR), the mechanical state of cells in average evolves an energy landscape with a high number of local minima [2,3,5-8]. The typical depth of these minima is much larger than the thermal noise, and thus the temporal evolution in this energy landscape proceeds due to activation energy such as a loading force in case of active micro-rheological measurements. As the frequency for the loading force is increased, G' increases as a power-law manner where the power-law exponent corresponds to a degree that the mechanical state of cell is suffering from hopping among local minima. At the higher frequency limit of $f = \Phi_0$ where the modulus $G' = g_0$ is unchanged, it is considered that the cell mechanical state is no longer able to escape from the trapped local minima. Hence, I assume that the time averaged storage modulus $\overline{G}'$ of each single cell is expressed as [2,5-6]

$$\overline{G}' = \overline{g}_0 \left(\frac{f}{\overline{\Phi}_0} \right)^{\alpha}, \tag{6.1}$$

in which the point ($\overline{\Phi}_0$, $\overline{g}_0$) can be estimated by extrapolating the $\overline{G}'$ vs. f curves measured under control (untreated) and cytoD-treated conditions. According to the soft glassy rheology model, the standard deviation of $G', \sigma_{\log G'}$, is approximately expressed

as [8,31]

$$\sigma_{\log G'} = \sigma_{\log g_0} + (\log \overline{\Phi}_0 - \log f)\sigma_\alpha , \tag{6.2}$$

in which $\sigma_{\log g_0}$ is the standard deviation of the storage modulus at around $f = \bar{\Phi}_0$ and σ_α is the standard deviation of power-law exponent α for different time states of single cell. The first term on the right-hand side is independent of *f*, and the second term is a frequency-dependent component, which is denoted as $\tilde{\sigma}_{\log G'}$. Similarly, $\sigma_{\log G'}$ can also be expressed as a function of $\log G'$ [8]:

$$\sigma_{\log G'} = \sigma_{\log g_0} + \frac{\sigma_\alpha}{\langle \alpha \rangle}(\log \overline{g}_0 - \log \overline{G}'), \tag{6.3}$$

where $\langle \alpha \rangle$ is the time mean value of α for different time states of single cell.

6.3 Results

Figure 6.2 (a) and (b) show a typical time course evolution of *G*′ and *G*″, respectively, at different frequencies measured at the center of a cell placed in the microarray well. It was clearly seen that *G*′ and *G*″ markedly fluctuated with time under control condition as observed by magnetic twisting cytometry (MTC) or laser tracking microrheology (LTM) [15,18] whereas the variation of the fluctuation amplitude in the time course of *G*′ and *G*″ became small after treated by cytoD. It was noted that the fluctuation profiles of time course in both *G*′ and *G*″ at different frequencies were highly synchronized, indicating the moduli follow a frequency-dependent function in time. Moreover, the ratio of *G*″ to *G*′ of cells at 10 Hz, *G*″/ *G*′, was converged around 0.2-0.4 in the control condition and markedly increased to around 0.7 in the cytoD-treated condition [Fig. 6.2 (c)], showing a structural damping behavior depending on the CSK structures.

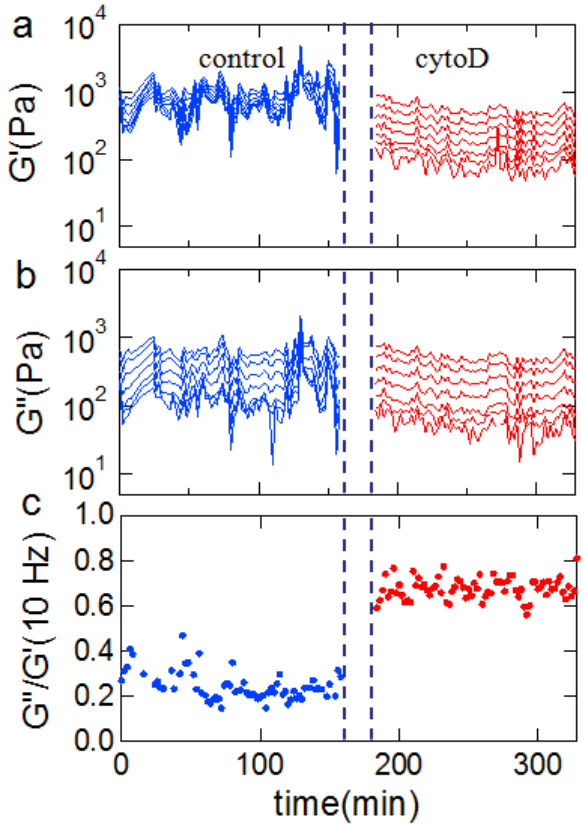

Figure 6.2 Time course of the rheological properties of NIH3T3 cell during the administration of cytoD at 160 min. G' (a) and G'' (b) became more stable after cytoD treatment, whereas G''/G' (10 Hz) (c) is transiently increased. The force modulation was examined at the center of the well with time interval 2 min.

Figure 6.3 shows the temporal distribution of G' and G''. Clearly, the distribution exhibited a log-normal, and the distribution became narrower with f. Moreover, it was found that the treatment with cytoD caused the decrease in the width of distribution and $\bar{G}^*$. Those features were the same as those observed in the ensemble distribution (see Chapters 3-5).

The frequency-dependence of $\bar{G}^*$ and the standard deviation, σ, of G^* distribution, $\sigma_{\log G*}$ shown in Fig. 6.3 is plotted in Fig. 6.4. $\bar{G}^*$ was well fitted to Eq. 6.1, showing that time-averaged value of G^* of cells followed the power-law rheology in the

frequency range of 2-180 Hz, as observed in ensemble experiments (see Chapters 3-5) [5-8]. The disruption of actin filament polymerization resulted in a decrease in G_0 and an increase in the power-law exponent α. For the temporal variation of those rheological parameters, it could be seen that G_0 and μ exhibited a log-normal distribution whereas α was a normal Gaussian (Fig. 6.5). Moreover, the variations of G_0 and α were reduced as the actin filaments were depolymerized with cytoD.

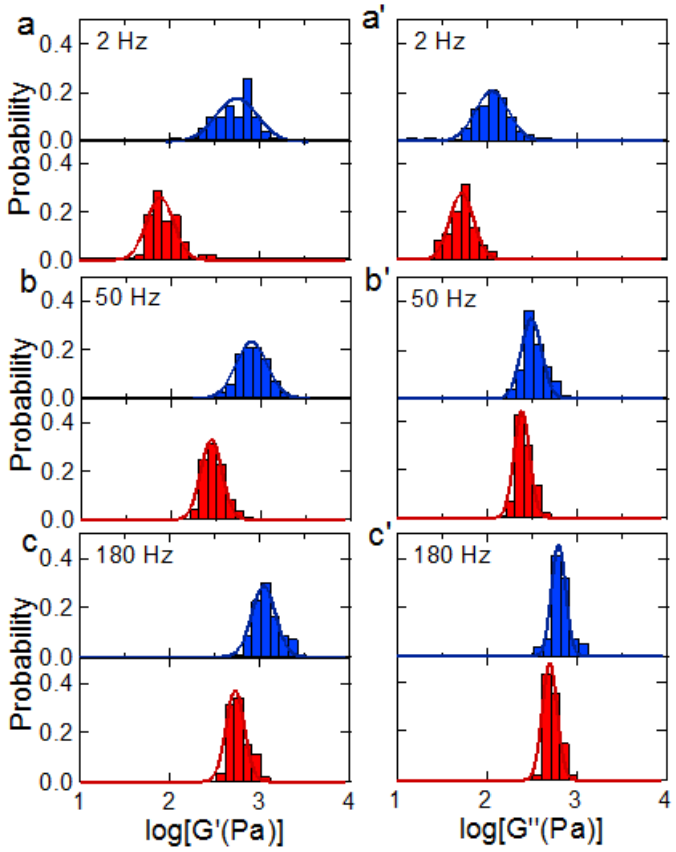

Figure 6.3 Temporal distributions of G' (left) and G'' (right) moduli of single cell of untreated condition (blue) and cytoD-treated condition (red) in microarray well at different frequencies: (a) 2, (b) 50 and (c) 180 Hz. The solid lines represent the fitted results of untreated and treated cells using a log-normal distribution function.

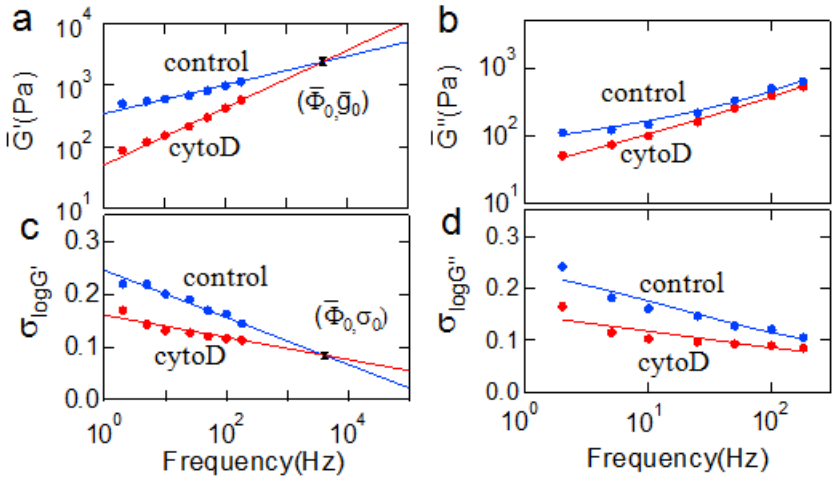

Figure 6.4 Frequency dependences of [$\bar{G}'$ (a) and $\bar{G}''$ (b)] of untreated (blue) and treated (red) conditions. Solid lines in (a) and (b) represent the fitted results to Eq. 1.1. The point where the curves of $\bar{G}'$ intersect is defined as $\bar{G}' = \bar{g}_0$ at $f = \bar{\Phi}_0$. Frequency dependences of $\sigma_{\log G'}$ (c) and $\sigma_{\log G''}$ (d) of untreated (blue) and treated (red) conditions. Solid lines in (c) and in (d) represent the fitted results using Eqs. 6.2 and A18, respectively.

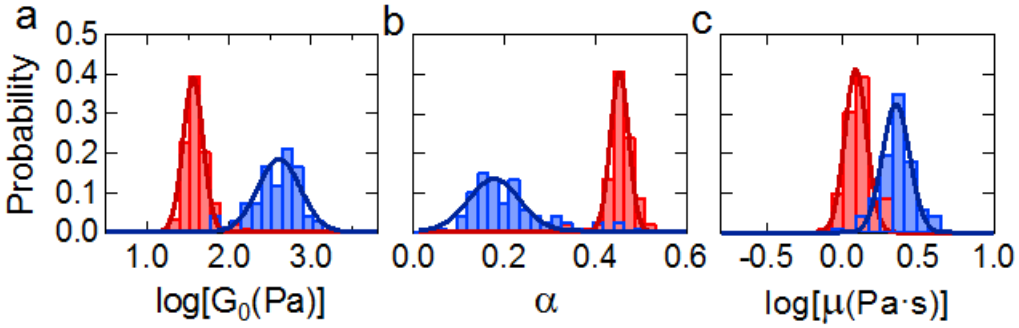

Figure 6.5 Temporal distributions of (a) G_0 on a logarithmic scale, (b) α on a linear scale and (c) μ on a logarithmic scale of untreated (blue) and treated (red) conditions of single cell. Solid lines represent the fitted results of untreated and treated cells using a normal distribution function (b) and a log-normal distribution function (a and c).

It was clearly shown in Fig. 6.4 (c) that the frequency-dependent $\sigma_{\log G'}$ was well fitted to Eq. 6.2 with the point ($\bar{\Phi}_0$, $\sigma_{\log g_0}$). Figure 6.6 showed the frequency-dependent component of $\sigma_{\log G'}$, $\tilde{\sigma}_{\log G'}$. The $\tilde{\sigma}_{\log G'}$ was reduced as the

actin filaments were depolymerized with cytoD. The reduction in $\tilde{\sigma}_{\log G'}$ was independent of logG' (see the inset of Fig. 6.6). This indicates that the temporal variation of G' is strongly coupled with the CSK such as the actin filaments structures and their remodeling.

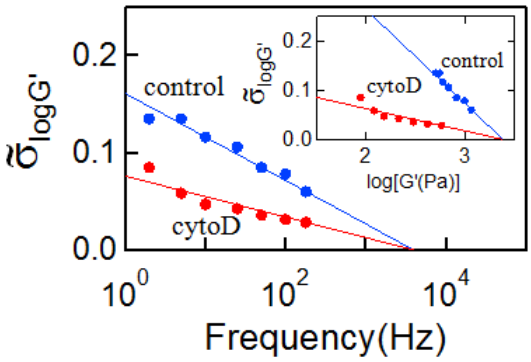

Figure 6.6 Plot of $\tilde{\sigma}_{\log G'}$, which represents $\sigma_{\log G'} - \sigma_{\log g_0}$, as a function of log$f$: (1) untreated condition (blue); (2) cytoD treated condition (red). Solid lines represent the fitted results using Eq. 6.2 in main figure. The inset is plotted $\sigma_{\log G'}$ as a function of $\log \overline{G}'$. Solid lines represent the fitted results using Eq. 6.3 in the inset.

6.4 Discussion

6.4.1 Relationship between ensemble and temporal variations

In different sets of ensemble variation experiments, the magnitude of $\sigma_{\log G'}$ is quite different owning to sample variation such as instrumental noise and day-to-day influences under in vitro culture. Thus, $\tilde{\sigma}_{\log G'}$ is used to compare after subtracting $\sigma_{\log g_0}$. Performing sample averaging in $\tilde{\sigma}_{\log G'}$ of different experiments leads to a mean value. Consistently, the mean value of the frequency-dependent component of the temporal variation $\tilde{\sigma}_{\log G'}$ (N ~ 7) and ensemble variation $\tilde{\sigma}_{\log G'}$ (N ~ 8) are compared in Fig. 6.7. I observed that $\tilde{\sigma}_{\log G'}$'s for temporal and ensemble variations exhibited

similar frequency-dependent behavior and had the same value. The same property was further observed in $\tilde{\sigma}_{\log G''}$ of temporal and ensemble variations (inset of Fig. 6.7). These mean that the variation of single cell resulted from the temporal remodeling of CSK is comparable to the individual differences, confirming that single cell under a confined condition behaves as an ergodic way. It is in contrast to previous study of Massiera *et al*. that no statistically ergodic behavior was observed in their experiment time [18]. Some possibilities are considered for the discrepancy. Firstly, Massiera *et al*. may not get enough measurement time to obtain the all possible states of single cell. Certainly, different cell types correspond to different characteristic time. Secondly, this ergodic behavior of single cell may only exist in the confined condition. Some experiments are needed to discrimination between these possibilities.

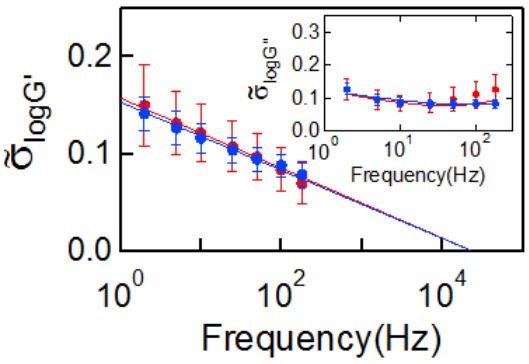

Figure 6.7 Comparison of frequency-dependent $\tilde{\sigma}_{\log G'}$ for temporal (blue) and ensemble variations (red). The inset is the comparison of frequency-dependent $\tilde{\sigma}_{\log G''}$ for temporal (blue) and ensemble variation (red). The data is the sample averaged result: N ~ 7 for temporal variation and N ~ 8 for ensemble variation. The solid lines represent the fitting result using Eqs. 6.2 and A18 [8].

6.4.2 Reserved aging process in time fluctuation of G^*

The obtained time course of G^* is seen to assess ongoing CSK remodeling events in single cell (Fig. 6.2). Recent studies reported that age-dependent changes in the

viscoelastic properties of soft glass material have been elucidated, in which a decrease or an increase in the network elasticity was found over time [16,32]. In the aging process, the system evolves slowly into more stable micro-configurations through intermittent transitions from one metastable state to another [32]. In my time series measurement, single cell rheology fluctuated with time whereas no softening or stiffing tendency was found. In contrast to some other reports, the aging process of single cell system is not obvious in this experimental measurement time within several hours. According to the report of Bursac *et al*., if the external force is added on the cell, the aging will be reversed and the system is rejuvenated [16].

6.4.3 Characterization of relaxation time of CSK remodeling

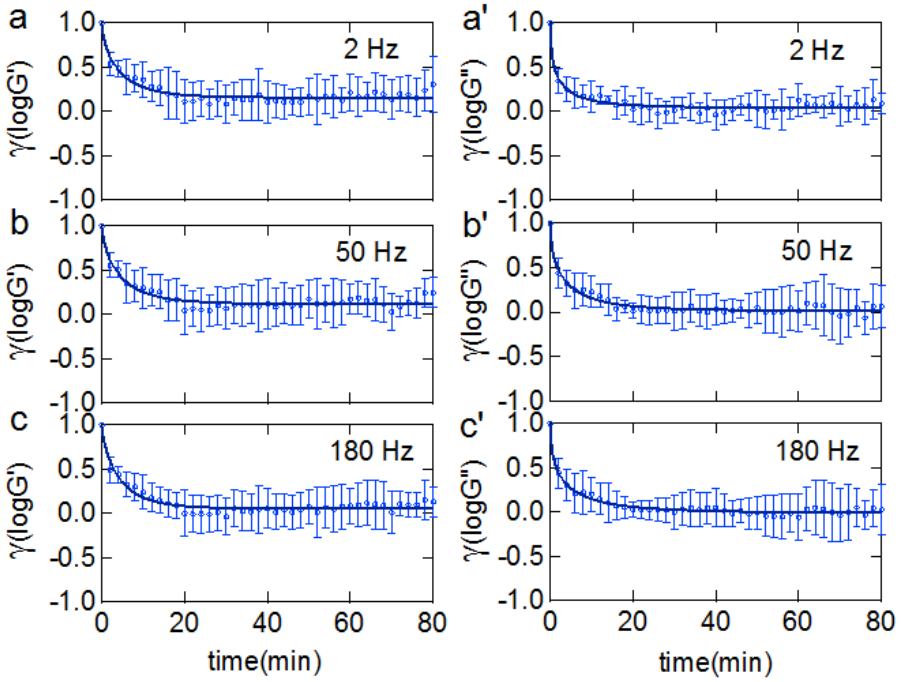

Figure 6.8 Autocorrelation function of $\gamma_{\log G'}$ (left) and $\gamma_{\log G''}$ (right) of untreated single cell at different frequencies: (a) 2, (b) 50 and (c) 180 Hz. The result is the mean value of seven single cells. The solid lines represent the fitted results by the stretching exponential function $\gamma_{\log G^*} \sim \gamma_0 + \gamma_A \exp\left[-(t/\tau_\gamma)^{\beta_\gamma}\right]$.

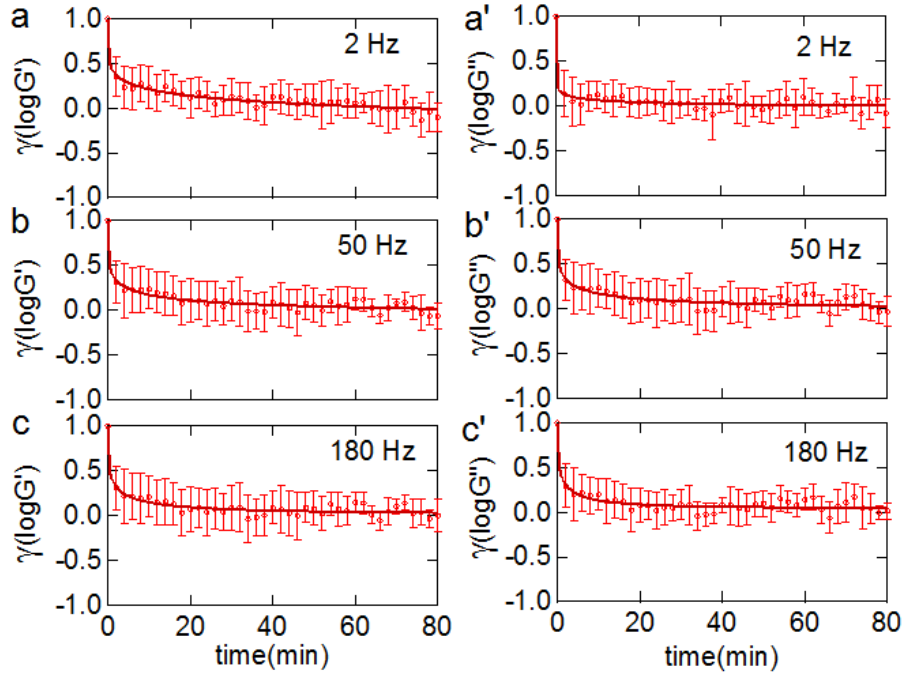

Figure 6.9 Autocorrelation function of $\gamma_{\log G'}$ (left) and $\gamma_{\log G''}$ (right) of treated single cell at different frequencies: (a) 2, (b) 50 and (c) 180 Hz. The result is the mean value of seven single cells. The solid lines represent the fitted results by stretching exponential function $\gamma_{\log G^*} \sim \gamma_0 + \gamma_A \exp\left[-(t/\tau_\gamma)^{\beta_\gamma}\right]$.

For a more detailed understanding of the time evolution of single cell rheology, the statistical properties of cell rheology were analyzed during a brief time interval. The corresponding autocorrelation of G^*, $\gamma_{\log G^*}$, was calculated for different frequencies under untreated and treated conditions (Figs. 6.8 and 6.9). $\gamma_{\log G^*}$ of both untreated cell and treated cell decreased quickly and became decorrelation over time. It seems likely that the magnitude of $\gamma_{\log G^*}$ exhibits frequency dependence at a given time. The magnitude of $\gamma_{\log G^*}$ that is related to the temporal heterogeneity controls the dynamics of the interaction network.

Correlation functions can be well fitted with the exponential stretching function

$\gamma_{\log G^*} \sim \gamma_0 + \gamma_A \exp\left[-(x/\tau_\gamma)^{\beta_\gamma}\right]$ (Fig. 6.10). Comparing correlation functions for different frequencies, G' and G'' of untreated cell show a same constant value of the characteristic time τ_γ of several minutes (Fig. 6.10). This means that the frequency does not influence the decorrelation process; in a word, they have the same speed of the decorrelation process in the single cell under untreated condition. One the other hand, the characteristic time τ_γ of treated cell is larger than that of untreated cell at low frequencies and the difference becomes small at high frequency. Moreover, depolymerization of actin filaments causes a decrease of fitting stretching exponent β_γ without the difference between G' and G''. For those results, it is conjectured that the decorrelation process becomes slowly owing to the enhancement of spatial homogeneity in actin networks by cytoD treatment.

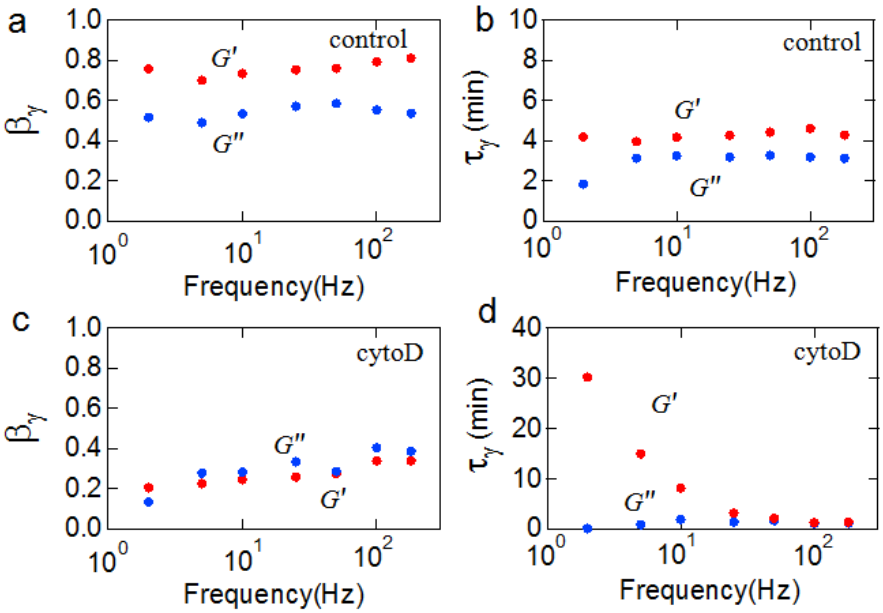

Figure 6.10 Frequency dependence of the stretching exponent β_γ (a, c) and the characteristic decay time τ_γ (b, d) of $\gamma_{\log G^*}$ for G' (red) and G'' (blue) of untreated cell (a, b) and treated cell (c, d). β_γ and τ_γ were extracted from the fit by an exponential function $\gamma_{\log G^*} \sim \gamma_0 + \gamma_A \exp\left[-(x/\tau_\gamma)^{\beta_\sigma}\right]$.

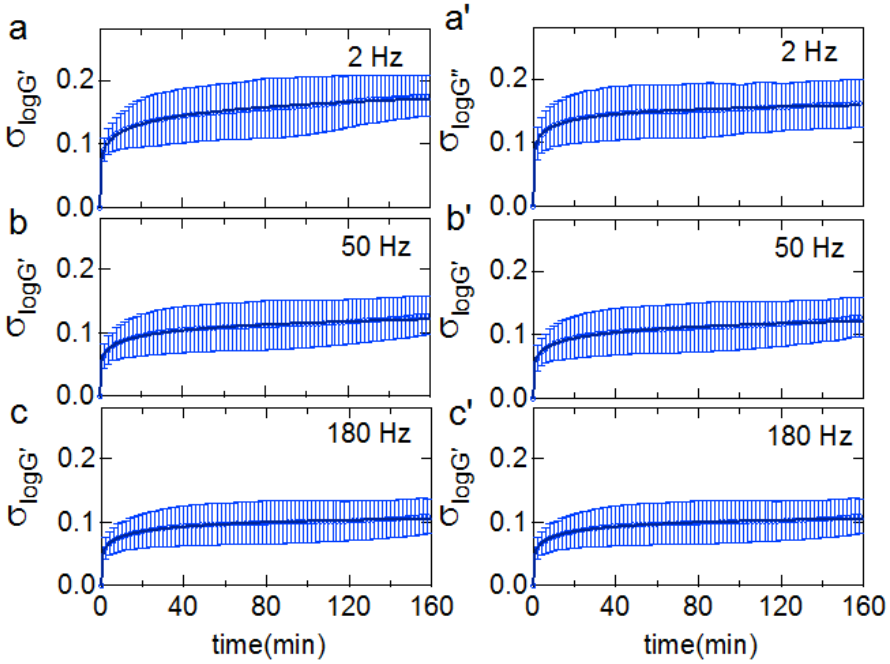

Figure 6.11 Time evolution of standard deviation $\sigma_{\log G'}$ (left) and $\sigma_{\log G''}$ (right) of untreated single cell at different frequencies: (a) 2, (b) 50 and (c) 180 Hz. The result is the mean value of seven single cells. The solid lines represent the fitted results by stretching exponential function $\sigma_{\log G^*} \sim \sigma_0 + \sigma_A \exp\left[-(t/\tau_\sigma)^{\beta_\sigma}\right]$.

To further understand the dynamical mechanics of cell rheology, the standard deviation $\sigma_{\log G^*}$ for G^* was calculated at different frequencies with time lapse. $\sigma_{\log G^*}$ based on the average of seven single cell samples and the corresponding error bar for both untreated cell and treated cell were respectively shown in Figs. 6.11 and 6.12. $\sigma_{\log G^*}$ increases quickly and gradually approaches a stationary state over time regardless of frequency, showing a time lag dependent. The corresponding characteristic time τ_σ was extracted from the fit by an exponential function $\sigma_{\log G^*} \sim \sigma_0 + \sigma_A \exp\left[-(t/\tau_\sigma)^{\beta_\sigma}\right]$, where a higher characteristic time τ_σ corresponds a

slower stabilization process (Fig. 6.13).

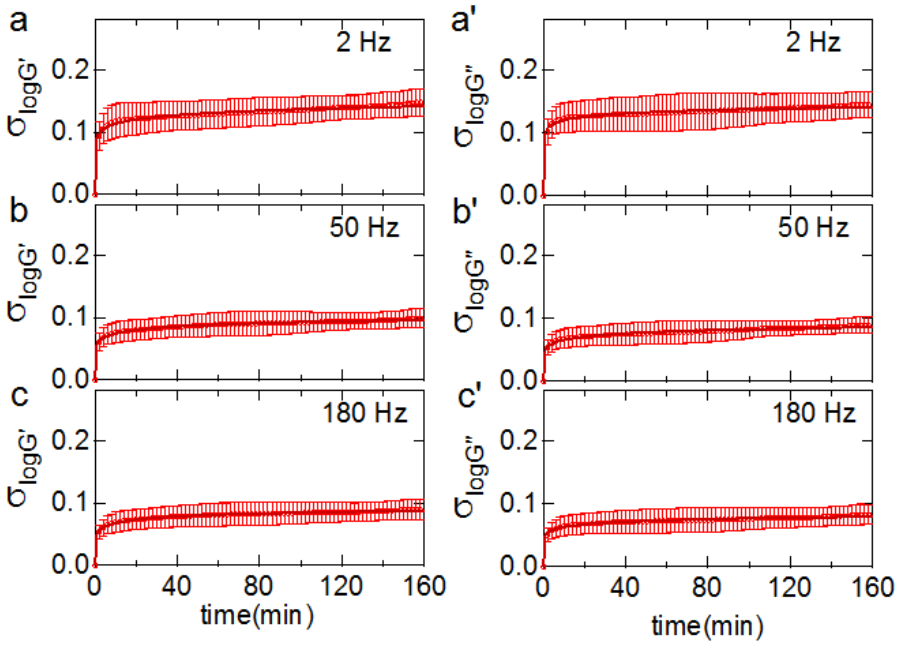

Figure 6.12 Time evolution of standard deviation $\sigma_{\log G'}$ (left) and $\sigma_{\log G''}$ (right) of treated single cell at different frequencies: (a) 2, (b) 50 and (c) 180 Hz. The result is the mean value of seven single cells. The solid lines represent the fitted results by stretching exponential function $\sigma_{\log G^*} \sim \sigma_0 + \sigma_A \exp\left[-(t/\tau_\sigma)^{\beta_\sigma}\right]$.

For both untreated and treated single cell, τ_σ is the same order, within several ten minutes, which is smaller than my experiment time 160 min. This shows that although the added external mechanical stress facilitated the system transition, a rapid stabilizing process was found in cell rheology, verifying the stationary of single cell rheology. Furthermore, the stretching exponent β_σ for the standard deviation appears to have no obvious change with cytoD-treatment around 0.2. The comparable τ_σ and β_σ values between untreated and treated cell indicated that the disruption of actin filament will slightly influence the stabilizing process and further the characteristic time.

From a biological point of view, combination of τ_σ and τ_γ can construct a model which sheds light on the mystery of the rearrangement of CSK over time and the integrated mechanical events in cells. According to SGR, my experimental results reveal that the fluctuations of cell rheological properties are not random manner but the rheological states transit in one small region then to others so that all the possible mechanical states of the ensemble one are traced.

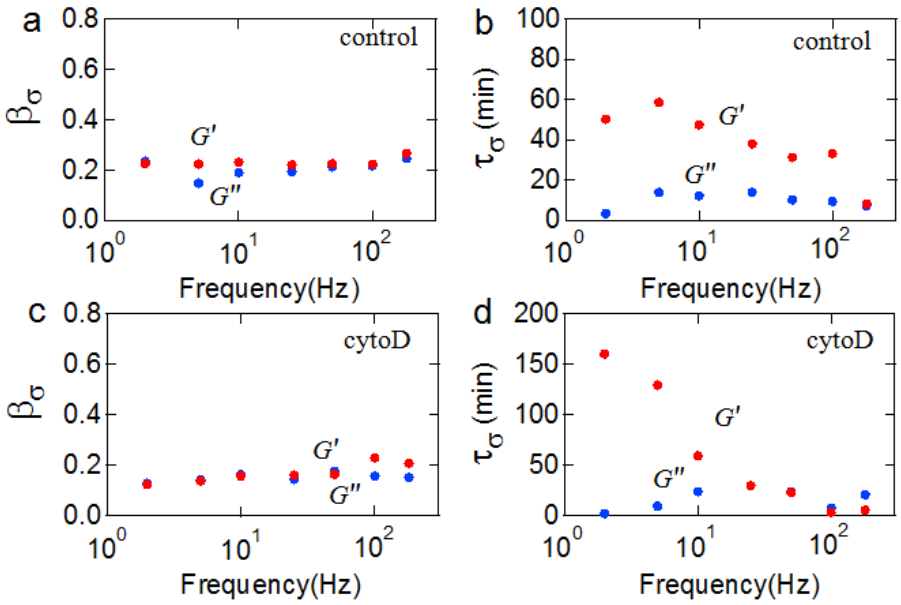

Figure 6.13 Frequency dependence of the stretching exponent β_σ(a, c) and the characteristic time τ_σ (b, d) of time lapse $\sigma_{\log G^*}$ for G' (red) and G'' (blue) of untreated cell (a, b) and treated cell (c, d). β_σ and τ_σ were extracted from the fit by an exponential function $\sigma_{\log G^*} \sim \sigma_0 + \sigma_A \exp\left[-(t/\tau_\sigma)^{\beta_\sigma}\right]$.

6.5 Conclusions

The temporal variation in rheological parameters measured via AFM oscillatory loading was estimated. The frequency-dependent component of temporal variation $\tilde{\sigma}_{\log G'}$ was quantified. It was found that $\tilde{\sigma}_{\log G'}$ of temporal variation was comparable to that of

ensemble one, indicating that single cell behaves as an ergodic way. Through the calculation of characteristic time τ_γ and τ_σ, it can extend the understanding of the mechanics of remodeling of CSK. The characteristic time τ_γ of time correlation function for control condition is smaller than that of actin filaments disrupted condition, representing that the decorrelation process of possible states of sing cell become slowly after the disruption of actin filaments and further proving that the transition of possible state is strongly associated with actin filaments. The comparable characteristic time τ_σ of time-lag standard deviation between untreated and treated cell indicates that stabilization process of possible states of sing cell is slightly related to actin filaments structure. Combination of τ_σ and τ_γ indicate that the fluctuations of cell rheological properties are not a random manner but transit from one small region to others with a characteristic time of about several to tens of minutes so that all the possible mechanical states of the ensemble one are traced.

6.6 References

1. Alberts, B., A. Johnson, J. Lewis, M. Raff, K. Roberts, and P. Walter. 2008. Molecular biology of the cell. 5th Edition. Garland Science, New York, NY.
2. Kollmannsberger, P. and B. Fabry. 2011. Linear and nonlinear rheology of living cells. Annu. Rev. Mater. Res. 41:75-97.
3. Pullarkat, P. A., P. A. Fernandez, and A. Ott. 2007. Rheological properties of the eukaryotic cell cytoskeleton. Phys. Rep. 449:29-53.
4. Chen, D. T. N., Q. Wen, P. A. Janmey, J. C. Crocker, and A. G. Yodh. 2010. Rheology of soft materials. Annu. Rev. Condens. Matter Phys. 1:301-322.
5. Trepat, X., G. Lenormand, and J. J. Fredberg. 2008. Universality in cell mechanics. Soft Matter 4:1750-1759.
6. Fabry, B., G. N. Maksym, J. P. Butler, M. Glogauer, D. Navajas, and J. J. Fredberg. 2001. Scaling the microrheology of living cells. Phys. Rev. Lett. 87:148102-1-148102-4.
7. Fabry, B., G. N. Maksym, J. P. Butler, M. Glogauer, D. Navajas, N. A. Taback, E. J. Millet, and J. J. Fredberg. 2003. Time scale and other invariants of integrative mechanical behavior in living cells. Phys. Rev. E 68:041914-1-041914-18.
8. Cai, P. G., Y. Mizutani, M. Tsuchiya, J. M. Maloney, B. Fabry, K. J. Van Vliet, and T. Okajima. 2013. Quantifying cell-to-cell variation in power-law rheology. Biophys. J. 105:1093-1102.
9. Laudadio, R. E., E. J. Millet, B. Fabry, S. S. An, J. P. Butler, and J. J. Fredberg. 2005. Rat airway smooth muscle cell during actin modulation: rheology and glassy dynamics. Am. J. Physiol. Cell Physiol. 289:C1388-C1395.
10. Smith, B. A., B. Tolloczko, J. G. Martin, and P. Grütter. 2005. Probing the

viscoelastic behavior of cultured airway smooth muscle cells with atomic force microscopy: stiffening induced by contractile agonist. Biophys. J. 88:2994-3007.

11. Van Citters, K. M., B. D. Hoffman, G. Massiera, and J. C. Crocker. 2006. The role of F-actin and myosin in epithelial cell rheology. Biophys. J. 91:3946-3956.
12. Lu, L., S. J. Oswald, H. Ngu, and F. C. –P. Yin. 2008. Mechanical properties of actin stress fibers in living cells. 95:6060-6071.
13. Rotsch, C. and M. Radmacher. 2000. Drug-induced changes of cytoskeletal structure and mechanics in fibroblasts: an atomic force microscopy study. Biophys. J. 78:520-535.
14. Khatau, S. B., C. M. Hale, P. J. Stewart-Hutchinson, M. S. Patel, C. L. Stewart, P. C. Searson, D. Hodzic, and D. Wirtz. 2009. A perinuclear actin cap regulates nuclear shape. Proc. Natl. Acad. Sci. USA 106:19017-19022.
15. Bursac, P., B. Fabry, X. Trepat, G. Lenormand, J. P. Butler, N. Wang, J. J. Fredberg, and S. S. An. 2007. Cytoskeleton dynamics: fluctuations within the network. Biochem. Bioph. Res. Co. 355:324-330.
16. Bursac, P., G. Lenormand, B. Fabry, M. Oliver, D. A. Weitz, V. Viasnoff, J. P. Butler, and J. J. Fredberg. 2005. Cytoskeletal remodelling and slow dynamics in the living cell. Nat. Mater. 4:557-561.
17. Schillers, H., M. Wälte, K. Urbanova, and H. Oberleithner. 2010. Real-time monitoring of cell elasticity reveals oscillating myosin activity. 99:3669-3646.
18. Massiera, G., K. M. Van Citters, P. L. Biancaniello, and J. C. Crocker. 2007. Mechanics of single cells: rheology, time dependence, and fluctuations. Biophys. J. 15:3703-3713.
19. Balland, M., N. Desprat, D. Icard, S. Fereol, A. Asnacios, J. Browaeys, S. Henon,

and F. Gallet. 2006. Power laws in microrheology experiments on living cells: comparative analysis and modeling. Phys. Rev. E 74:021911-1-021911-17.

20. Desprat, N., A. Richert, J. Simeon, and A. Asnacios. 2005. Creep function of a single living cell. Biophys. J. 88:2224-2233.
21. Deng, L. H., X. Trepat, J. P. Butler, E. Millet, K. G. Morgan, D. A. Weitz, and J. J. Fredberg. 2006. Fast and slow dynamics of the cytoskeleton. Nat. Mater. 5:636-640.
22. Hiratsuka, S., Y. Mizutani, M. Tsuchiya, K. Kawahara, H. Tokumoto, and T. Okajima. 2009. The number distribution of complex shear modulus of single cells measured by atomic force microscopy. Ultramicroscopy 109:937-941.
23. Miyaoka, A., Y. Mizutani, M. Tsuchiya, K. Kawahara, and T. Okajima. 2011. Rheological properties of growth-arrested fibroblast cells under serum starvation measured by atomic force microscopy. Jpn. J. Appl. Phys. 50:08LB16-1-08LB16-4.
24. Mizutani, Y., M. Tsuchiya, S. Hiratsuka, K. Kawahara, H. Tokumot, and T. Okajima. 2008. Elasticity of living cells on a microarray during the early stages of adhesion measured by atomic force microscopy. Jpn. J. Appl. Phys. 47:6177-6180.
25. Alcaraz, J., L. Buscemi, M. Grabulosa, X. Trepat, B. Fabry, R. Farre, and D. Navajas. 2003. Microrheology of human lung epithelial cells measured by atomic force microscopy. Biophys. J. 84:2071-2079.
26. Mahaffy, R. E., S. Park, E. Gerde, J. Kas, and C. K. Shih. 2004. Quantitative analysis of the viscoelastic properties of thin regions of fibroblasts using atomic force microscopy. Biophys. J. 86:1777-1793.
27. Alcaraz, J., L. Buscemi, M. Puig-de-Morales, J. Colchero, A. Baro, and D. Navajas. 2002. Correction of microrheological measurements of soft samples with atomic

force microscopy for the hydrodynamic drag on the cantilever. Langmuir 18:716-721.

28. Landau, L. and E. M. Lifshitz. 1986. Theory of elasticity. Oxford: Pergamon Press.
29. Radmacher, M., R. W. Tillmann, M. Fritz, and H. E. Gaub. 1992. From molecules to cells: imaging soft samples with the atomic force microscope. Science 257:1900-1905.
30. Fredberg, J. J. and D. Stamenovic. 1989. On the imperfect elasticity of lung-tissue. J. Appl. Physiol. 67:2408-2419.
31. Maloney, J. M. and K. J. Van Vliet. 2011. On the origin and extent of mechanical variation among cells. arXiv:1104.0702v2.
32. Lieleg, O., J. Kayser, G. Brambilla, L. Cipelletti, and A. R. Bausch. 2011. Slow dynamics and internal stress relaxation in bundled cytoskeletal networks. Nature. 10:236-242.

Chapter 7: Conclusions

The dissertation describes the features of the frequency-dependent components of the spatial dependent cell-to-cell and temporal variations in cell rheology with CSK modifications. The following conclusions were given:

In **Chapter 3**, the frequency-dependent component of cell-to-cell variation was quantified as a standard deviation, $\tilde{\sigma}_{\ln G'}$, in term of SGR. $\tilde{\sigma}_{\ln G'}$ observed for different cell populations under the same conditions was almost identical. The reduction of value of $\tilde{\sigma}_{\ln G'}$ of cells by cytoD-treatment indicated that $\tilde{\sigma}_{\ln G'}$ can be varied by perturbing the cytoskeleton at least via altering actin polymerization. Moreover, $\tilde{\sigma}_{\ln G'}$ measured at the center of microarray wells containing single cells was larger than that measured within the cell nucleus boundaries away from the well centers, suggesting that frequency-dependent component of cell-to-cell variation of G' also exhibits a subcellular spatial dependence related to cytoskeletal organization.

In **Chapter 4**, the parameters in cell-to-cell variation were characterized at the center and off-center locations of microarray wells by single power-law SGR. The results showed that the parameters $\bar{\Phi}_0$, $\bar{g}_0$ and $\sigma_{\log g_0}$ were almost the same in the center and off-center locations in wells. Moreover, the spatial dependence of the frequency-dependent component of the cell-to-cell variation in G' was preserved even the spatial heterogeneities of G' were largely varied among cell samples.

In **Chapter 5**, the effect of the interaction between actin filaments and myosin on the cell-to-cell variation in cell rheology was investigated. The enhancement of myosin II with calyculin A had no distinct change in the ensemble-averaged G^*, but led to an apparent increase of the cell-to-cell variation of G^*, $\sigma_{\log G^*}$, showing that the calyculin A-treated cells had more heterogeneous CSK structures than untreated cells. Moreover,

the inhibition of myosin II with blebbistatin led to a significant decrease in both the ensemble averaged G^* and $\sigma_{\log G^*}$, showing that blebbistatin-treated cells had homogenous CSK structures rather than untreated cells. These results indicate that the interaction between actin and myosin II regulates the heterogeneities of CSK structures and enhances the cell-to-cell variation in cell rheology.

In **Chapter 6**, the frequency-dependent component of temporal variation $\widetilde{\sigma}_{\log G'}$ was quantified. $\widetilde{\sigma}_{\log G'}$ of temporal variation is comparable to that of ensemble one, indicating that single cell behaves as an ergodic way. The characteristic time τ_γ of time correlation function is smaller than that of time-lag standard deviation, τ_σ, indicating that the fluctuations of cell rheological properties are not a random manner but transit from one small region to others so that all the possible mechanical states of the ensemble one are traced.

In this study, based on the single power-law model, the frequency-dependent components of the spatial dependent cell-to-cell (ensemble) and temporal variations in the storage modulus G', $\widetilde{\sigma}_{\log G'}$, were characterized. The results in this study revealed that the frequency-dependent component of variations in G' is proportional to logarithmic frequency. These findings contribute to the observation that, despite the enormous complexity of the underlying structures of cells, cellular microrheology seems to obey a universal and a defined empirical law. Moreover, it was found that the variations in cell rheology sensitively changed depending on the structural details of the constituents as well as the interaction between actin and myosin. This reveals one main source of the variations in cell rheology that is originated from the actin-myosin

complex structure. Comparison between the temporal and ensemble variations shows the same value of those two variations. This reveals the underlying physical mechanism that the time fluctuation of the rheological property of single cell behaves an ergodic way. The AFM combined microarray technique used here allows us to estimate the frequency-dependent components of variations in cell rheology and thus is expected to be useful in the future to provide mechanical identification and sorting of different cell states such as cancerous cell states.

Appendix

Quantifying Cell-to-Cell Variation in Power-Law Rheology

1. Cumulative distributions of lnμ and μ

Figure A1 (a) and (b) shows the cumulative distributions of lnμ and μ, respectively. The cumulative distributions of lnμ for both treated and untreated cells are well fitted to the error function, compared with those of μ. This indicates that μ follows a log-normal distribution rather than a normal Gaussian.

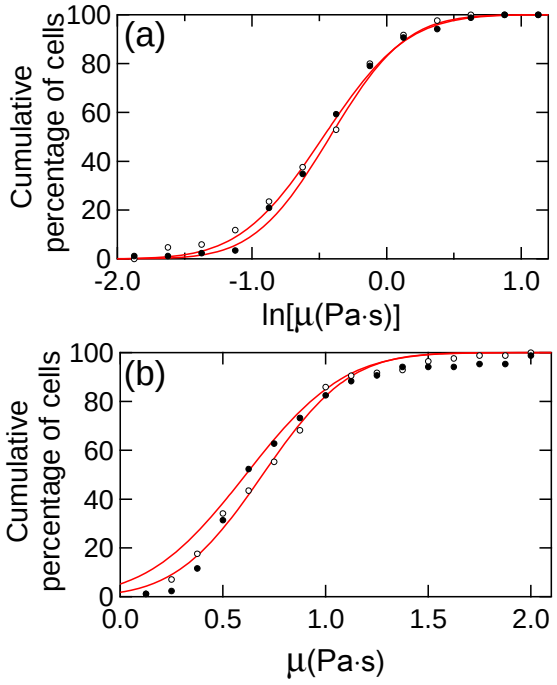

Figure A1 Cumulative percentages of cells for lnμ (a) and μ (b) under control condition (open circle) and cytoD treatment (closed circle). The red solid line represents the fitting result using the error function.

2. **Relation between $\sigma_{\ln G^*}$ and ln*G** in cells untreated and treated with cytochalasin D**

The standard deviation σ_X of quantity X with normal Gaussian depends on the magnitude of X: The k-fold increase in the i-th data X_i results in the same fold increase of σ_X,

$$\sigma_{kX}^2 = \frac{1}{n-1}\sum_{i=1}^{n}\left(kX_i - \langle kX\rangle\right)^2 = k^2\sigma_X^2,$$

and thus

$$\frac{\sigma_{kX}}{\sigma_X} = k. \qquad \text{(A1)}$$

I observed that the magnitude of $\ln\overline{G}^*$ was changed for cells treated with cytoD [Fig. 3.3 (a) and (b)]. According to Eq. A1, the reduction of $\ln\overline{G}^*$ leads to the change in the standard deviation, $\sigma_{\ln G^*}$. I plotted in Fig. A2 $R(\sigma_{\ln G^*})$, as a function of $R(\ln\overline{G}^*)$, where $R(X)$ represents the ratio of the variable X of the treated cells to that of the untreated cells. From Eq. A1, the relation $R(\sigma_{\ln G^*}) = R(\ln\overline{G}^*)$ should be satisfied if ln$G$* for each cells changes in the same manner. However, as shown in Fig. A2 (a) and (b), I found the relation $R(\sigma_{\ln G^*}) < R(\ln\overline{G}^*)$ at most of frequencies measured, showing that $\sigma_{\ln G^*}$ for the treated cells is largely reduced, compared with that expected from Eq. A1. Moreover, as shown in Fig. A2 (c) and (d), such a large reduction mentioned above is found for the frequency-dependent component of the cell-to-cell variation of cell rheology (see Discussion in Section 3.4), $\tilde{\sigma}_{\ln G^*}$, at every frequency.

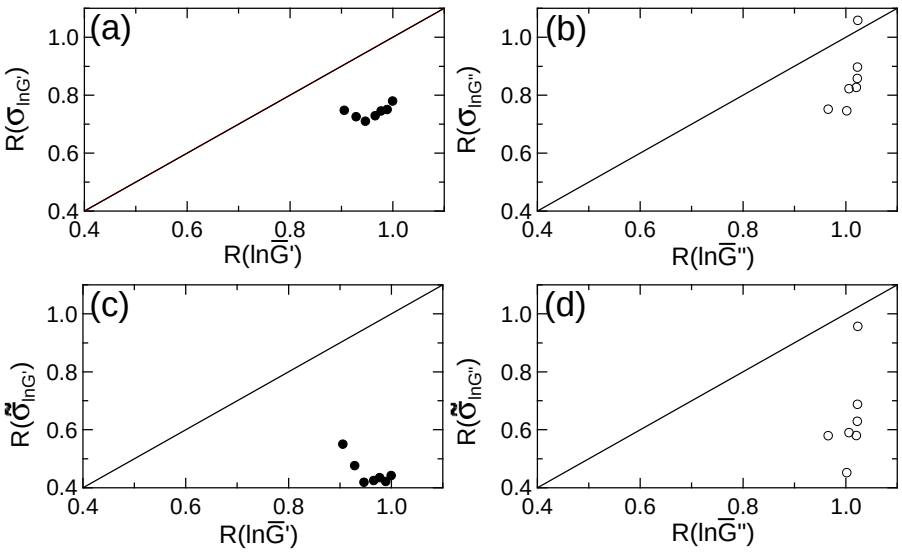

Figure A2 Plots of $R(\sigma_{\ln G'})$ vs. $R(\ln \overline{G'})$ (a), $R(\sigma_{\ln G''})$ vs. $R(\ln \overline{G''})$ (b), $R(\tilde{\sigma}_{\ln G'})$ vs. $R(\ln \overline{G'})$ (c) and $R(\tilde{\sigma}_{\ln G''})$ vs. $R(\ln \overline{G''})$ (d), where $\tilde{\sigma}_{\ln G*}$ represents the frequency-dependent component of the cell-to-cell variation of cell rheology (see Discussion in Section 3.4). $R(X)$ represents the ratio of the variable X of the cytoD-treated cells to that of the untreated cells. The solid line represents a linear line with the slope of one through the origin.

3. Relation between $\sigma_{\ln G^*}$ and $\ln \overline{G}^*$ obtained from the AFM measurements

The $\sigma_{\ln G^*}$ as a function of $\ln \overline{G}^*$ is shown in Fig. A3 (a) and (b), for untreated and treated cells and in Fig. A3 (c) and (d), for cells measured at the center and off-center of wells.

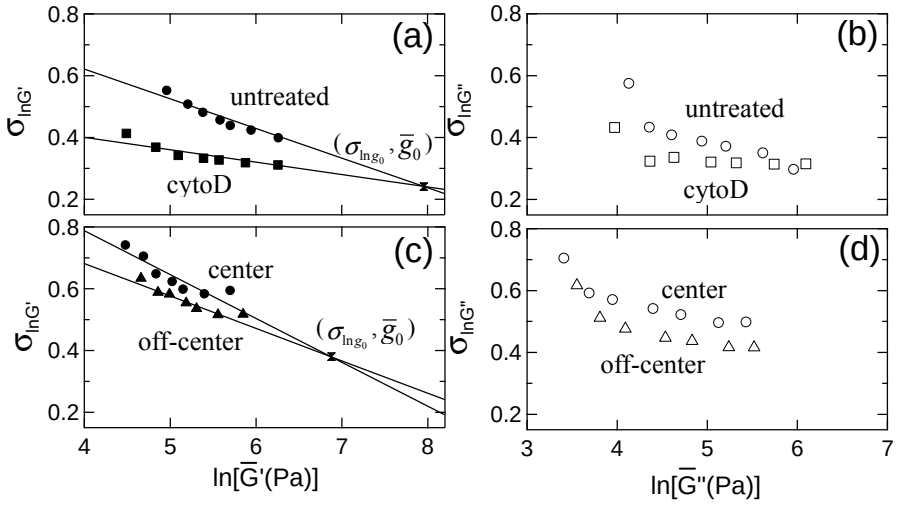

Figure A3 Plots of $\sigma_{\ln G^*}$ as a function of $\ln \overline{G}'$ (closed, a and c) and $\ln \overline{G}''$ (open, b and d) of two pairs of experimental conditions: (1) untreated cells (circle, a and b) and cytoD treated cells (square, a and b); (2) cells measured at the center (circle, c and d) and off-center (triangle, c and d) of wells. Solid lines in (a) and (c) represent the fitted results using Eq. 3.4 (see Discussion in Section 3.4).

4. Plot of g_0 and Φ_0 for each cells

The cross-point value, (Φ_0, g_0), at which the curves of G' measured for each cells intersect is plotted in Fig. A4.

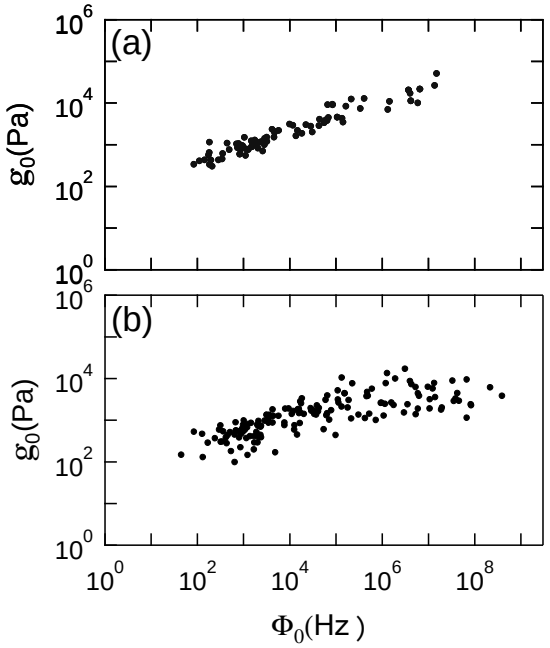

Figure A4 Plots of g_0 vs. Φ_0 estimated from G' as a function of f for each cells (a) untreated and treated with cytoD and (b) measured at the center and off-center of the wells.

5. Relation among power-law parameters derived from power-law rheology

According to Eq. 1.1 (2, 3), lnG' is expressed as

$$\ln G' = \ln G_0 + \ln g(\alpha) + \alpha \ln\left(\frac{f}{f_0}\right). \tag{A2}$$

Assuming that G' for each cells is g_0 at a cross-point frequency $f = \Phi_0$, I express Eq. 1.1 as

$$\ln G' = \ln g_0 + \alpha(\ln f - \ln \Phi_0). \tag{A3}$$

From Eqs. A2 and A3, I obtain the following relation:

$$\ln G_0 = \ln g_0 - \ln g(\alpha) - \alpha(\ln \Phi_0 - \ln f_0). \tag{A4}$$

Since ln$g(\alpha)$ is approximately proportional to α [Fig. A5 (a)], I obtain from Eq. A2

$$\ln G' = \ln G_0 + \left[\ln\left(\frac{f}{f_0}\right) + \frac{d \ln g(\alpha)}{d\alpha}\right]\alpha, \tag{A5}$$

and from Eq. A4

$$\ln G_0 = \ln g_0 - \left[\ln\left(\frac{\Phi_0}{f_0}\right) + \frac{d \ln g(\alpha)}{d\alpha}\right]\alpha.$$

For ensemble averaged data (2, 3), it is expressed as

$$\ln G_0 = \ln \overline{g}_0 - \left[\ln\left(\frac{\overline{\Phi}_0}{f_0}\right) + \frac{d \ln g(\alpha)}{d\alpha}\right]\alpha, \tag{A6}$$

showing that lnG_0 is negatively proportional to α and the slope is a function of f_0, which is arbitrarily determined.

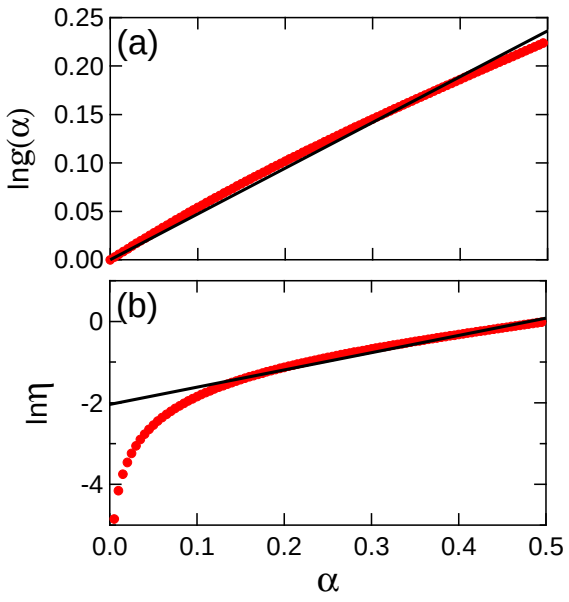

Figure A5 Plots of $\ln g(\alpha)$ vs. α (a) and $\ln\eta$ vs. α (b). Solid lines represent a linear function.

6. $\sigma_{\ln G^*}$ derived from the power-law rheology

The standard deviation of the sum of two quantities, X and Y, with normal Gaussian, σ_{X+Y}, is defined as

$$\sigma_{X+Y}^2 = \left[\frac{1}{n-1}\sum_{i=1}^{n}\left\{(X_i+Y_i)^2 - \langle X+Y\rangle^2\right\}\right]^{1/2}. \tag{A7}$$

Thus, σ_{X+Y} is given by

$$\sigma_{X+Y} = \sqrt{\sigma_X^2+\sigma_Y^2+2\sigma_{XY}} = \sqrt{\sigma_X^2+\sigma_Y^2+2\gamma_{XY}\sigma_X\sigma_Y}\,, \tag{A8}$$

where σ_{XY} represents the covariance of X and Y, which is defined as

$$\sigma_{XY} = \frac{1}{n-1}\sum_{i=1}^{n}(X_i-\langle X\rangle)(Y_i-\langle Y\rangle) = \frac{1}{n-1}\sum_{i=1}^{n}\left(X_iY_i-\langle X\rangle\langle Y\rangle\right). \tag{A9}$$

The γ_{XY} is the correlation coefficient, which is defined as

$$\gamma_{XY} = \frac{\sigma_{XY}}{\sigma_X \sigma_Y}. \tag{A10}$$

In the case that X and Y are completely independent, i.e., $\gamma_{XY} = 0$, σ_{X+Y} is given by

$$\sigma_{X+Y} = \sqrt{\sigma_X^2 + \sigma_Y^2}. \tag{A11}$$

On the other hand, in the case that X and Y are completely correlated each other, i.e., $\gamma_{XY} = \pm 1$, σ_{X+Y} is expressed by

$$\sigma_{X+Y} = \left| \sigma_X \pm \sigma_Y \right|. \tag{A12}$$

Since ln$G$' is a linear combination of lnG_0 and α (Eq. A5), $\sigma_{\ln G'}$ is composed of $\sigma_{\ln G_0}$ and σ_α (Eq. A8). As the relation $\gamma_{\ln G_0 \cdot \alpha} = -1$ is approximately satisfied [Fig. 3.9 (a)], I express $\sigma_{\ln G'}$ as

$$\sigma_{\ln G'} = \sigma_{\ln G_0} - \left[\ln\left(\frac{f}{f_0} \right) + \frac{d \ln g(\alpha)}{d\alpha} \right] \sigma_\alpha. \tag{A13}$$

Therefore, $\sigma_{\ln G'}$ at $f = \overline{\Phi}_0$, $\sigma_{\ln g_0}$, is expressed as

$$\sigma_{\ln g_0} = \sigma_{\ln G_0} - \left[\ln\left(\frac{\overline{\Phi}_0}{f_0} \right) + \frac{d \ln g(\alpha)}{d\alpha} \right] \sigma_\alpha. \tag{A14}$$

From Eqs. A13 and A14, I finally obtain

$$\sigma_{\ln G'} = \sigma_{\ln g_0} + \left(\ln \overline{\Phi}_0 - \ln f \right) \sigma_\alpha, \tag{A15}$$

showing that $\sigma_{\ln G'}$ decreases with increasing ln$f$ (4) and becomes $\sigma_{\ln g_0}$, which represents the global mechanical variation, at $f = \overline{\Phi}_0$. I define the frequency-dependent component of the cell-to-cell variation of cell rheology, $\tilde{\sigma}_{\ln G'}$, as $\tilde{\sigma}_{\ln G'} = \sigma_{\ln G'} - \sigma_{\ln g_0}$.

Using a first-order Taylor series expansion, $\ln G''$ is approximated as

$$\ln G'' = \ln G''(\ln \overline{G}_0, \langle\alpha\rangle, \ln \overline{\mu}) + \frac{\partial \ln G''}{\partial \ln G_0}(\ln G_0 - \ln \overline{G}_0) + \frac{\partial \ln G''}{\partial \alpha}(\alpha - \langle\alpha\rangle) + \frac{\partial \ln G''}{\partial \ln \mu}(\ln \mu - \ln \overline{\mu}). \quad \text{(A16)}$$

By using (Eq. A8), $\sigma_{\ln G''}$ is expressed as

$$\begin{aligned}\sigma_{\ln G''}{}^2 = &\left(\frac{\partial \ln G''}{\partial \ln G_0}\right)^2 \sigma_{\ln G_0}{}^2 + \left(\frac{\partial \ln G''}{\partial \alpha}\right)^2 \sigma_\alpha{}^2 + \left(\frac{\partial \ln G''}{\partial \ln \mu}\right)^2 \sigma_{\ln \mu}{}^2 \\ &+ 2\gamma_{\ln G_0 \cdot \alpha} \frac{\partial \ln G''}{\partial \ln G_0}\frac{\partial \ln G''}{\partial \alpha}\sigma_{\ln G_0}\sigma_\alpha \\ &+ 2\gamma_{\ln G_0 \cdot \ln \mu} \frac{\partial \ln G''}{\partial \ln G_0}\frac{\partial \ln G''}{\partial \ln \mu}\sigma_{\ln G_0}\sigma_{\ln \mu} \\ &+ 2\gamma_{\alpha \cdot \ln \mu} \frac{\partial \ln G''}{\partial \alpha}\frac{\partial \ln G''}{\partial \ln \mu}\sigma_\alpha \sigma_{\ln \mu}. \end{aligned} \quad \text{(A17)}$$

It is assumed that $\ln G_0, \ln\mu$ and α have linear relations such as $\gamma_{\ln G_0 \cdot \alpha} = -1$, $\gamma_{\ln G_0 \cdot \ln \mu} = 1$, and $\gamma_{\alpha \cdot \ln \mu} = -1$ (Figs. 3.9 and A6) and $\ln\eta$ is a linear function of α [Fig. A5 (b)]. Then, $\sigma_{\ln G''}$ is given by

$$\sigma_{\ln G''} = \left| \frac{\partial \ln G''}{\partial \ln G_0}\sigma_{\ln G_0} - \frac{\partial \ln G''}{\partial \alpha}\sigma_\alpha + \frac{\partial \ln G''}{\partial \ln \mu}\sigma_{\ln \mu} \right|,$$

or

$$\begin{aligned}\sigma_{\ln G''} = &\left[\sigma_{\ln G_0} - \left(\ln \frac{f}{f_0} + \frac{d \ln g(\alpha)}{d\alpha} + \frac{\pi}{\sin \pi \langle\alpha\rangle} \right)\sigma_\alpha \right] \frac{\overline{\eta}\,\overline{G}}{\overline{\eta}\,\overline{G} + \overline{\mu} f} \\ &+ \frac{\overline{\mu} f}{\overline{\eta}\,\overline{G} + \overline{\mu} f}\sigma_{\ln \mu}, \end{aligned} \quad \text{(A18)}$$

where $\overline{\eta}$, $\overline{G}'$, and $\overline{\mu}$ are the respective values at $G_0 = \overline{G}_0$, $\alpha = \langle\alpha\rangle$ and $\mu = \overline{\mu}$. Using the relation of the cross-point of $(\overline{\Phi}_0, \overline{g}_0)$, I finally obtain

$$\sigma_{\ln G''} = \left(\sigma_{\ln g_0} + \tilde{\sigma}_{\ln G'} - \frac{\pi}{\sin \pi \langle \alpha \rangle} \sigma_\alpha \right) \frac{\overline{\eta}\,\overline{G}}{\overline{\eta}\,\overline{G} + \overline{\mu} f} + \frac{\overline{\mu} f}{\overline{\eta}\,\overline{G} + \overline{\mu} f} \sigma_{\ln \mu} . \tag{A19}$$

Eliminating the effect of $\sigma_{\ln g_0}$ from $\sigma_{\ln G''}$, I obtain

$$\tilde{\sigma}_{\ln G''} = \sigma_{\ln G''} - \sigma_{\ln g_0} \overline{\eta}\,\overline{G} / (\overline{\eta}\,\overline{G} + \overline{\mu} f) .$$

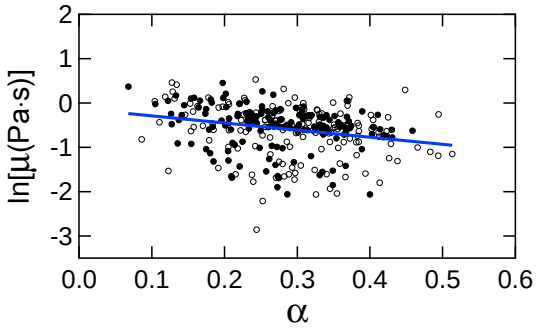

Figure A6 Plot of $\ln\mu$ vs. α of cells measured at the center and off-center of wells shown in Figs. 3.5–3.7.

7. Relation between $\sigma_{\ln G^*}$ and $\ln \overline{G}^*$ derived from power-law rheology

For ensemble averaged power-law rheology of cells with the cross-point $(\overline{\Phi}_0, \overline{g}_0)$, $\ln \overline{G}'$ is expressed by:

$$\ln \overline{G}' = \ln \overline{g}_0 + \langle \alpha \rangle \left(\ln f - \ln \overline{\Phi}_0 \right) . \tag{A20}$$

Combining Eqs. A15 and A20, the relation between $\sigma_{\ln G'}$ and $\ln \overline{G}'$ is given by

$$\sigma_{\ln G'} = \sigma_{\ln g_0} + \frac{\sigma_\alpha}{\langle a \rangle} (\ln \overline{g}_0 - \ln \overline{G}') , \tag{A21}$$

showing that $\sigma_{\ln G'}$ decreases with increasing $\ln \overline{G}'$ and becomes $\sigma_{\ln g_0}$ at $\overline{G}' = \overline{g}_0$.

8. Apparent Young's modulus for each cells

The apparent Young's modulus, *E*, estimated from the approaching force curve in the untreated cells is shown in Fig. A7. In the force curve measurements, the scan speed of the cantilever in the Z direction corresponded to a frequency of approximately 1 Hz, in which higher frequency components were contained during the indentation as the Z-piezo was linearly moved as a function of time. Moreover, in this case, the indentation time was much shorter than 1 s. Thus, the cell modulus was not completely relaxed during the indentation, and the measured *E* contains frequency components higher than that for Z-scan.

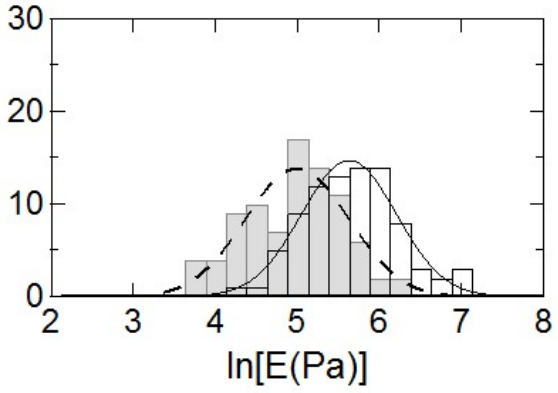

Figure A7 Distribution of apparent Young's modulus, *E*, estimated from the approaching force curve in the untreated cells (white) and cytoD-treated cell (gray).

References

1. Hiratsuka, S., Y. Mizutani, M. Tsuchiya, K. Kawahara, H. Tokumoto, and T. Okajima. 2009. The number distribution of complex shear modulus of single cells measured by atomic force microscopy. Ultramicroscopy 109:937-941.
2. Fabry, B., G. N. Maksym, J. P. Butler, M. Glogauer, D. Navajas, and J. J. Fredberg. 2001. Scaling the microrheology of living cells. Phys. Rev. Lett. 87:148102-148105.
3. Fabry, B., G. N. Maksym, J. P. Butler, M. Glogauer, D. Navajs, N. A. Taback, E. J. Millet, and J. J. Fredberg. 2003. Time scale and other invariants of integrative mechanical behavior in living cells. Phys. Rev. E. 68:041914-041931.
4. Maloney, J. M. and K. J. Van Vliet. 2011. On the origin and extent of mechanical variation among cells. arXiv:1104.0702v2.

List of Publications

Papers

学術論文

1. P. G. Cai, Y. Mizutani, M. Tsuchiya, J. M. Maloney, B. Fabry, K. J. Van Vliet, and T. Okajima. 2013. “Quantifying cell-to-cell variation in power-law rheology”. Biophys. J. 105:1093-1102. (IF = 3.832)
2. P. G. Cai and T. Okajima. 2015. “Precision of cell-to-cell variation in power-law rheology characterized by atomic force microscopy”. Jpn. J. Appl. Phys. 54:037001-1-037001-5. (IF = 1.057)

査読付国際学会プロシーディング

1. P. G. Cai, R. Takahashi, K. Kuribayashi-shigetomi, A. Subagyo, K. Sueoka, and T. Okajima. 2014. “Temporal change in complex shear modulus of cells: an atomic force microscopy study”. DOI: 10.1109/MHS.2014.7006107.
2. S. Hiratsuka, Y. Mizutani, P. G. Cai, M. Tsuchiya, H. Tokumoto, K. Kawahara, and T. Okajima. 2010. “Statistics of single cell mechanics investigated by atomic force microscopy”. Mater. Res. Soc. Symp. Proc. 1261:1261-U01-08.

Presentations

国際会議

1. P. G. Cai and T. Okajima. “Origin of cell-to-cell mechanical variation investigated by atomic force microscopy”. The 22nd International Colloquium on Scanning Probe Microscopy. Atagawa Heights, Japan, December, 2014.

2. P. G. Cai, R. Takahashi, K. Kuribayashi-Shigetomi, A. Subagyo, K. Sueoka, and T. Okajima. “Temporal change in complex shear modulus of cells: an atomic force microscopy study”. 25th Anniversary MHS2014. Nagoya, Japan, November, 2014.

3. P. G. Cai, Y. Mizutani, M. Tsuchiya, and T. Okajima. “Time distribution of single cell rheology investigated by atomic force microscopy”. The 5th International Symposium on Global COE Program of Center for Next-Generation Information Technology Based on Knowledge Discovery and Knowledge Federation. Sapporo, Japan, January, 2012.

4. P. G. Cai, Y. Mizutani, K. Kawahara, and T. Okajima. “Temporal variation of single cell rheology investigated by atomic force microscopy”. The 19th International Colloquium on Scanning Probe Microscopy. Toyaho Manseikaku, Hokkaido, Japan, December, 2011.

5. P. G. Cai, Y. Mizutani, M. Tsuchiya, K. Kawahara, and T. Okajima. “Change in the number distribution of complex shear modulus of single cells by actin cytoskeleton modifications measured by atomic force microscopy”. Biophysical Society 55th Annual Meeting. Baltimore, America, March, 2011.

6. P. G. Cai, Y. Mizutani, M. Tsuchiya, K. Kawahara, and T. Okajima. “Rheology of single cells in the modulation of microtubules measured by atomic force microscopy”. The 4nd International Symposium on Global COE Program of Center for Next-Generation Information Technology Based on Knowledge Discovery and Knowledge Federation. Sapporo, Japan, January, 2011.

7. P. G. Cai, Y. Mizutani, M. Tsuchiya, K. Kawahara, and T. Okajima. “Time and space dependent studies in cell rheology by atomic force microscopy.” The 18th International Colloquium on Scanning Probe Microscopy. Atagawa, Japan,

December, 2010.

8. P. G. Cai, Y. Mizutani, M. Tsuchiya, K. Kawahara, and T. Okajima. “Rheological properties of drug-treated single cells investigated by atomic force microscopy”. International Conference on Nanoscience and Technology. Beijing, China, August, 2010.

9. P. G. Cai, Y. Mizutani, M. Tsuchiya, K. Kawahara, and T. Okajima. “Drug-induced change of single cell rheology investigated by atomic force microscopy”. The 12th International Scanning Probe Microscopy Conference. Sapporo, Japan, May, 2010.

10. P. G. Cai, Y. Mizutani, A. Miyaoka, M. Tsuchiya, K. Kawahara, and T. Okajima. “Viscoelastic properties of single cells cultured on microarray measured by atomic force microscopy”. The 3nd International Symposium on Global COE Program of Center for Next-Generation Information Technology Based on Knowledge Discovery and Knowledge Federation. Sapporo, Japan, January, 2010.

11. P. G. Cai, Y. Mizutani, A. Miyaoka, M. Tsuchiya, K. Kawahara and T. Okajima. “Mechanics of single cells cultured on microarray measured by atomic force microscopy”. The 17th International Colloquium on Scanning Probe Microscopy, Atagawa, Japan, December, 2009.

12. P. G. Cai, S.J. Yu, X.J. Xu, M.G. Chen, and T. Okajima. “Stress relief patterns of Ni films deposited on silicone oil surfaces”. The 2nd International Symposium on Global COE Program of Center for Next-Generation Information Technology Based on Knowledge Discovery and Knowledge Federation. Sapporo, Japan, January, 2009.

国内学会

1. P. G. Cai, R. Takahashi, K. Kuribayashi-Shigetomi, A. Subagyo, K. Sueoka, and T. Okajima, “Temporal fluctuation of single cell rheology investigated by atomic force microscopy”, ゆらぎと構造の協奏–非平衡系における普遍法則の確立、第二領域研究会（2014 年 8 月）.

2. P. G. Cai, Y. Mizutani, M. Tsuchiya, K. Kawahara, and T. Okajima, “The role of

myosin in single cell rheology investigated by an atomic force microscopy", 第 4 回 若手研究者支援のための産学協同 GCOE シンポジウム 2011（2011 年 10 月）.

3. P. G. Cai, Y. Mizutani, M. Tsuchiya, K. Kawahara, and T. Okajima, "Precise Analysis of Variation of Single Cell Rheology Using Atomic Force Microscopy", 2011 年秋季 第 72 回 応用物理学会学術講演会（2011 年 8 月）.

4. P. G. Cai, Y. Mizutani, A. Miyaoka, K. Kawahara, and T. Okajima, "Single Cell Rheology in the Maculation of Cytoskeleton Investigated by Atomic Force Microscopy", 2011 年春季 第 58 回 応用物理学関係連合講演会（2011 年 3 月）.

5. P. G. Cai, Y. Mizutani, A. Miyaoka, K. Kawahara, and T. Okajima, "Atomic Force Microscopy Study on Drug-Induced Changes of Single Cell Rheology", 第 3 回 若手研究者支援のための産学協同 GCOE シンポジウム 2010（2010 年 10 月）.

6. P. G. Cai, Y. Mizutani, M. Tsuchiya, K. Kawahara, and T. Okajima, "Effect of Drug on Single Cell Rheology Investigated by Atomic Force Microscopy", 第 2 回 若手研究者による知の創出のための異分野共同セミナー（2010 年 3 月）.

7. P. G. Cai, Y. Mizutani, A. Miyaoka, K. Kawahara, and T. Okajima, Universality of Single Cells Rheology Investigated by Atomic Force Microscopy, 2010 年春季 第 57 回 応用物理学関係連合講演会（2010 年 3 月）.

8. P. G. Cai, Y. Mizutani, A. Miyaoka, K. Kawahara, and T. Okajima, "Local Measurements of Viscoelastic Properties of Single Cells by Atomic Force Microscopy", 第 2 回 若手研究者支援のための産学協同 GCOE シンポジウム 2009（2009 年 9 月）.

その他

本論文に関係した特許 1 件

岡嶋孝治、蔡萍根、水谷祐輔、土屋雅博. "単一細胞の力学特性の計測方法および計測装置". 特願 2011-184403（2011.8.26）.

Acknowledgements

The present dissertation collected the studies performed under the direction of Professor Takaharu Okajima during 2008-2014 at Hokkaido University Japan.

I would like to express the deepest and sincere appreciation to Professor Takaharu Okajima for his valuable advices, helpful discussions, and continuous encouragement throughout these works. I have learned passionate attitude for research from Professor Okajima. Professor Okajima has taught me a great deal about cell rheology and AFM, encouraged me to have a confidence in research as well as in living and shown a good example of excellent researcher.

I also would like to express the sincere thanks to Professor Krystyn J. Van Vliet, Professor Ben Fabry, Professor Koichi Kawahara, and Dr. John M. Maloney for their valuable comments and helpful suggestions. All the members in Laboratory of Cellular and Tissue Engineering offered kind assistance. I should sincerely appreciate them for their kind experimental supports and sacrificial help.

Great thanks to Hokkaido University (Japan) and Zhejiang University of Technology for giving me the chance to study in Japan and learn the culture and daily life of Japanese.

Finally, I would like to thank my parents, my relatives and my friends for their love, support, advice and spiritual encouragement. Special thanks to my husband JieYu Wu who always supports and encourages me all the time and for the many sacrifices. This dissertation is dedicated to them.

PingGen Cai

Laboratory of Cellular and Tissue Engineering

Graduate School of Information Science and Technology

Hokkaido University

Dec. 2014